โฟโตออกซิเดชันของสารประกอบออร์แกโนซัลเฟอร์ที่เร่งปฏิกิริยาด้วยอนุพันธ์ของไอโอโดโบดิพี
ภายใต้การฉายแสงในช่วงที่ตามองเห็น

นางสาวปิยมาภรณ์ ตั้งเกษมสำราญ

วิทยานิพนธ์นี้เป็นส่วนหนึ่งของการศึกษาตามหลักสูตรปริญญาวิทยาศาสตรมหาบัณฑิต
สาขาวิชาปิโตรเคมีและวิทยาศาสตร์พอลิเมอร์
คณะวิทยาศาสตร์ จุฬาลงกรณ์มหาวิทยาลัย
ปีการศึกษา 2560
ลิขสิทธิ์ของจุฬาลงกรณ์มหาวิทยาลัย

PHOTOOXIDATION OF ORGANOSULFUR COMPOUNDS CATALYZED BY IODO-
BODIPY DERIVATIVES UNDER VISIBLE LIGHT IRRADIATION

Miss Piyamaporn Tangkasemsamran

จุฬาลงกรณ์มหาวิทยาลัย
CHULALONGKORN UNIVERSITY

A Thesis Submitted in Partial Fulfillment of the Requirements

for the Degree of Master of Science Program in Petrochemistry and Polymer Science

Faculty of Science

Chulalongkorn University

Academic Year 2017

Thesis Title   PHOTOOXIDATION OF ORGANOSULFUR COMPOUNDS CATALYZED BY IODO-BODIPY DERIVATIVES UNDER VISIBLE LIGHT IRRADIATION

By   Miss Piyamaporn Tangkasemsamran

Field of Study   Petrochemistry and Polymer Science

Thesis Advisor   Associate Professor Sumrit Wacharasindhu, Ph.D.

Thesis Co-Advisor   Professor Mongkol Sukwattanasinitt, Ph.D.

    Accepted by the Faculty of Science, Chulalongkorn University in Partial Fulfillment of the Requirements for the Master's Degree

                      Dean of the Faculty of Science

    (Professor Polkit Sangvanich, Ph.D.)

THESIS COMMITTEE

                      Chairman

    (Assistant Professor Warinthorn Chavasiri, Ph.D.)

                      Thesis Advisor

    (Associate Professor Sumrit Wacharasindhu, Ph.D.)

                      Thesis Co-Advisor

    (Professor Mongkol Sukwattanasinitt, Ph.D.)

                      Examiner

    (Chatr Panithipongwut Kowalski, Ph.D.)

                      External Examiner

    (Nopporn Thasana, Ph.D.)

ปิยมาภรณ์ ตั้งเกษมสำราญ : โฟโตออกซิเดชันของสารประกอบออร์แกโนซัลเฟอร์ที่เร่งปฏิกิริยาด้วย อนุพันธ์ของไอโอโดโบดิพีภายใต้การฉายแสงในช่วงที่ตามองเห็น (PHOTOOXIDATION OF ORGANOSULFUR COMPOUNDS CATALYZED BY IODO-BODIPY DERIVATIVES UNDER VISIBLE LIGHT IRRADIATION) อ.ที่ปรึกษาวิทยานิพนธ์หลัก: รศ. ดร. สัมฤทธิ์ วัชรสินธุ์, อ.ที่ปรึกษาวิทยานิพนธ์ ร่วม: ศ. ดร. มงคล สุขวัฒนาสินิทธิ์, 97 หน้า.

งานวิจัยนี้ได้สังเคราะห์อนุพันธ์ไอโอโดโบดิพี I-GB, 3I-GB, I-RB, 3I-RB และใช้เป็นตัวเร่งปฏิกิริยาเชิงแสง ในปฏิกิริยาออกซิเดชันของสารประกอบออแกโนซัลเฟอร์ เช่น ไทออลและไทโออีเทอร์เป็นไดซัลไฟด์และซัลฟอกไซด์ ตามลำดับ เปรียบเทียบกับโรสเบงกอลซึ่งเป็นตัวเร่งปฏิกิริยามาตรฐาน โบดิพีทั้งหมดถูกสังเคราะห์ได้สำเร็จในร้อย ละผลผลิตที่ดี (36-80%) ผ่านปฏิกิริยาควบแน่นระหว่าง 4-ไอโอโดเบนซัลดีไฮด์และไพโรล ตามด้วยปฏิกิริยา ออกซิเดชันกับ DDQ และปฏิกิริยาสร้างสารประกอบเชิงซ้อนกับ $BF_3 \cdot OEt_2$ จากโบดิพีทั้งหมดที่ถูกสังเคราะห์ 3I-GB และ 3I-RB มีควอนตัมยีลด์ต่ำ (0.053-0.054) ซึ่งสัมพันธ์กับประสิทธิภาพในการสร้างซิงเกิลต์ออกซิเจนที่สูงภายใต้ แสงสีเขียว บ่งชี้ว่าอนุพันธ์ทั้งสองชนิดเป็นตัวเร่งปฏิกิริยาเชิงแสงที่ดีสำหรับปฏิกิริยาออกซิเดชันของสารประกอบ ซัลเฟอร์ ในกรณีของปฏิกิริยาออกซิเดชันของ 4-คลอโรไทโอฟีนอล 3I-GB และ 3I-RB ทำให้ปฏิกิริยาเกิดสมบูรณ์ ภายใน 6 ชั่วโมง (92-100%) และภายใต้เงื่อนไขเดียวกัน ตัวเร่งปฏิกิริยาชนิดอื่นให้ร้อยละผลผลิตเพียง 4-56 ภายใต้ แสงสีเขียว นอกจากนี้ 3I-GB และ 3I-RB สามารถถูกใช้เป็นตัวเร่งปฏิกิริยาเชิงแสงในปฏิกิริยาออกซิเดชันของสารตั้ง ต้นไทออลชนิดอื่น เช่น เฮทเทอร์โรไซคลิก (11, 13), อะโรมาติก (7, 9) และเบนซิลิก (13) ไทออล ให้ร้อยละผลผลิต 79-100 สำหรับปฏิกิริยาออกซิเดชันของไทโออะนีโซล 3I-GB และ 3I-RB แสดงให้เห็นความสามารถในการเป็น ตัวเร่งปฏิกิริยาที่ดีกว่า I-GB, I-RB และโรสเบงกอล โดยให้ร้อยละผลผลิตของสารประกอบซัลฟอกไซด์ประมาณ 80 ภายใต้แสงสีเขียวเป็นเวลา 24 ชั่วโมง ขณะที่สารประกอบไทโออีเทอร์ชนิดอื่นเช่นเฮทเทอร์โรไซคลิกและอะลิฟาติก ไม่สามารถถูกกระตุ้นได้ด้วยตัวเร่งปฏิกิริยาของเรา สำหรับกลไกการเกิดปฏิกิริยาของปฏิกิริยาออกซิเดชันของ สารประกอบซัลเฟอร์ที่ถูกกระตุ้นด้วยตัวเร่งปฏิกิริยาเชิงแสง เราเสนอว่าเมื่อโบดิพีถูกใช้เป็นตัวเร่งปฏิกิริยา ปฏิกิริยา จะเกิดผ่านการถ่ายโอนพลังงานและซิงเกิลต์ออกซิเจนจะเกิดขึ้นระหว่างกลไกการเร่งปฏิกิริยา สำหรับโรสเบงกอล กลไกของปฏิกิริยาออกซิเดชันเชิงแสงจะเกิดผ่านการถ่ายโอนอิเล็กตรอนแทน

สาขาวิชา ปิโตรเคมีและวิทยาศาสตร์พอลิเมอร์	ลายมือชื่อนิสิต	_____
ปีการศึกษา 2560	ลายมือชื่อ อ.ที่ปรึกษาหลัก	_____
	ลายมือชื่อ อ.ที่ปรึกษาร่วม	_____

5871990023 : MAJOR PETROCHEMISTRY AND POLYMER SCIENCE

KEYWORDS: BODIPY, PHOTOCATALYST

PIYAMAPORN TANGKASEMSAMRAN: PHOTOOXIDATION OF ORGANOSULFUR COMPOUNDS CATALYZED BY IODO-BODIPY DERIVATIVES UNDER VISIBLE LIGHT IRRADIATION. ADVISOR: ASSOC. PROF. SUMRIT WACHARASINDHU, Ph.D., CO-ADVISOR: PROF. MONGKOL SUKWATTANASINITT, Ph.D., 97 pp.

In this work, iodo-BODIPY derivatives, I-GB, 3I-GB, I-RB, were synthesized and used as photocatalysts for oxidation of organosulfurs such as thiols and thioethers into the corresponding disulfides and sulfoxides, respectively, as well as compared with benchmark photocatalyst, rose bengal. All BODIPY derivatives were successfully synthesized in good yields (36-80%) via condensation reaction between 4-iodobenzaldehyde and corresponding pyrroles, followed by oxidation with DDQ and complexation with $BF_3 \cdot OEt_2$. Among all synthesized BODIPYs, 3I-GB and 3I-RB showed relatively low quantum yield (0.053-0.054) with high singlet oxygen generation efficiency under green LED suggesting that both of them could serve as good photocatalysts for sulfur oxidation in visible light. In case of 4-chlorothiophenol (7) oxidation, 3I-GB and 3I-RB catalysts drove the reaction completely within 6 hours (92-100%), while other catalysts provided only 4-56% under the same condition irradiating by green LED. Moreover, 3I-GB and 3I-RB can be used as excellent photocatalysts in oxidation of others thiol substrates such as heterocyclic (11, 13), aromatic (7, 9), and benzylic (13) thiols giving the desired disulfides in 79%-quantitative yields. For the oxidation of thioanisole (19), 3I-GB and 3I-RB demonstrated higher catalytic activity comparing to I-GB, I-RB, and rose bengal providing sulfoxide (20) around 80% under green LED irradiation for 24 hours. Unfortunately, other unreactive thioethers such as heterocyclic and aliphatic substrates, were unable to oxidize using our catalysts. For mechanism of sulfur oxidation catalyzed by photocatalysts, we proposed that when BODIPYs is used as catalysts, the reaction proceeds through energy transfer and singlet oxygen is produced during the catalytic circle while the electron transfer process involves in the photooxidation catalyzed by rose bengal.

.

Field of Study:	Petrochemistry and Polymer Science	Student's Signature	-----------------------------------
Academic Year:	2017	Advisor's Signature	-----------------------------------
		Co-Advisor's Signature	-----------------------------------

ACKNOWLEDGEMENTS

CONTENTS

LIST OF SCHEMES

LIST OF FIGURES

จุฬาลงกรณ์มหาวิทยาลัย
CHULALONGKORN UNIVERSITY

LIST OF TABLES

LIST OF EQUATION

LIST OF ABBREVIATIONS

Ar	aromatic
hv	light energy
rt	room temperature
h	hour(s)
equiv	equivalent(s)
PrOH	propanol
EtOH	ethanol
LED	Light-emitting diode
MeCN	acetronitrile
THF	tetrahydrofuran
TLC	thin layer chromatography
^{1}H-NMR	proton nuclear magnetic resonance spectroscopy
^{13}C-NMR	carbon-13 nuclear magnetic resonance spectroscopy
δ	chemical shift
$CDCl_3$	deuterated chloroform
s	singlet (NMR)
d	doublet (NMR)
m	multiplet (NMR)
λ	wavelength
$λ_{ex}$	excitation wavelength
$λ_{abs}$	absorption wavelength
ε	molar absorptivity
UV	ultraviolet
Φ	quantum yield
R_f	retardation factor
m/z	mass per charge ratio
obsd	observed
calcd	calculated

% yield	percentage yield
% NMR yield	percentage yield via nuclear magnetic resonance analysis
J	coupling constant
ESI-MS	electrospray ionization mass spectrometer
DMSO	dimethyl sulfoxide
TFA	trifluoroacetic acid
DDQ	2,3-dichloro-5,6-dicyano-1,4-benzoquinone
DIPEA	N,N-diisopropylethylamine
ADPA	anthracene-9,10-dipropionic acid disodium salt

CHAPTER 1

INTRODUCTION

1.1 Overview

The oxidation of organosulfur compound is an important reaction in many industries such as vulcanization process for modify rubber or associated polymer to be more enduring material [1], increasing stability of some proteins [2], synthesis of drugs and intermediates [3-5], and removal of thiols from petroleum product by changing thiols to disulfides. [6] To perform the reaction, many researchers use metal catalysts or strong oxidizing agent to facilitate the oxidation reaction. However, the use of organometallic complexes as catalysts has many drawbacks such as high toxicity, requiring stoichiometric amount of catalyst, complicated workup step and high cost. [7-9] In addition, use of strong oxidizing agents have generated toxic waste as byproducts and difficult to handle the reaction. [10, 11] Recently, organic dyes had been in spotlight as photocatalysts because of theirs good stability, high reaction rate and high efficiency for sulfur compound oxidation. [8, 12] Then, our research group is interested in developing the greener chemistry by using boron dipyrromethene as photocatalyst dyes which is less toxic to environment and less expensive for oxidation of organosulfur compound.

1.2 Introduction to photocatalyst

Photocatalyst is acceleration of chemical reaction by a catalyst with suitable light source. When the oxygen is involved in the reaction, it is called as aerobic photooxidation. It has been used in various applications such as small organic molecule oxidation, [13, 14] preparing precursor in pharmaceutical industry [15] and continuous flow oxidation processes. [16] This wide adoption of aerobic photooxidation is driven by lower waste, less toxicity oxidant, inexpensive, high selectivity and high efficiency. [17] Mechanistically, photocatalyst can be performed

through electron or energy transfer processes to substrate when irradiated by light. There are two possible pathways for aerobic photooxidation. First, when photocatalyst is irradiated by visible light, either the electron transfer or energy transfer process are possibly occurred. For the electron-transfer process, substrate radical cation will be generated from the reduction of excited state photocatalyst (PC^*). After that, excited state photocatalyst become a radical anion ($PC^{\bullet-}$) and subsequently react with oxygen molecule to form an oxygen radical anion ($O_2^{\bullet-}$). This oxygen species will react with substrate or active compound (I) providing the product and hydrogen peroxide and water as byproduct as seen in figure 1.1a. [18] In case of energy transfer process, photocatalyst is excited by light source then converted into singlet excited state photocatalyst ($^1PC^*$). After intersystem crossing happens, the singlet excited state photocatalyst will become triplet excited state ($^3PC^*$) then react with oxygen molecule to generate singlet oxygen ($^1O_2$). Such singlet oxygen oxidizes substrate to give a product as seen in figure 1.1b.

PC = photocatalyst, S = substrate, I = intermediate, P = product, ISC = intersystem crossing
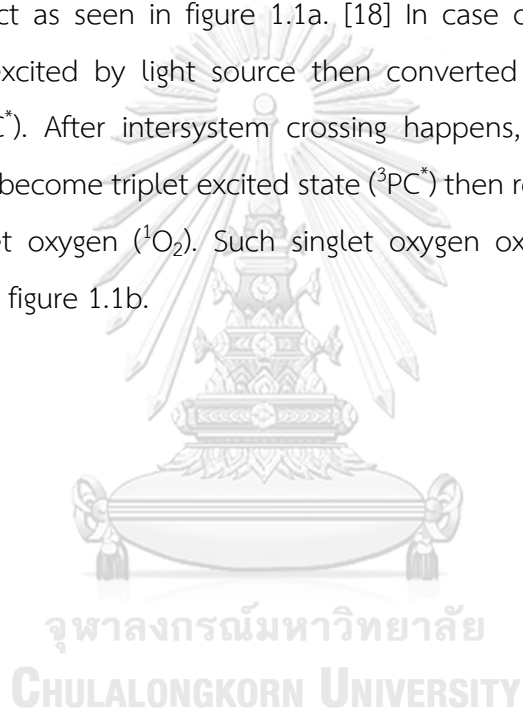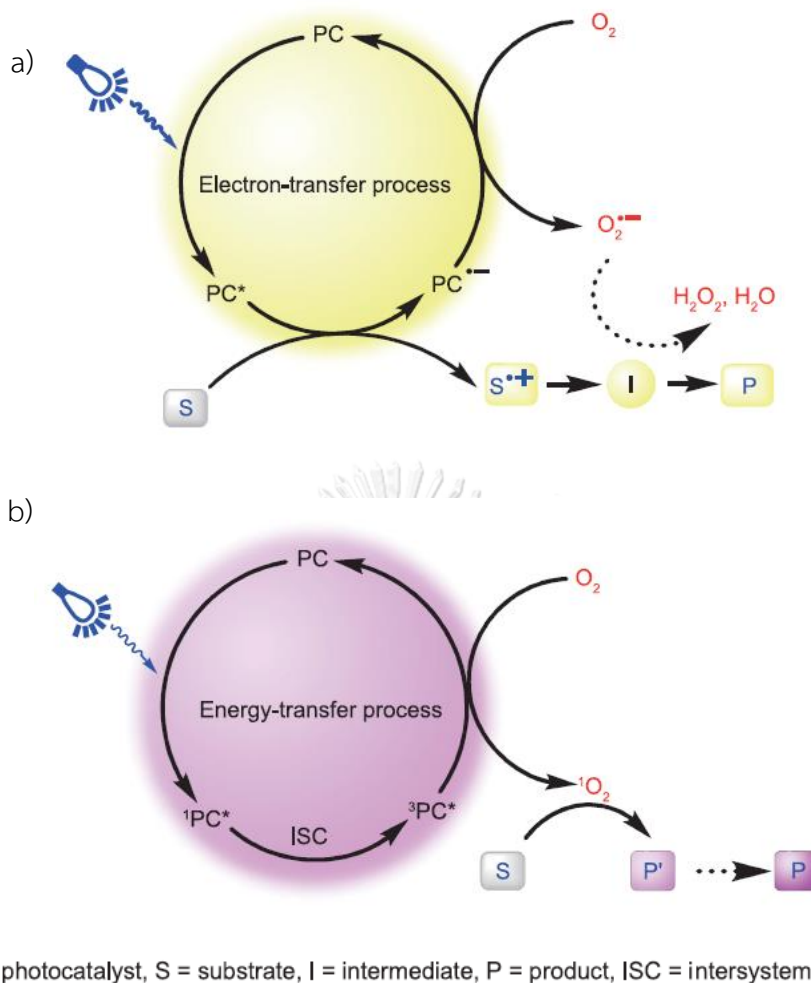
Figure 1.1 Outline of mechanism of visible-light-driven aerobic oxidation a) electron-transfer process b) energy-transfer process

For example, in 2014, Hari and co-workers [19] proposed mechanism through electron-transfer process for oxidative coupling of tetrahydroisoquinolines catalyzed by Eosin Y as shown in scheme 1.1. Eosin Y (EY) was excited by the suitable wavelength of light source generating excited state of Eosin Y. A singlet electron is transferred from tetrahydroisoquinoline (**1**) to EY*. Then, the electron is transferred to oxygen to give oxygen radical anion which can react with aminyl radical cation (**2**) to get the iminium ion (**3**) and hydrogen peroxide as by-product. Finally, the iminium ion (**3**) was reacted with nucleophile to give product (**4**).
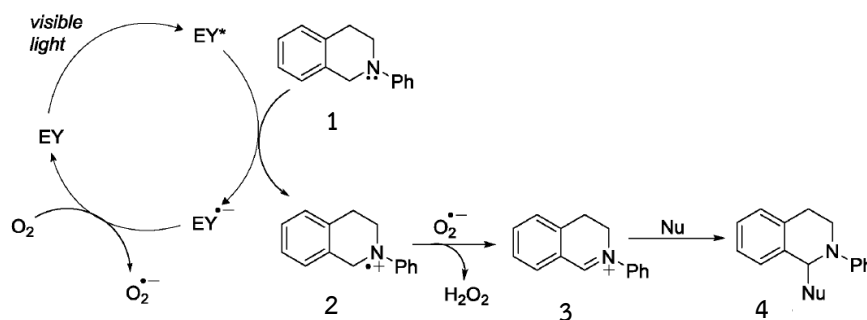
Scheme 1.1 The proposed mechanism for oxidative coupling of tetrahydroisoquinolines catalyzed by Eosin Y

1.3 Introduction to BODIPY

BODIPY was first discovered by Treibs and Kreuzer in 1968. [20] The structure of boron dipyrromethene (4,4-difluoro-4-bora-3a,4a-diaza-s-indacene) or BODIPY was shown in figure 1.2. It consists of disubstituted boron atom (BF_3) and complex of dipyrromethene. Recently, many researchers reported the BODIPY as photocatalysts because of their following properties such as small stroke shift, high fluorescence quantum yields (Φ_f), large molar absorption coefficient (ε). [21] These effects come from the low of degree of freedom caused by high rigidity of the BODIPY core structure. Moreover, it can be dissolved in many organic solvents [22] and tunable photophysical properties by introducing substituent groups at the peripheral position of BODIPY core. [23] According to the above-mentioned properties, BODIPY has been widely used in many applications such as photocatalysts, [24] optical sensor, [25] fluorescence markers [26] and photodynamic therapy. [27]
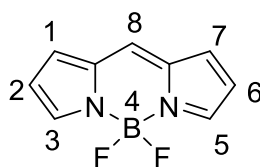
Figure 1.2 The structure of BODIPY

1.4 Literature review as catalyst for thiol oxidation

1.4.1 Oxidative coupling of thiol catalyzed by metal catalysts

In 2010, Kasem and co-worker [28] used tributylammonium fluorochromate (TBAFC) and tributylammonium chlorochromate (TBACC) absorbed on silica gel as catalysts for oxidation of different thiols into disulfides (68-93%yields) as seen in scheme 1.2. The advantages of their works are shorter reaction time, lower oxidant molar ratio, higher yields, and ease of separation of products.
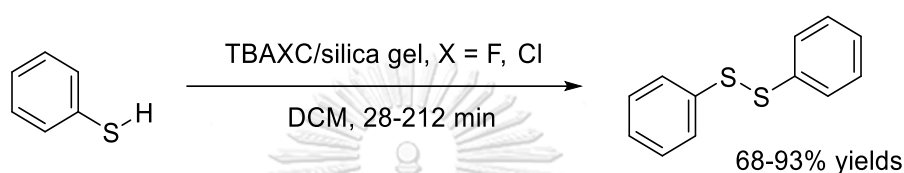
Scheme 1.2 Oxidation of thiols catalyzed by TBAFC or TBACC

In 2011, Oba and co-workers [29] reported the oxidative coupling of thiol catalyzed by diaryl tellurides such as bis(4-methoxyphenyl)telluride catalyst. The reaction provided the disulfide products in excellent yield as shown in scheme 1.3. The reaction need to perform in the presence of air atmospheric in dichloromethane at 0^oC.

$$2\ RSH\ \xrightarrow[\text{DCM or benzene or IPA, }0^oC,\ 15\text{-}60\ \text{min}]{\text{An}_2\text{Te (1 mol\%), tetraphenylporphyrin (0.1 mM)}}\ RS{-}SR$$

77-99 %yields
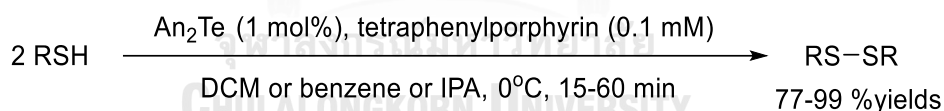
Scheme 1.3 Oxidation of thiol catalyzed by bis(4-methoxyphenyl)telluride

In 2014, Dharmarathna and co-workers [30] synthesized disulfide product using inexpensive manganese octahedral molecular sieve (OMS-2) as catalyst in oxidation of thiol as shown in scheme 1.4. The reaction was performed in acetonitrile at 100^oC and provided products around 18-100% yields.

18-100% yields
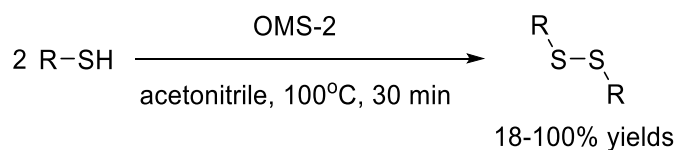
Scheme 1.4 Oxidation of thiol catalyzed by manganese octahedral molecular sieve

1.4.2 Oxidative coupling of thiol catalyzed by enzyme

In 2013, Abdel-Mohsen and co-workers [31] reported the oxidative coupling of heterocyclic thiols catalyzed by laccase. The reaction performed in aqueous media and provided coupling product in moderate yield (40-59%) at room temperature as shown in scheme 1.5.

laccase (T. *versicolor*), ABTS
0.2 M acetate buffer pH 4.4
MeOH 10 %

air, rt, 24 h

40-59 %conversion
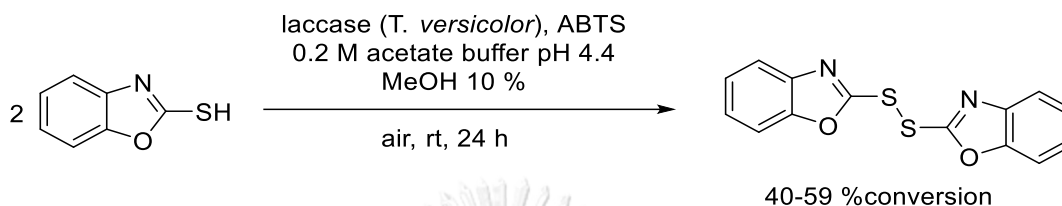
Scheme 1.5 Oxidation of thiol catalyzed by laccase

1.4.3 Photooxidation of thiol catalyzed by metal catalyst

In 2016, Liu and co-workers [18] reported the photooxidation of thiol catalyzed by TiO_2/MoS_2 nanocomposite and disulfide product was obtain in 85-99% yield at 8 hours as shown in scheme 1.6. Even though this protocol provided excellent yields of disulfide and the catalyst can be reused, TiO_2 nanoparticle causes oxidative damage in mesothelial cell of human. [32]

$$2 \text{ RSH} \xrightarrow[\text{TiO}_2/\text{MoS}_2]{\text{visible light, EtOH, air, rt, 8 h}} \text{RS–SR}$$
85-99% yields
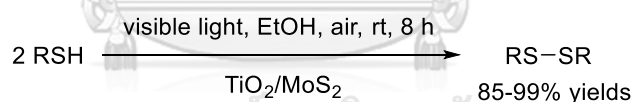
Scheme 1.6 Photooxidation of thiol catalyzed by TiO_2/MoS_2 nanocomposite

1.4.4 Photooxidation of thiol catalyzed by dye

In 2015, Talla and co-workers [33] reported the synthesis of disulfides in both batch and continuous-flow methods using Eosin Y as photocatalyst and tetramethylethylenediamine (TMEDA) as acid scavenger as shown in scheme 1.7. The reaction proceeded with white LED as a light source in the presence of air and provided the disulfide product in good to excellent yields within 20 minutes.
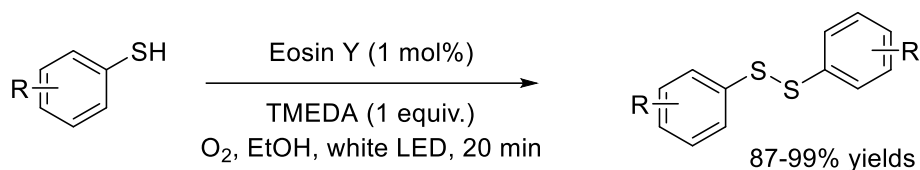
Scheme 1.7 Photooxidation of thiol into disulfide catalyzed by Eosin Y

For mechanism of this reaction (scheme 1.8), they proposed that thiols were oxidized by excited state Eosin Y and converted to thiol radical. In the same time, thiols were deprotonated by TMEDA to generate thiol anion. Then, it couples with another thiol radical to generate disulfide product.
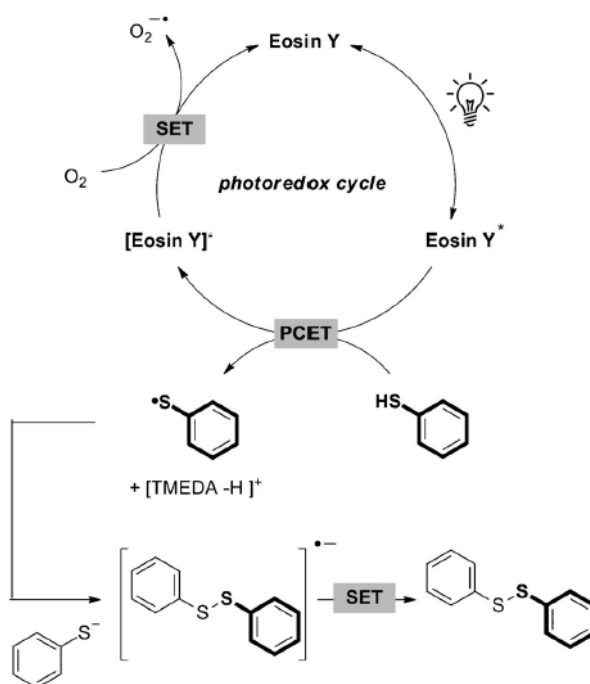
Scheme 1.8 The plausible mechanism for photooxidation of thiols using Eosin Y as catalyst

Similarly, in 2016, our research group [34] successfully synthesized disulfide product by oxidative coupling of thiol using rose bengal as photocatalyst. The reaction

proceeded in isopropanol at room temperature irradiated by white LED and provided the product in good to excellent yields within 3-15 hours as shown in scheme 1.9.

$$R-SH \xrightarrow[\text{white LED, PrOH}]{\text{5\% Rose Bengal}} R-S-S-R$$

R = aliphatic, 15 h, 84-94%
aromatic, 6 h, 75-92%
heterocyclic, 3 h, 81-92%
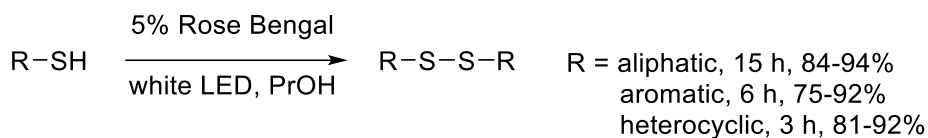
Scheme 1.9 Photooxidation of thiol catalyzed by rose bengal

The proposed mechanism was different from the above-mentioned research. We proposed that the product is generated through the energy transfer mechanism. The singlet excited state rose bengal ($^1RB^*$) is generated when ground state rose bengal (RB) is excited by light source. After that, intersystem crossing occurred and changed the spin multiplicity of electron to triplet ($^3RB^*$). Then, such triplet excited state rose bengal transfer energy to triplet oxygen molecule producing singlet oxygen species. The thiol substrate will be oxidized by singlet oxygen to give thiol radical and hydroperoxyl radical. Then, homocoupling reaction is occurred to provide disulfides as product and hydrogen peroxide as byproduct.
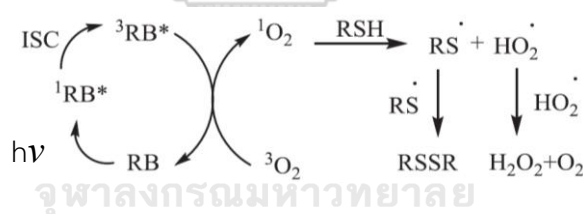
Scheme 1.10 Mechanism for photooxidation of thiols into disulfides

According to the previously reported literatures, the metal catalysts or oxidizing agent used in thiols oxidation still have some drawbacks, such as high toxicity, low selectivity, low yield and harsh condition. Even though there are some good literatures using photocatalyst in oxidation reaction of thiol, such catalyst still cannot provide appecable product yield and the mechanism for this type of reaction is still unclear. Therefore, in this work, we aim to develop the non-toxic and higher efficiency of photocatalysts based on BODIPY which allow us to modify its structure systematically

for oxidation of thiols. This will not only provide more efficient photocatalyst but also mechanistic information for photooxidation on BODIPY-based catalyst.

1.5 Literature review to catalyst in oxidation of thioanisole

1.5.1 Oxidation of thioanisole catalyzed by metal catalyst

In 2006, Mba and co-workers [11] reported the oxidation of sulfide substrate catalyzed by titanium compound in the presence of stoichiometric hydrogen peroxide as oxidizing agent. The reaction underwent smoothly at room temperature and provided sulfoxide product in 61-93% yield at 2-4 hours as shown in scheme 1.11. Due to the strong oxidizing power of the catalyst, the overoxidation product, sulfone, was observed in the reaction condition.
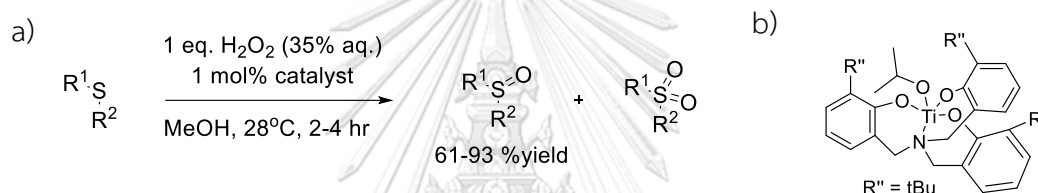
Scheme 1.11 a) oxidation of sulfide substrate catalyzed by titanium compound

b) Structure of titanium compound using as catalyst

In 2009, Yang and co-workers [35] synthesized tetra-(tetraalkylammonium) octamolybdate as catalysts and also used hydrogen peroxide as co-oxidizing agent for oxidation of sulfides to sulfoxides. The reaction proceeded in methanol as solvent at room temperature giving product in 92-100% yield as seen in scheme 1.12. According to the results, this catalyst shows high catalytic activity and is recyclable. However, this reaction provided sulfone as overoxidized byproduct.
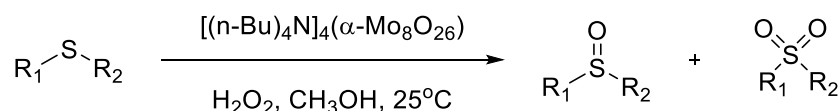
Scheme 1.12 oxidation of sulfides into sulfoxides catalyzed by molybdenum catalyst

In 2010, Das and co-workers [36] synthesized sulfoxides through oxidation of sulfides using CuBr$_2$ as catalyst and t-BuOOH as co-oxidizing agent at 0.75-24 h giving

sulfoxide products in 80-94% yield as shown in scheme 1.13. According to the reaction catalyzed by this catalyst, it showed high selectivity and gave good yields. However, the high temperature condition from refluxing was required to proceed the reaction completely.
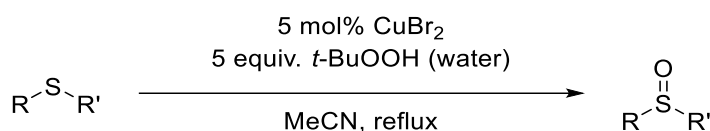
Scheme 1.13 oxidation of sulfides into sulfoxide catalyzed by Cu(II)

1.5.2 Photooxidation of thioanisole catalyzed by organic dyes

In 2013, Gu and co-workers [37] reported the photooxidation of thioanisole catalyzed by rose bengal under fluorescent lamp and sulfoxide product was isolated in 67-99% yield at 6-48 hours as shown in scheme 1.14. This reaction provided high selectivity, excellent yield, and unwanted waste is not produced. However, the acid catalyst was required to perform the reaction and might be reacted with other functional group in some compound.
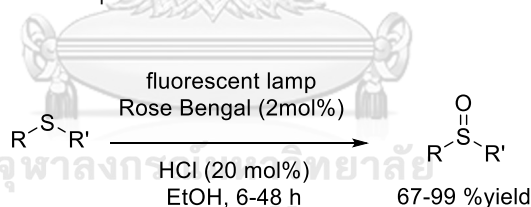
Scheme 1.14 Photooxidation of thioanisole catalyzed by rose bengal

In 2013 Li and co-workers [38] reported the synthesis of sulfoxide compound by oxidation of thioanisole using BODIPY derivatives as photocatalysts as shown in scheme 1.15. The BODIPY that has iodine atoms at 2 and 6 positions called I-BDP and the BODIPY without iodine atom called BDP. The results showed that I-BDP gave sulfoxide product to quantitative conversion in 3-33 hours which is faster than non-iodo BODIPY (BDP). They reported that the iodinated BODIPYs gave higher singlet oxygen generation efficiency compared to non-iodinated BODIPYs owing by heavy atom effect.

a)

BODIPY, 5 mol%

methanol, air, 3-33 h

96-100 %conversion

b)

I-BDP

BDP

I-BDP, X= H, methyl, phenyl

BDP, Y= H, methyl, phenyl, *p*-iodo-phenyl
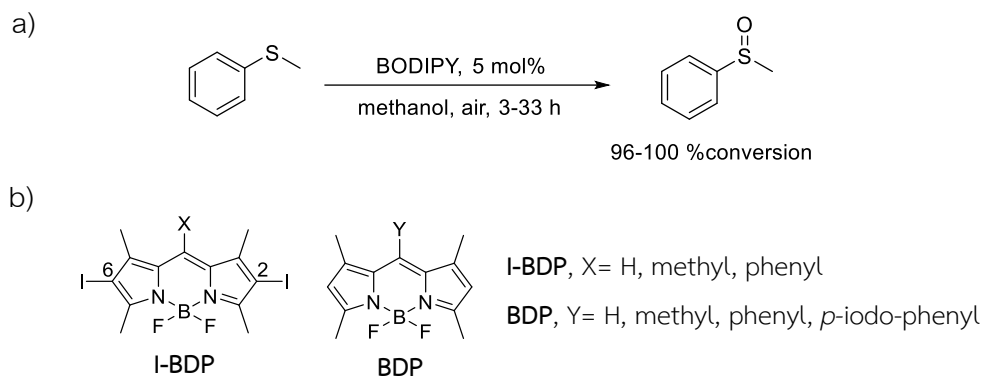
Scheme 1.15 a) Photooxidation of thioanisole catalyzed by I-BDP and BDP

b) Structures of I-BDP and BDP using as photocatalysts

They proposed the mechanism for the oxidation of thioanisole as shown in scheme 1.16. When BODIPY is excited by the appropriate wavelength, it undergoes to singlet excited state $^1BODIPY^*$ and goes down from lowest excited state energy level (S_1). If it falls to ground state and gives fluorescent emission, this is a competitive pathway which is not consider as photocatalyst. On the other hand, if $^1BODIPY^*$ changes electronic spin multiplicity called intersystem crossing process (ISC) to generate $^3BODIPY^*$ and goes back to ground state resulting in phosphorescent emission, consequently, the energy will be transferred from $^3BODIPY^*$ to triplet state oxygen molecule ($^3O_2$) to form singlet state oxygen molecule ($^1O_2$). Then, $^1O_2$ which is reactive oxygen species can react with thioanisole in the reaction to obtain desired product.
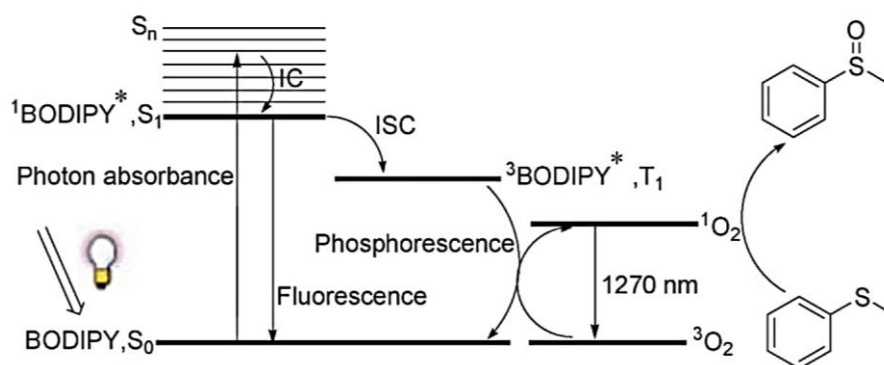
Scheme 1.16 The proposed mechanism for photooxidation of thioanisole

In 2014, Quan and co-workers [24] reported the oxidation of thioanisole catalyzed by BODIPY derivatives to get sulfoxide product in 7-100% conversion as shown in scheme 1.17. This type of catalysts can provide metal-free reaction which is environmental friendly.
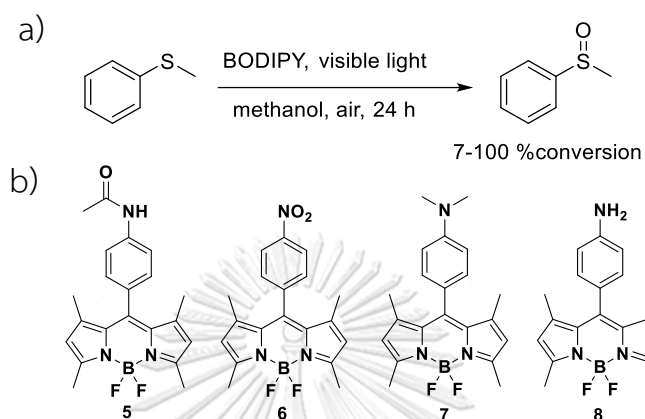
Scheme 1.17 a) Photooxidation of thioanisole catalyzed by BODIPY derivatives

b) Structures of BODIPY derivatives using as photocatalysts

1.6 Objective of this research

From the literature reviews, there are many ways to oxidize thiols and thioethers but most of them involve the use of toxic metal catalysts and strong oxidizing agent. On the other hand, the use of photocatalysts as an oxidant shows the promising properties due to the milder condition in the reaction. Herein, we aim to develop the novel iodo-BODIPY derivatives as photocatalysts in oxidation of 4-chlorothiophenol and oxidation of thioanisole as shown in scheme 1.18. The systematic modification of BODIPYs in this work include 1) the increase of phenyl groups at 3 and 5 positions (**I-GB** *vs.* **I-RB** and **3I-GB** *vs.* **3I-RB**) to extend conjugation system which increase intersystem crossing rate 2) the addition of iodine atoms at 2 and 6 positions (**I-GB** *vs.* **3I-GB** and **I-RB** *vs.* **3I-RB**) to increase heavy atom effect leading to higher singlet oxygen generation caused by higher spin orbit coupling process. Furthermore, we will study the photocatalytic activity of BODIPY compared to rose bengal as a benchmark catalyst in photooxidation of the sulfur substrates. The

singlet oxygen generation efficiency of all photocatalysts will be investigated. The optimum conditions will be studied in effect of light source, amount of catalyst, and reaction time. Moreover, we will extend our optimization into photooxidation of other thiol and thioether substrates and provide the mechanism for photooxidation.
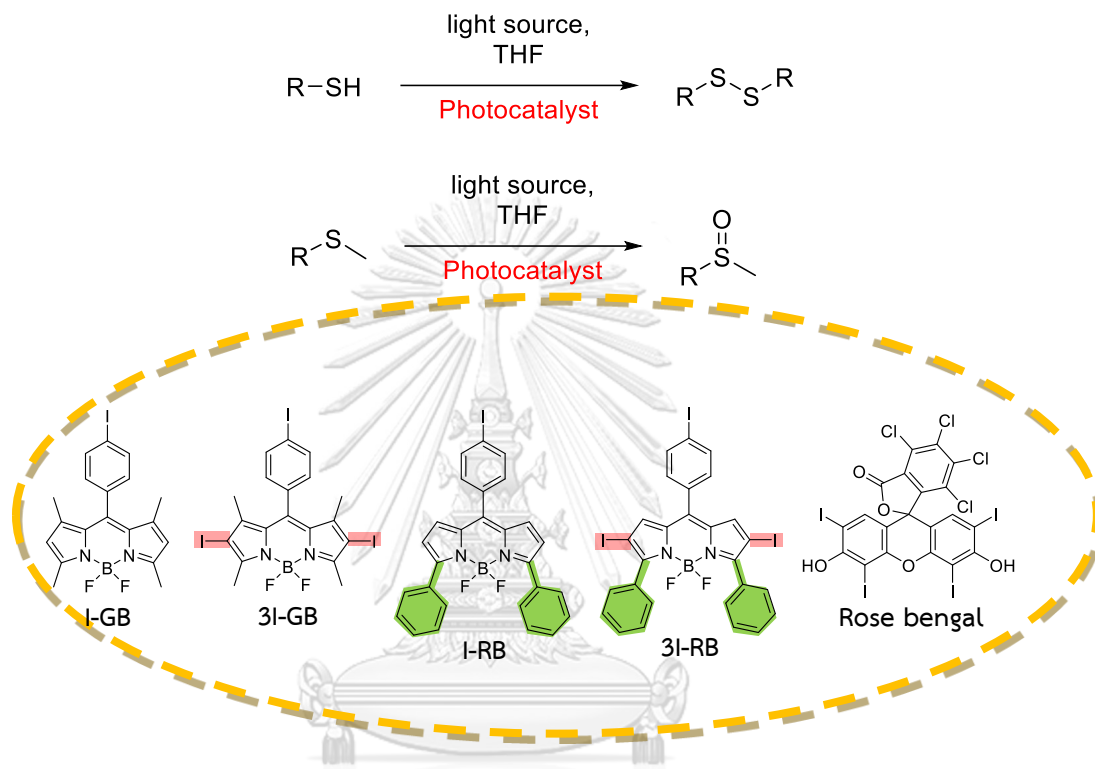
Scheme 1.18 Scope of our work

CHAPTER 2

EXPERIMENTAL

All chemicals were purchased from Sigma-Aldrich, Merck® (Germany) or Fluka® (Switzerland) and were applied without cumulative purification. All solvents were flowed with nitrogen before handling in the reaction. Analytical thin-layer chromatography (TLC) was operated on Kieselgel F-254 pre-coated plastic TLC plates from EM Science. Column chromatography was performed silica gel (60 Å, 230-400 mesh) from ICN Silitech. Visualization was carried out with a 254 nm ultraviolet lamp. The ^{1}H and ^{13}C NMR spectra were recorded on a Varian or bruker NMR spectrometer, operating at 400 MHz for ^{1}H and 100 MHz for ^{13}C nuclei (Varian Company, CA, USA). The chemical shifts (δ) of ^{1}H and ^{13}C NMR spectra were shown in parts per million (ppm) using remaining solvent, chloroform (δ 7.26 for ^{1}H, δ 77.00 for ^{13}C) and methanol (δ 4.87 for ^{1}H, δ 49.15 for ^{13}C), as standards. Coupling constants (J) were recount in Hertz (Hz). Splitting pattern of signal was establish as s (singlet), d (doublet), t (triplet), q (quartet), and m (multiplet). High resolution mass spectra were acquired from electrospray ionization mass spectrometer (ESI-MS). LED reactors were operated from a 1000 mL beaker lined with a commercial belt LED (1.5 W228). Fluorescent lamp was carried on whiting bulb (32W). Varian Cary 50 UV-Vis spectrophotometer (Varian, USA) was used to record the UV-Visible spectra from 300 to 700 nm at ambient temperature using isopropanol and tetrahydrofuran as solvents. Fluorescence emission spectra and fluorescence quantum efficiency were obtained by using Perkin Elmer precisely LS45. Fluorescein and rhodamine b were used as standards.

2.1 Part of synthesis

2.1.1 Preparation of acetophenone oxime
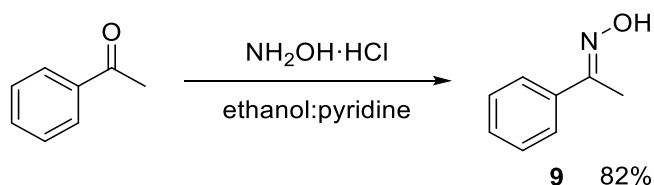
Scheme 2.1 Synthesis of acetophenone oxime

Acetophenone (2.0 g, 0.017 mol) and hydroxylamine hydrochloride (2.3 g, 0.033 mol) in ethanol:pyridine (20:2 mL) in 100 mL round bottom flask with magnetic bar. The mixture was refluxed at 100℃ for 4 hours. The solution was precipitated and washed with cool water. After that, the product was purified by crystallized in hexane to give acetophenone oxime in 1.846 g as white needle (82%).

^{1}H-NMR (400 MHz, CDCl$_3$) δ 2.32 (s, 3H), 7.37-7.42 (m, 3H), 7.61-7.66 (m, 2H)

2.1.2 Preparation of 2-phenyl pyrrole
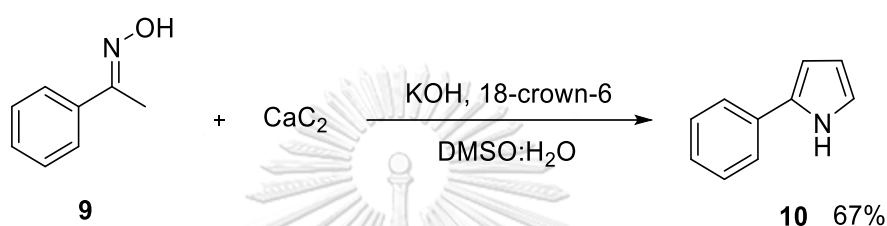
Scheme 2.2 Synthesis of 2-phenyl pyrrole

In a seal tube, acetophenone oxime (200 mg, 1.48 mmol), calcium carbide (569 mg, 8.88 mmol), potassium hydroxide (125 mg, 2.22 mmol) and 18-crown-6 (3 mol%) as a catalyst were added in DMSO:H$_2$O (18:2 mL) and stirred at 100℃ for 18 hours as shown in scheme 2.2. The solution was cooled at room temperature and added deionized water to remove acetylene gas. Then, the mixture was extracted with diethyl ether (3x20 mL), brine (3x20 mL) and dried over anhydrous sodium sulfate. After evaporation, the mixture was purified by column chromatography on aluminum oxide to get 2-phenyl pyrrole 134 mg (0.944 mmol, 67%) as purple solid, mp 127-128 ℃.

^{1}H-NMR (400 MHz, CDCl$_3$) δ 6.47 (s, 1H), 6.72 (s, 1H), 6.84 (s, 1H), 7.35 (s, 1H), 7.46 (s, 2H), 7.53 (s, 2H), 8.35 (s, 1H)

2.1.3 Preparation of 4,4-difluoro-8-(4'-iodophenyl)-1,3,5,7-tetramethyl-4-bora-3a,4a-diaza-s-indancene (I-GB)
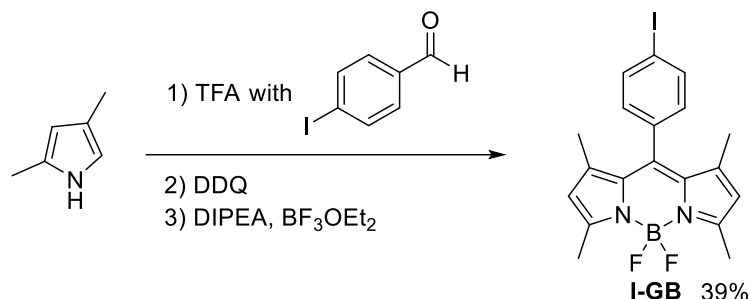
Scheme 2.3 Synthesis of **I-GB**

In a round bottom flask, 4-iodobenzaldehyde (300 mg, 1.30 mmol) and 2,4-dimethylpyrrole (0.264 mL, 2.61 mmol) were stirred in dichloromethane (40 mL) at 0°C under nitrogen atmosphere for 5 minutes. Trifluoroacetic acid (0.1 mL, 1.03 mmol) was added in the solution and stirred under nitrogen atmosphere for 3 hours. Then, 2,3-dichloro-5,6-dicyano-1,4-benzoquinone (295 mg, 1.3 mmol) was put in the reaction mixture and stirred at room temperature under nitrogen atmosphere for 30 minutes. The solution was charged with N,N-diisopropylethylamine (1.6 mL, 9.1 mmol) and boron trifluoride diethyl etherate (1.6 mL, 13.0 mmol). The mixture solution was stirred at 0°C under nitrogen atmosphere for 16 hours. The resulting solution was washed with sodium bicarbonate (2x50 mL), brine (2x50 mL) and dried over anhydrous sodium sulfate. After evaporation, the mixture was purified by column chromatography on silica gel to provide **I-GB** (231.0 mg, 39%) as orange solid (scheme 2.3), R_f 0.50 (40% CH_2Cl_2/hexane).

^{1}H-NMR (400 MHz, CDCl$_3$) δ 1.41 (s, 6H), 2.55 (s, 6H), 5.99 (s, 2H), 7.04 (d, J = 8.4 Hz, 2H), 7.84 (d, J = 8.4 Hz, 2H); ^{13}C-NMR (100 MHz, CDCl$_3$) δ 15.1, 95.2, 121.9, 130.4, 131.6, 135.0, 138.8, 140.5, 143.4, 156.4; HR-ESI-MS m/z obsd 451.0654 [(M+H)$^+$], calcd 451.0649 [(M+H)$^+$, M = $C_{19}H_{18}BF_2IN_2$].

2.1.4 Preparation of 4,4-difluoro-8-(4'-iodophenyl)-3,5-diphenyl-4-bora-3a,4a-diaza-s-indancene (I-RB)
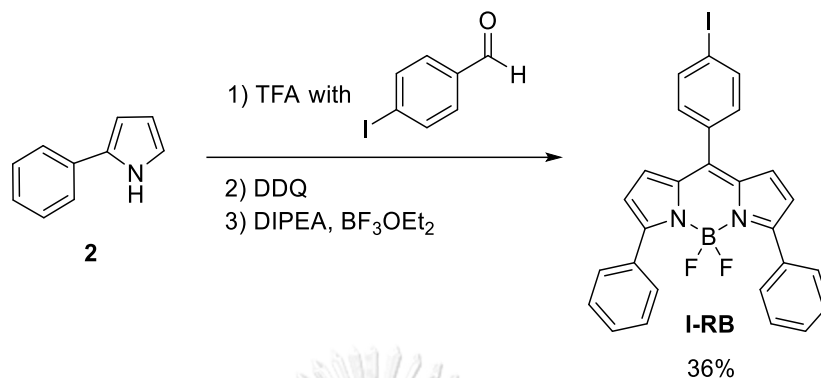
Scheme 2.4 Synthesis of **I-RB**

In a round bottom flask, 4-iodobenzaldehyde (300 mg, 1.30 mmol) and 2-phenylpyrrole (373 mg, 2.61 mmol) were stirred in dichloromethane (40 mL) at 0°C under nitrogen atmosphere for 5 minutes. Trifluoroacetic acid (0.1 mL, 1.03 mmol) was added in the solution and stirred under nitrogen atmosphere for 3 hours. Then, 2,3-dichloro-5,6-dicyano-1,4-benzoquinone (295 mg, 1.3 mmol) was put in the reaction mixture and stirred at room temperature under nitrogen atmosphere for 30 minutes. The solution was charged with N,N-diisopropylethylamine (1.6 mL, 9.1 mmol) and boron trifluoride diethyl etherate (1.6 mL, 13.0 mmol). The mixture solution was stirred at 0°C under nitrogen atmosphere for 16 hours. The resulting solution was washed with sodium bicarbonate (2x50 mL), brine (2x50 mL) and dried over anhydrous sodium sulfate. After evaporation, the mixture was purified by column chromatography on silica gel to provide **I-RB** (256 mg, 36%) as a deep red solid (scheme 2.4). R_f 0.35 (10% EtOAc/hexane).

^{1}H-NMR (400 MHz, CDCl$_3$) δ 6.64 (d, J = 4.4 Hz, 2H), 6.87 (d, J = 3.6 Hz, 2H), 7.33 (d, J = 8.4 Hz, 2H), 7.37 – 7.49 (m, 6H), 7.81 – 7.95 (m, 6H); ^{13}C-NMR (100 MHz, CDCl$_3$) δ 96.4, 121.0, 128.1, 129.3, 129.4, 130.4, 131.9, 132.3, 133.7, 135.9, 137.4, 142.4, 159.2; HR-ESI-MS m/z obsd 569.0466 [(M+Na)$^+$], calcd 569.0468 [(M+Na)$^+$, M = C$_{27}$H$_{18}$BF$_2$IN$_2$].

2.1.5 Preparation of 4,4-difluoro-2,6-diiodo-8-(4'-iodophenyl)-1,3,5,7-tetramethyl-4-bora-3a,4a-diaza-s-indancene (3I-GB).
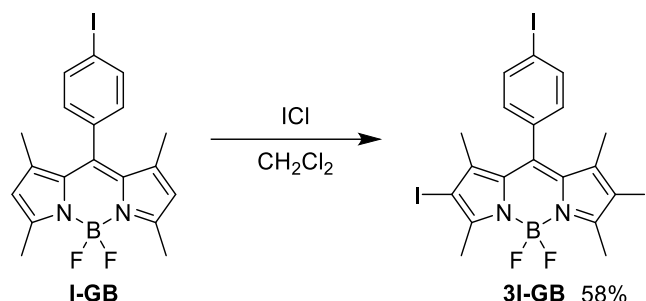
Scheme 2.5 Synthesis of **3I-GB**

In a round bottom flask, **I-GB** (200 mg, 0.445 mmol) and iodine monochloride (47 µL, 0.890 mmol) were dissolved in dichloromethane (30 mL) and stirred at room temperature under nitrogen atmosphere for 60 minutes as shown in scheme 2.5. The resulting solution was extracted with sodium thiosulfate (3x30 mL) and dried over anhydrous sodium sulfate. After evaporation, the mixture was purified by column chromatography on silica gel to provide **3I-GB** (54 mg, 58%) as red solid. R_f 0.50 (30% CH_2Cl_2/hexane).

^{1}H-NMR (400 MHz, $CDCl_3$) δ 1.43 (s, 6H), 2.64 (s, 6H), 7.01 (d, J = 8.4 Hz, 1H), 7.88 (d, J = 8.0 Hz, 1H); ^{13}C-NMR (100 MHz, $CDCl_3$) δ 16.1, 17.3, 95.3, 129.7, 131.0, 134.0, 134.3, 138.7, 139.7, 145.1, 157.2; HR-ESI-MS m/z obsd 724.8409 [(M+Na)$^+$], calcd 724.8401 [(M+Na)$^+$, M = $C_{19}H_{16}BF_2I_3N_2$].

2.1.6 Preparation of 4,4-difluoro-2,6-diiodo-8-(4'-iodophenyl)-3,5-diphenyl-4-bora-3a,4a-diaza-s-indancene (3I-RB).
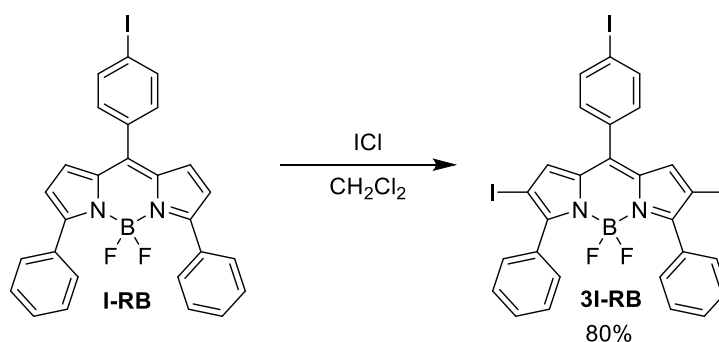
Scheme 2.6 Synthesis of **3I-RB**

In round bottom flask, **I-RB** (500 mg, 0.916 mmol) and iodine monochloride (216 µL, 4.12 mmol) were dissolved in chloroform:methanol (120:60 mL) and refluxed at 70°C for 16 hours as shown in scheme 2.6. The resulting solution was extracted with sodium thiosulfate (3x30 mL) and dried over anhydrous sodium sulfate. After evaporation, the mixture was purified by column chromatography on silica gel to provide **3I-RB** (585 mg, 80%) as purple solid. R_f 0.40 (30% CH_2Cl_2/hexane).

^{1}H-NMR (400 MHz, CDCl$_3$) δ 7.14 (s, 2H), 7.34 (d, J = 8.1 Hz, 2H), 7.41-7.43 (m, 6 H), 7.52-7.55 (m, 4 H), 7.94 (d, J = 8.1 Hz, 2H); ^{13}C-NMR (100 MHz, CDCl$_3$) δ 96.3, 123.2, 127.6, 129.9, 130.0, 130.8, 131.7, 132.7, 135.5, 137.6, 137.8, 138.2, 161.5; HR-ESI-MS m/z obsd 820.8415 [(M+Na)$^+$], calcd 820.8401 [(M+Na)$^+$, M = $C_{27}H_{16}BF_2I_3N_2$].

2.2 Determination of singlet oxygen generation efficiency of photocatalyst
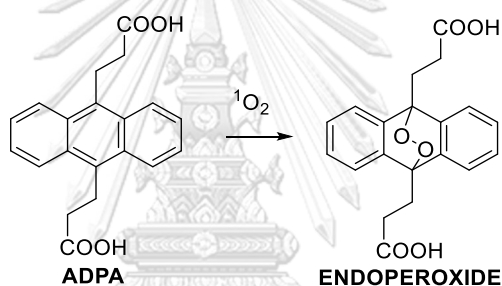
Scheme 2.7 Trapping mechanism by ADPA

Singlet oxygen generation efficiency could be measured using ADPA trapping mechanism (scheme 2.7) by observing the change of absorption of ADPA's at 381 nm over time when the mixture containing ADPA and photocatalyst was irradiated by light as shown in Figure 2.1. ADPA in water:THF solution (1:9) was used as a control experiment.
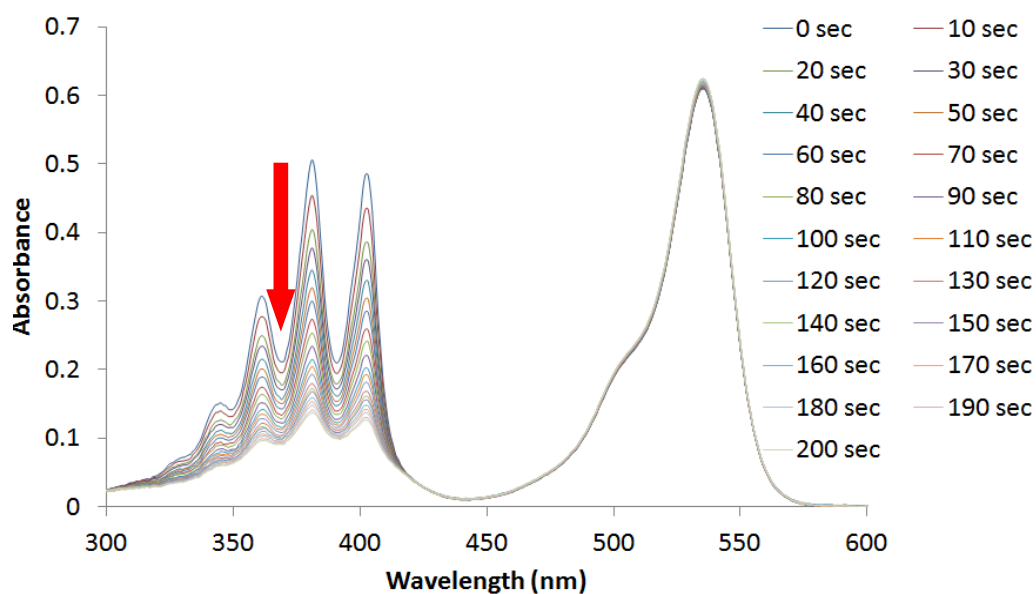
Figure 2.1 The absorption spectra of ADPA and photocatalyst under light source over time

2.3 Determination of percent NMR yield of the resulting solution in self-oxidation of 4-chlorothiophenol by ^{1}H-NMR spectroscopy

After the solvent of resulting reaction was evaporated, the mixture was dissolved in methanol-d and investigated percent yield by ^{1}H-NMR spectroscopy. The calculating percent NMR yield of product from photooxidation could be analyzed from Equation 2.1.

$$\%NMR\ yield = \frac{integration\ of\ product}{integration\ of\ product + integration\ of\ substrate}\ x\ 100$$

Equation 2.1 equation for determination of percent NMR yield

For investigated percent NMR yield, we chose the peak of 4-chlorothiphenol in the blue edge as substrate and the peak of disulfide product in the red edge as shown in Figure 2.2. Similarly, we indicated the peak of thioanisole in the blue edge as substrate and the peak of sulfoxide product in the red edge as shown in Figure 2.3.
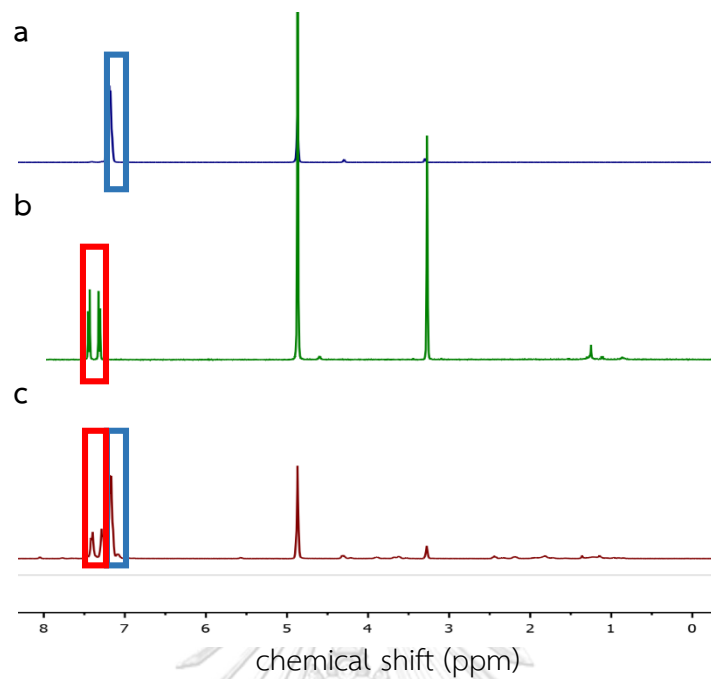
Figure 2.2 ^{1}H-NMR spectra of **a)** 4-chlorothiophenol **b)** disulfide product
c) mixture of thiol and disulfide (MeOD, 400 MHz)
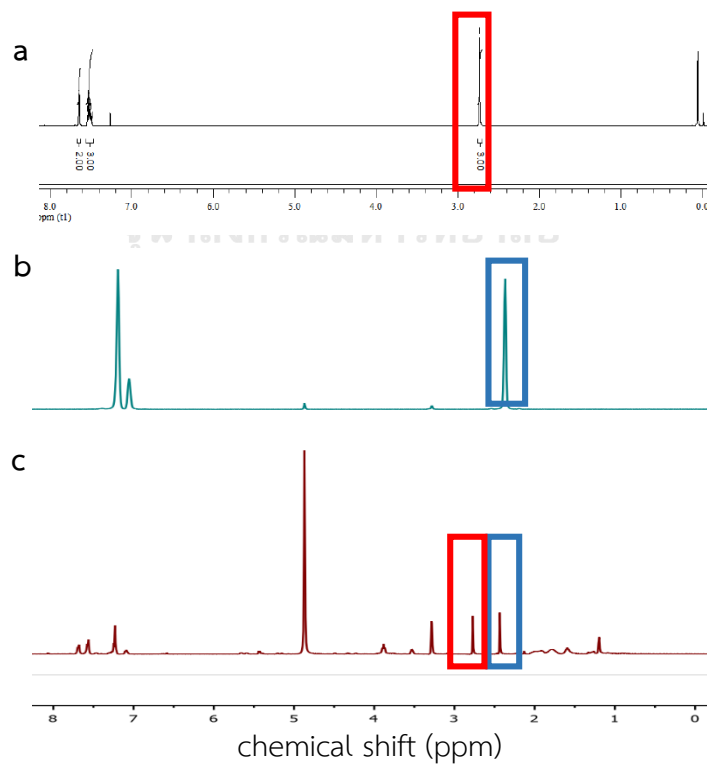
Figure 2.3 ^{1}H-NMR spectra of **a)** sulfoxide product [39] **b)** thioanisole
c) mixture of thioanisole and sulfoxide (MeOD, 400 MHz)

2.4 Determination of photocatalytic activity by using iodo-BODIPY catalysts with other substrates

After we used iodo-BODIPYs as catalyst in photooxidation of 4-chlorothiophenol, we studied the photocatalytic activity in oxidation reaction by using iodo-BODIPY catalysts with other substrates. We chose the other substrates by evaluated from aliphatic, aromatic and heterocyclic structure as shown in Figure 2.4.
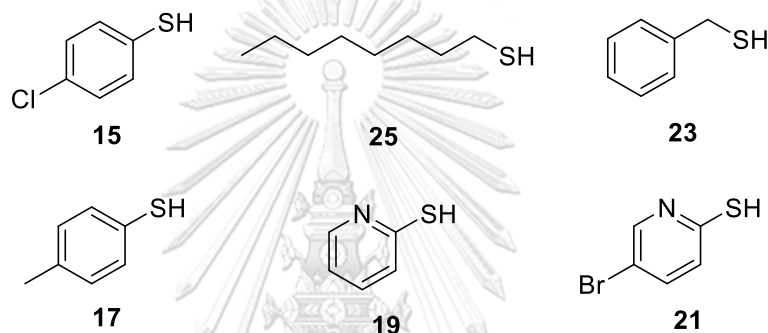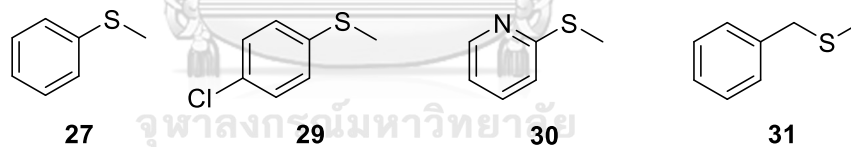
Figure 2.4 substrates scope

CHAPTER 3

RESULTS AND DISCUSSION

3.1 Synthesis of iodo-BODIPY derivatives

In this work, we planned to prepare four BODIPY based photocatalysts **I-GB**, **3I-GB**, **I-RB** and **3I-RB** as shown in figure 3.1. Structurally, all four BODIPY catalysts have iodo-benzene substituted on C8-position on BODIPY core but the number of iodine at C2 and C6 positions as well as number of phenyl group at C3 and C5 positions are different. **I-GB** has no extra conjugated phenyl group, while **3I-GB** and **3I-RB** contain 2 extra iodo-substituted groups at C2 and C6 positions. Based on previous literatures [38, 40], increasing iodine atoms at C2 and C6 positions of BODIPY core leads to the better photocatalytic activity. This result is probably due to the heavy atom effect (HAE) that can increase spin-orbit coupling providing high intersystem crossing (ISC). This will cause a high singlet oxygen generation on BODIPY derivatives. [21] Moreover, the incorporation of phenyl group at C3 and C5 positions will increase the conjugation system that allowed the absorption of light at longer wavelength in catalysts as we designed for **I-RB** and **3I-RB**.
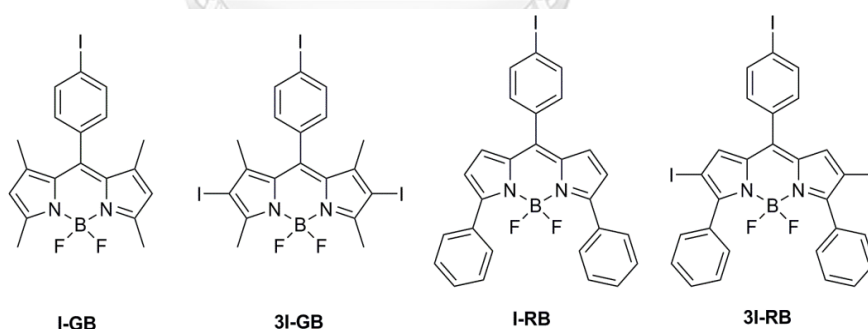
Figure 3.1 Photocatalyst molecules **I-GB**, **3I-GB**, **I-RB** and **3I-RB**

We planned to synthesize four photocatalysts as displayed in retro-synthetic scheme 3.1. For **3I-GB**, it will be synthesized *via* beta iodination of **I-GB** catalyst. The **I-GB** catalyst is received from 2,4-dimethylpyrrole (**1**) *via* the BODIPY formation. Similarly, the **3I-RB** catalyst is prepared from beta-iodination of **I-RB** which is

synthesized by BODIPY formation of phenyl pyrrole (**3**) received from Trofimov reaction between acetophenone oxime (**2**) and calcium carbide. [41]
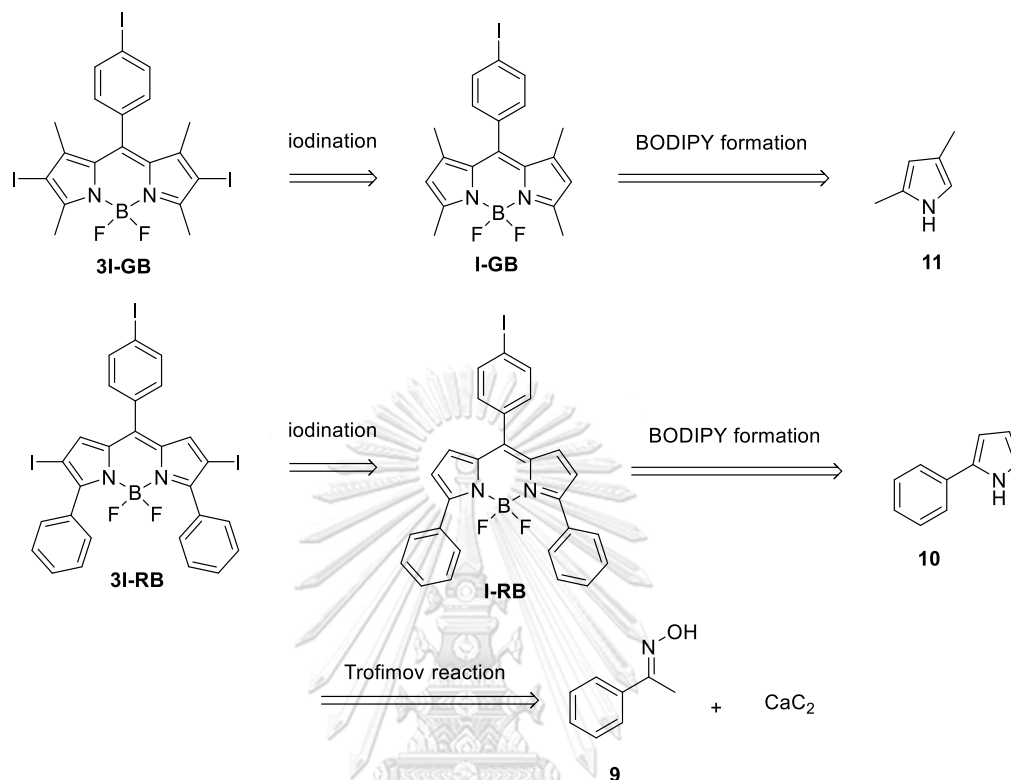
Scheme 3.1 Retro synthetic plan for **3I-GB**, **I-GB**, **3I-RB**, **I-RB** catalysts

3.1.1 Synthesis and characterization of acetophenone oxime (9)

Acetophenone oxime (**9**) was synthesized by the imination between 1 equivalent of acetophenone and 2 equivalents of hydroxylamine hydrochloride in 82% yield as shown in scheme 3.2. Structure of compound **9** was confirmed by ^{1}H-NMR spectrum which was consistenced to a reported literature [41] as displayed in figure 3.2. The proton signals at 7.63 ppm (b), 7.39 ppm (c and d) belonged to aromatic protons and peak at 2.32 ppm (a) corresponded to methyl group.
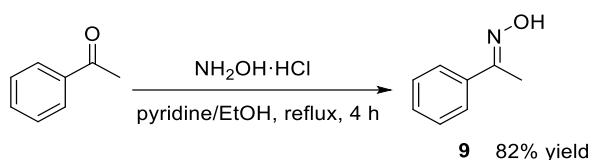
Scheme 3.2 Synthesis of acetophenone oxime (**9**)
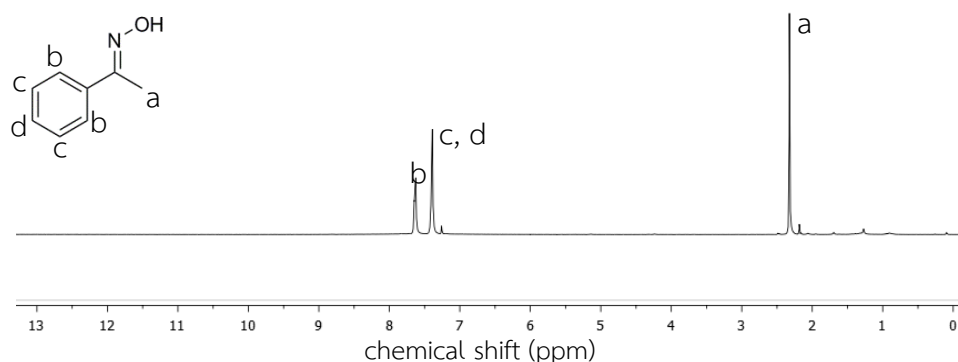
Figure 3.2 ^{1}H-NMR spectrum of acetophenone oxime (**9**) (CDCl$_3$, 400 MHz)

3.1.2 Synthesis and characterization of 2-phenyl pyrrole (10)

For synthesis of 2-phenyl pyrrole (**10**), acetophenone oxime (**9**) was used as a starting material for [3+2] cycloaddition reacting with calcium carbide to give 2-phenyl pyrrole (**10**) in 67% yield as shown in scheme 3.3. [41] ^{1}H-NMR spectrum of product (**10**) was corresponded to the reported literature [41] as seen in figure 3.3. The absence of a methyl peak at 2.32 ppm of oxime (**9**) was observed along with the formation of new broad peak of secondary amine (-NH) in 2-phenyl pyrrole at 8.35 ppm (g). Moreover, the characteristic aromatic peaks of pyrrole were shown at 6.47 (c) and 6.72 ppm (b) confirming the formation of pyrrole ring.
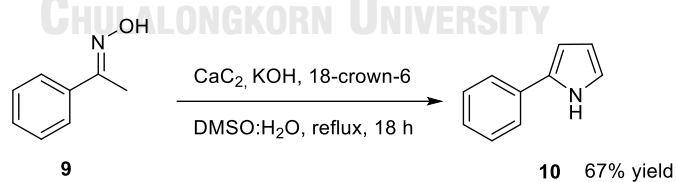
Scheme 3.3 Synthesis of 2-phenylpyrrole (**10**)
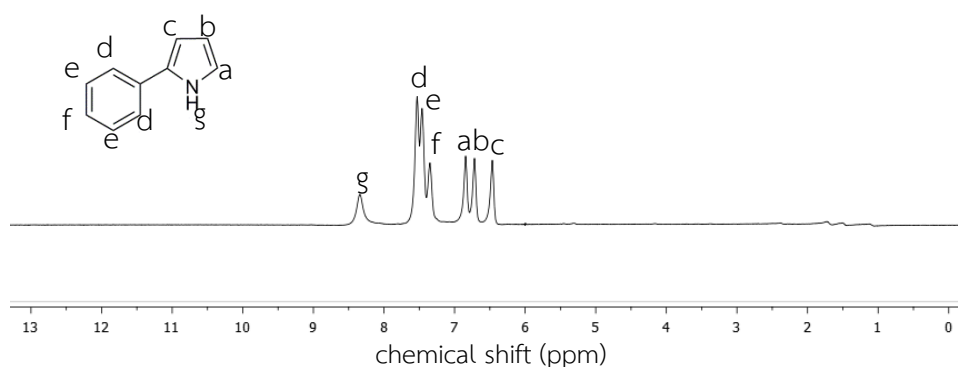
Figure 3.3 ^{1}H-NMR spectrum of 2-phenylpyrrole (**10**) (CDCl$_3$, 400 MHz)

3.1.3 Synthesis and characterization of 4,4-difluoro-8-(4'-iodophenyl)-1,3,5,7-tetramethyl-4-bora-3a,4a-diaza-s-indancene (I-GB)

The synthesis of **I-GB** started with a condensation reaction between 2,4-dimethylpyrrole (**11**) and 4-iodobenzaldehyde to give the dipyrrole intermediated (**12**) as shown in scheme 3.4. Then, the crude product (**12**) was further used without purification and subsequently oxidized with 2,3-dichloro-5,6-dicyano-1,4-benzoquinone (DDQ) to give compound **13**. Finally, treatment of compound **13** with boron trifluoride diethyl etherate provided **I-GB** in 39% yield for three steps.
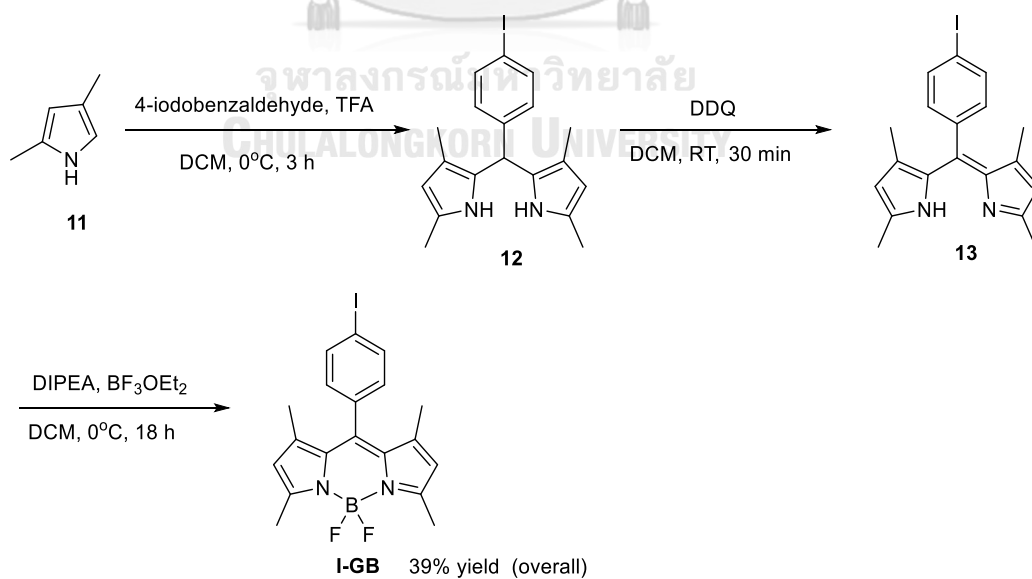
Scheme 3.4 Synthetic procedure of **I-GB**

^{1}H-NMR spectrum of **I-GB** was shown in figure 3.4. All proton signals were corresponded to the previously reported literature [42]. The peaks of 2,4-dimethylpyrrole of the BODIPY core at 5.99 ppm (d) and iodo-benzene peak at 7.04 ppm (a) and 7.84 ppm (b) were observed. Moreover, ^{13}C-NMR spectrum was assigned and matched with **I-GB** as shown in figure 3.5. Also molecular ion peak of **I-GB** at m/z 451.0654 [(M+H)$^+$] was detected by HR-ESI-MS confirming the successful synthesis of **I-GB** (figure A.5).
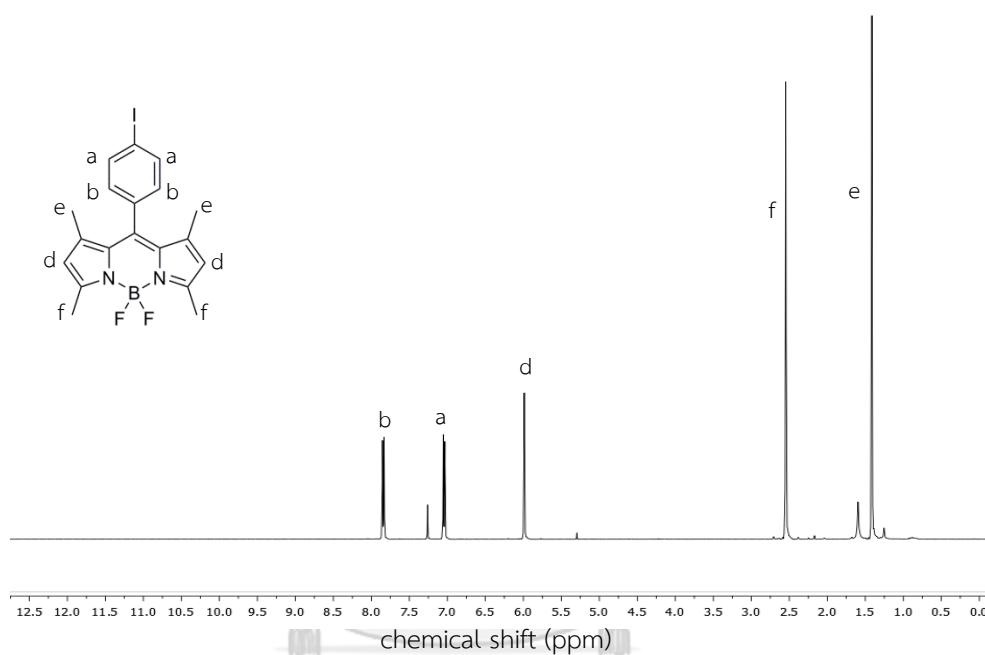
Figure 3.4 ^{1}H-NMR spectrum of **I-GB** (CDCl$_3$, 400 MHz)
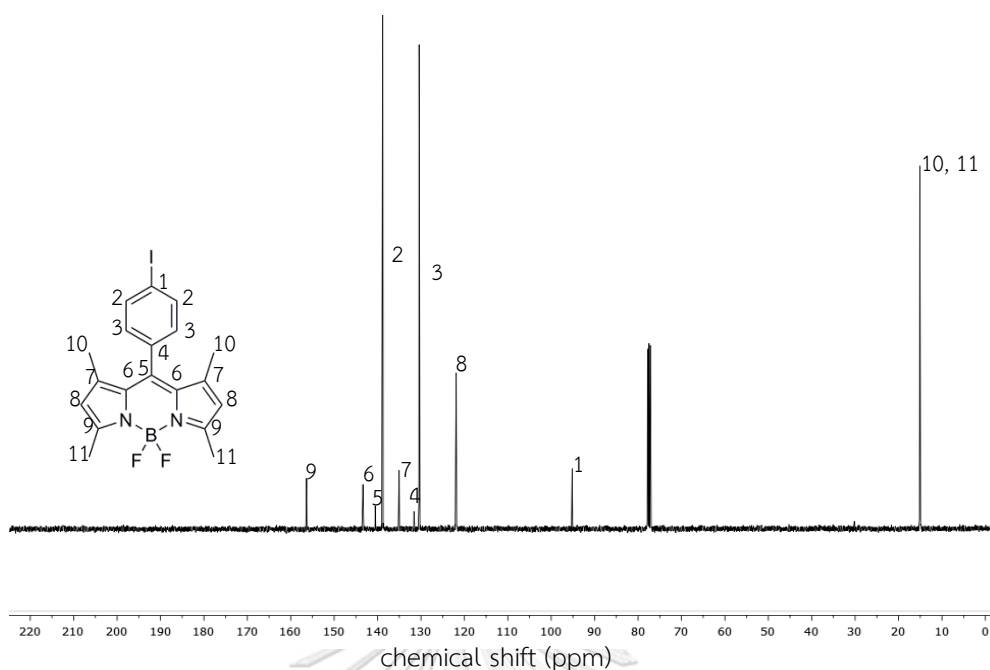
Figure 3.5 ^{13}C-NMR spectrum of **I-GB** (CDCl$_3$, 100 MHz)

3.1.4 Synthesis and characterization of 4,4-difluoro-2,6-diiodo-8-(4'-iodophenyl)-1,3,5,7-tetramethyl-4-bora-3a,4a-diaza-s-indancene (3I-GB)

For **3I-GB**, the beta-iodination reaction of **I-GB** with 2 equivalent of iodine monochloride was accomplished at room temperature and the crude product was purified by column chromatography to give **3I-GB** in 58% yield as shown in scheme 3.5.
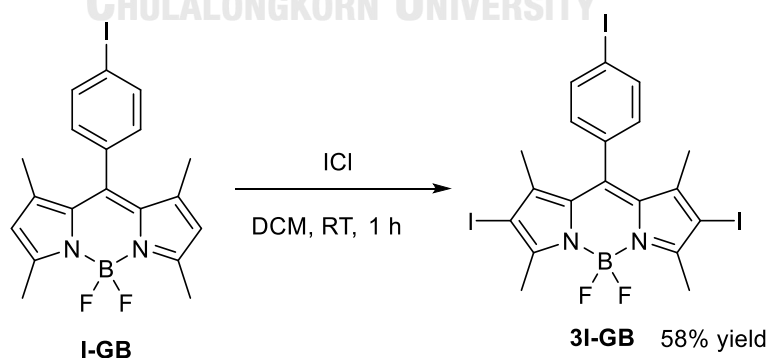
Scheme 3.5 Synthetic procedure of **3I-GB**

The ^{1}H-NMR spectrum of the product was assigned as seen in figure 3.6. [43] The proton signals of 2,4-dimethylpyrrole at BODIPY peripheral position at 5.99 ppm

(d, figure 3.4) disappeared suggesting the completion of iodination reaction. Comparing between C8 of **I-GB** (figure 3.5) and **3I-GB** (figure 3.7), we observed the downfield shifting from 121.3 to 129.3 ppm which was due to the substitution by iodine having higher electronegativity compared to hydrogen. In addition, we detected a molecular ion peak **of 3I-GB** at m/z 724.8409 [(M+Na)$^+$] by HR-ESI-MS as shown in appendix (figure A.8).
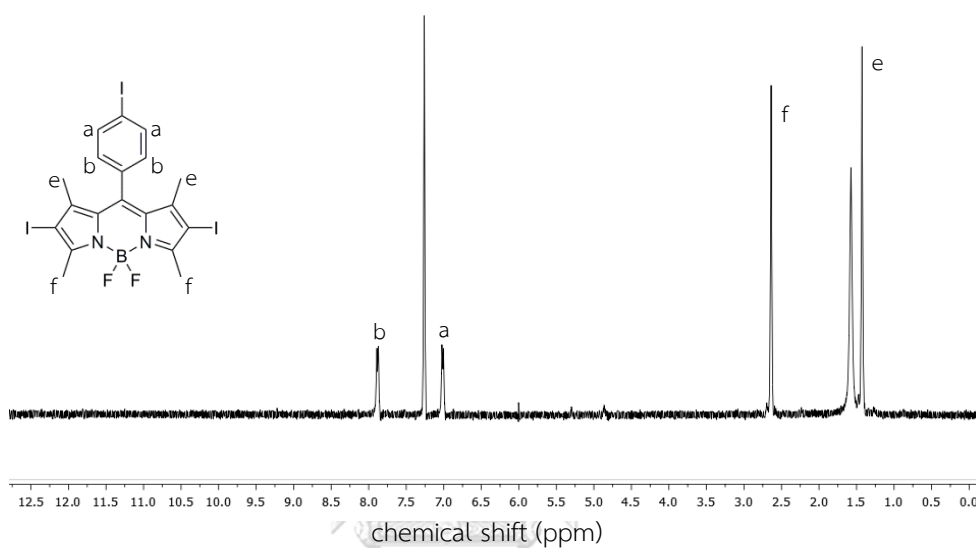
Figure 3.6 ^{1}H-NMR spectrum of **3I-GB** (CDCl$_3$, 400 MHz)
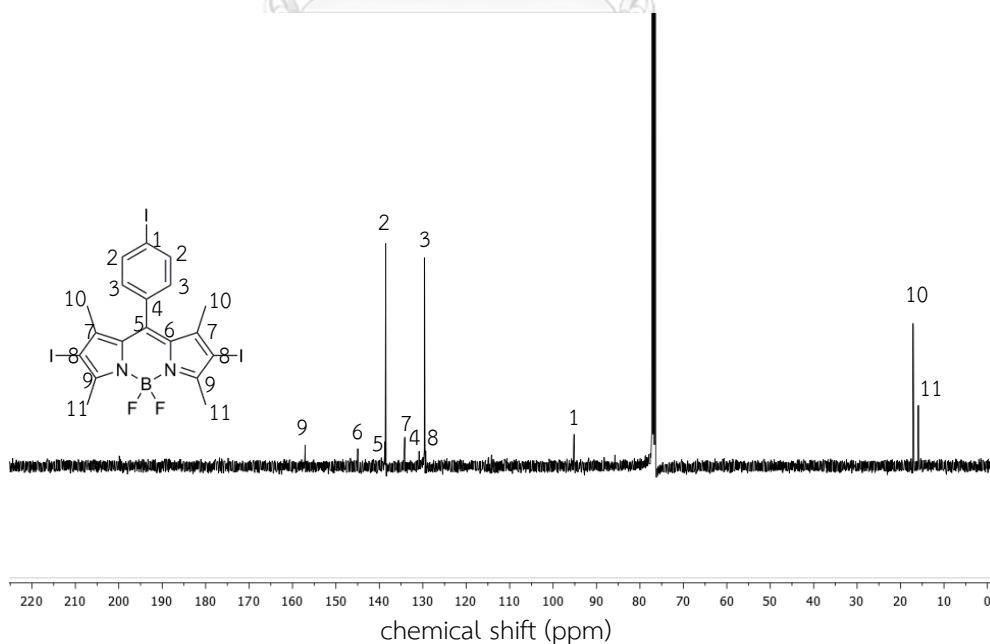
Figure 3.7 ^{13}C-NMR spectrum of **3I-GB** (CDCl$_3$, 100 MHz)

3.1.5 Synthesis and characterization of 4,4-difluoro-8-(4'-iodophenyl)-3,5-diphenyl-4-bora-3a,4a-diaza-s-indancene (I-RB)

Similar to **I-GB,** the synthesis of **I-RB** was initiated with condensation reaction between 2 equivalents of 2-phenylpyrrole (**10**) and 1 equivalent of 4-iodobenzaldehyde, followed by oxidation with 1 equivalent of 2,3-dichloro-5,6-dicyano-1,4-benzoquinone (DDQ) and complexation with 10 equivalent of boron trifluoride diethyl etherate to give **I-RB** in 36% yield for three steps as shown in scheme 3.6.
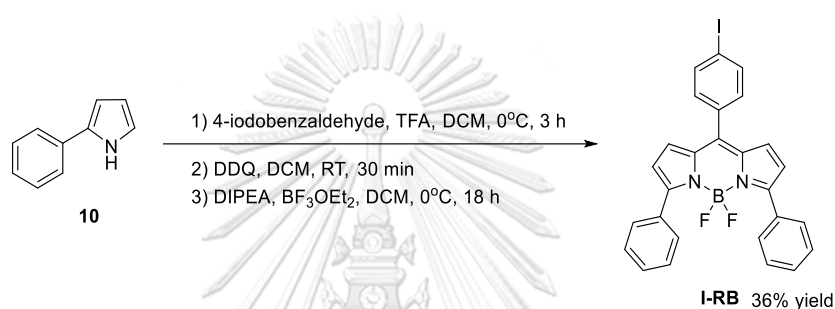
Scheme 3.6 Synthetic procedure of **I-RB**

^{1}H-NMR and ^{13}C-NMR spectra of the **I-RB** were assigned as shown in figure 3.8 and figure 3.9, respectively, which were corresponded to the reported literature [44]. For ^{1}H-NMR spectrum, the peak of pyrrole in the BODIPY core appeared at 6.64 ppm (d) and 6.87 ppm (c), while the proton signals of phenyl substituents were observed at around 7.42 ppm (h and i). Additionally, a molecular ion peak of **I-RB** at m/z 569.0466 [(M+Na)$^+$] was detected by HR-ESI-MS as shown in appendix (figure A.11).
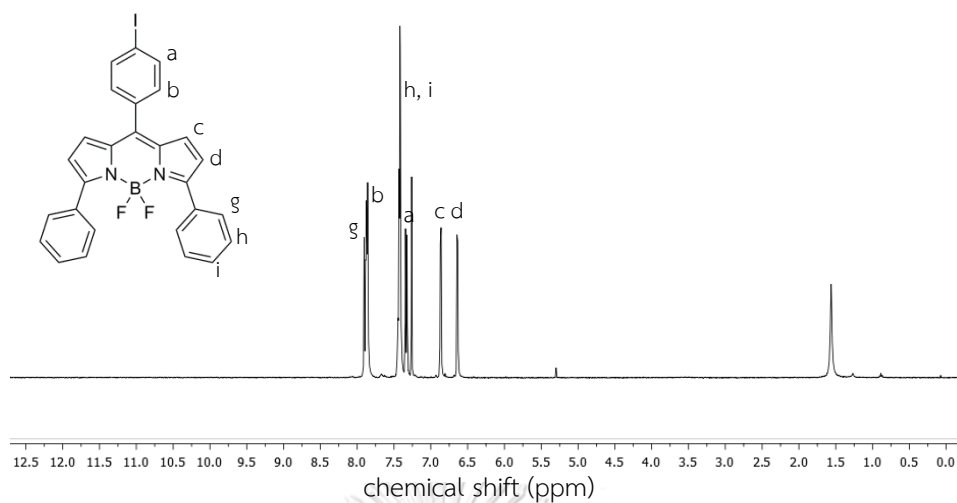
Figure 3.8 ^{1}H-NMR spectrum of **I-RB** (CDCl$_3$, 400 MHz)
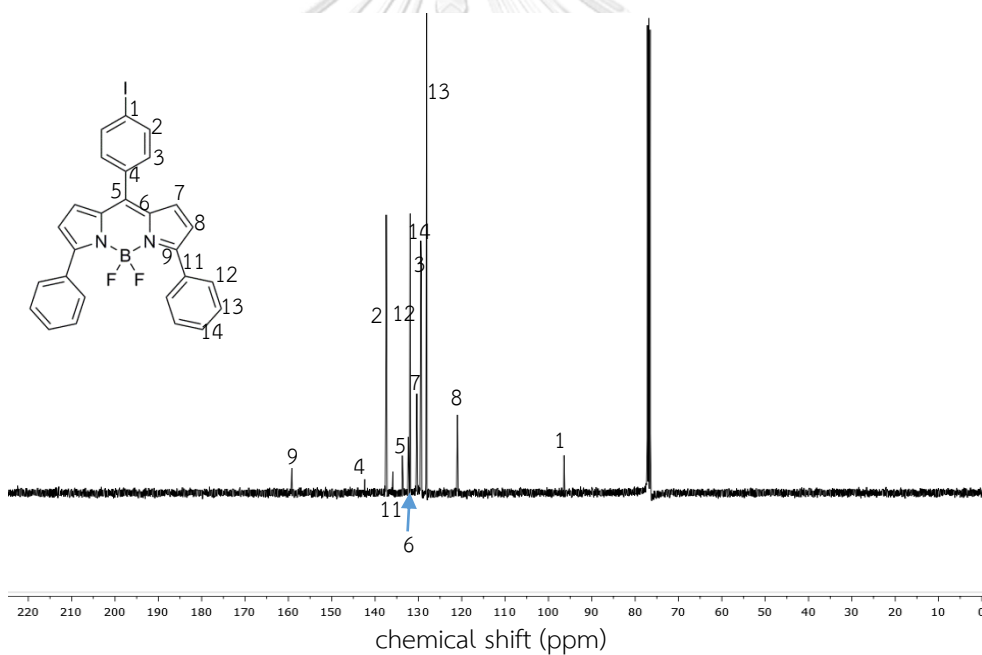
Figure 3.9 ^{13}C-NMR spectrum of **I-RB** (CDCl$_3$, 100 MHz)

3.1.6 Synthesis and characterization of 4,4-difluoro-2,6-diiodo-8-(4'-iodophenyl)-3,5-diphenyl-4-bora-3a,4a-diaza-s-indancene (3I-RB)

Finally, treatment of an excess iodine monochloride with **I-RB** at reflux to ensure the completion of beta-iodination reaction gave **3I-RB** in 80% yield as major

product shown in scheme 3.7. We would like to note that when the reaction was performed at room temperature under identical condition as **3I-GB**'s condition, it gave no reaction and mostly starting material was recovered. These is probably due to the steric hindrance from extra phenyl groups at C3 and C5 of **I-RB**. The product was then fully characterized by spectroscopic techniques.
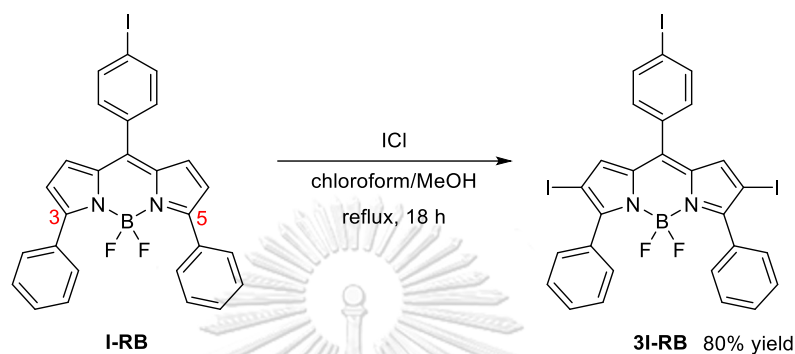
Scheme 3.7 Synthetic procedure of **3I-RB**

The ^{1}H-NMR spectrum and ^{13}C-NMR spectrum of **3I-RB** were obtained as shown in figure 3.10 and figure 3.11. From ^{1}H-NMR spectrum, the disappearance of the peak belonging to pyrrole unit in **3I-RB** at around 6.64 ppm (d) in figure 3.8 suggested that the double iodinations were successful. Moreover, chemical shift of proton at C7 of **3I-RB** (peak c) was slightly downfield when compared with original **I-RB** (6.86 ppm to 7.14 ppm) owing to the high electronegativity of iodine atom. [21] In comparison between ^{13}C-NMR of **I-RB** and **3I-RB** (figure 3.9 and figure 3.11), the downfield shifting of C8 from 121.0 to 123.2 ppm was also observed. The molecular weight of **3I-RB** was also confirmed by the detection of molecular ion peak at 820.8415 m/z [(M+Na)$^+$] by HR-ESI-MS as seen in appendix (figure A.14).
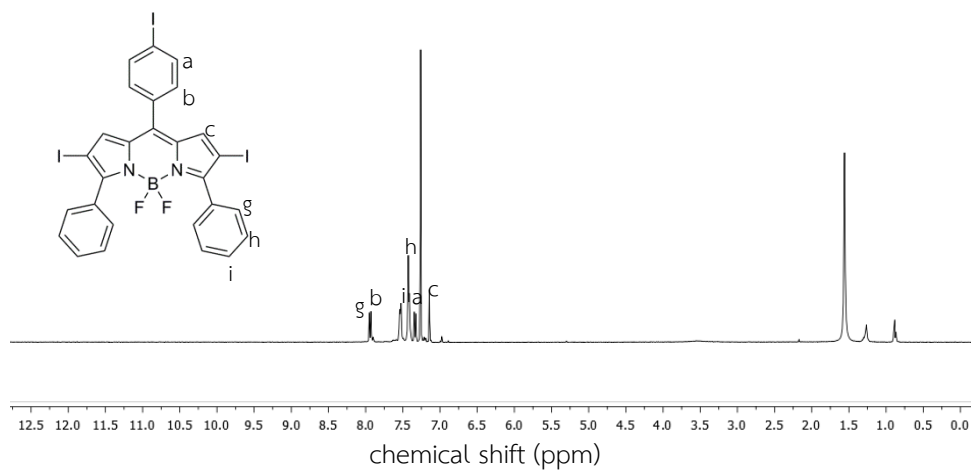
Figure 3.10 ^{1}H-NMR spectrum of **3I-RB** (CDCl$_3$, 400 MHz)
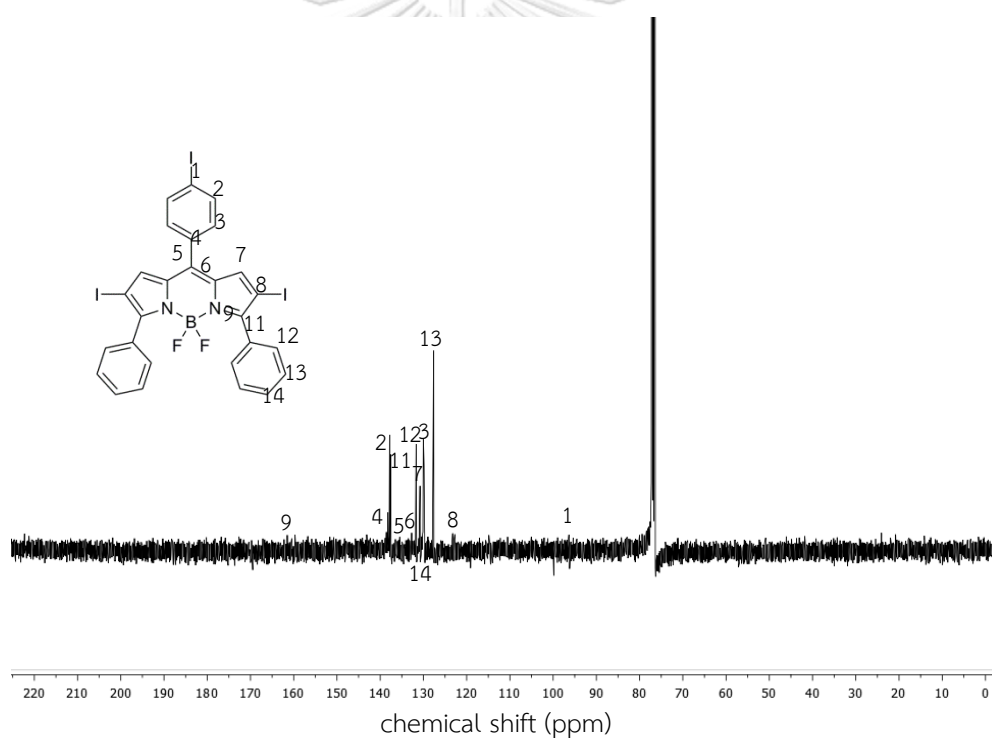
Figure 3.11 ^{13}C-NMR spectrum of **3I-RB** (CDCl$_3$, 100 MHz)

3.2 Solubility of photocatalysts

After the all BODIPY catalysts were prepared, we tested the solubility of all BODIPY derivatives in common organic solvents which are isopropanol (IPA) and tetrahydrofuran (THF, table 3.1). According to the results, **I-GB**, **I-RB**, and rose bengal

were completely dissolved in isopropanol and color of catalyst solutions showed as orange, purple, and deep pink, respectively, as seen in table 3.1. While **3I-RB** and **3I-GB** were partially dissolved in isopropanol and provided light pink and light violet solutions. Then, switching solvent from polar protic solvent IPA to polar aprotic solvent THF, it showed better solubility comparing with IPA. All BODIPY catalysts, **I-GB**, **I-RB**, **3I-GB**, **3I-RB**, and rose bengal completely dissolved in THF and showed more intense color than IPA. Based on the above survey, we selected THF as the solvent for studying photophysical properties and catalytic activity of our catalysts.

Table 3.1 The solubility of photocatalysts

	I-GB	3I-GB	I-RB	3I-RB	Rose Bengal
IPA					
THF					

*substrates concentration: 2.5 mg/mL

3.3 Photophysical properties of photocatalysts

With all four catalysts in hand, we began to study the photophysical properties of synthesized catalysts. The absorptions of synthesized BODIPYs were evaluated in THF as shown in figure 3.12. All iodo-BODIPY catalysts showed broad absorption band in visible region. For example, **I-GB** absorbed at the wavelength between 400-520 nm and center at 502 nm which appeared as orange color. In case of **I-RB**, the absorption maximum shifted to 592 nm and displayed purple color. This is probably due to the increase of conjugation system [45] from the extra phenyl group at C3 and C5 positions of BODIPY. Similarly, the maximum absorption wavelength of **3I-GB** increased to 535

nm displaying pink color. This result attributes to the high conjugation of iodine at C2 and C6 positions of **I-GB**. [23] For **3I-RB**, the additional of phenyl groups at C3 and C5 and iodine atoms at C2 and C6 positions caused the red shift showing the maximum absorption at 573 nm along with violet color. This compound not only showed the longest maximum absorption among all prepared catalysts but its absorption spectrum was broadest which covered most of visible region between 450-650 nm. This property should make **3I-RB** suitable as a photocatalyst under visible light.
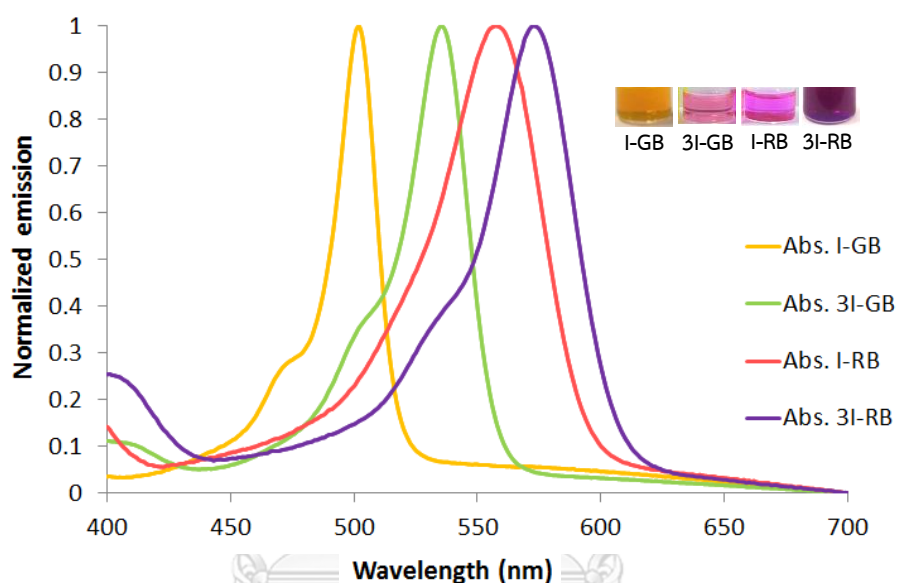
Figure 3.12 Normalized absorption spectra of iodo-BODIPY derivatives in THF. Insets show colors of catalyst solutions under visible light.

In a similar manner, the emissions of BODIPYs were measured in THF and results were shown in figure 3.13. **I-GB** and **I-RB** displayed maximum emissions at 513 and 592 nm and appeared as green and yellowish orange under black light, respectively. Again, the long maximum emission in **I-RB** responded from extra phenyl group at C3 and C5 positions. In case of **3I-GB** and **3I-RB**, emission maxima shifted to longer wavelength at 554 and 604 nm when compared to parent compounds, **I-GB** and **I-RB**. Similarly, this is probably due to the heavy atom effect from increase of iodine atom at C2 and C6 positions. Under the black light, **3I-GB** and **3I-RB** displayed as yellow and red color.
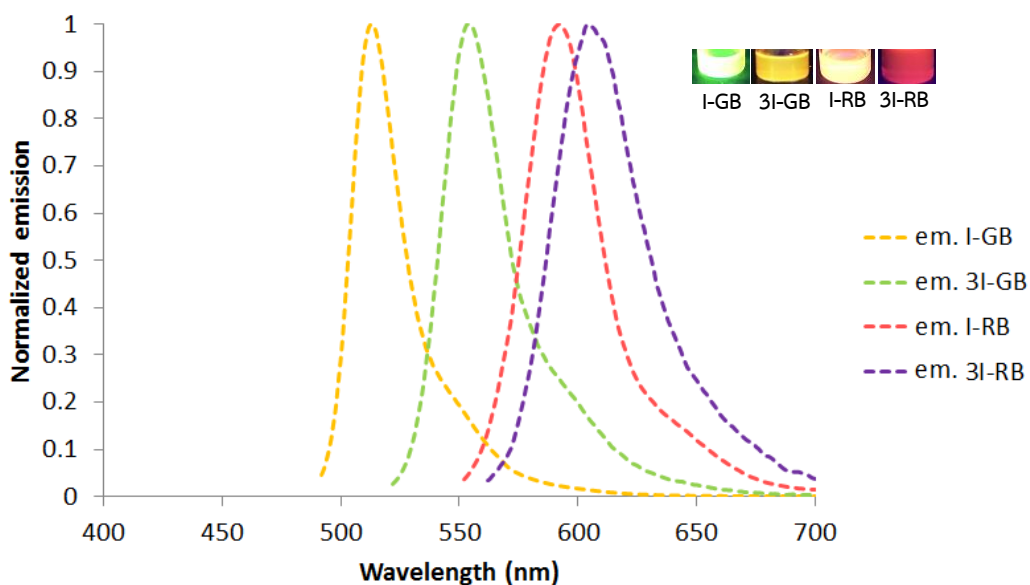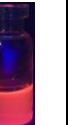
Figure 3.13 Normalized emission spectra of iodo-BODIPY derivatives in THF. Insets show colors of catalyst solutions under black light.

The summarized photophysical properties of all BODIPYs were shown in table 3.2. The order of molar absorptivities of BODIPY dyes from high to low was **I-GB**, **3I-GB**, **I-RB** and **3I-RB**, respectively. The decrease of molar absorptivity could be explained by the higher conjugation of the additional phenyl group when compared between GB and RB series resulting from energy losing in vibrational relaxation process. It should be noted that when the number of iodine atoms increase, the molar absorptivity will be lower due to the more complicated molecular orbital energy level in the presence of f-block atom. These results were also observed in a fluorescence quantum yield in a similar pattern. For all prepared BODIPYs, relatively lower fluorescent quantum yields were obtained between 0.053-0.377. Especially, **3I-GB** and **3I-RB** showed the lowest fluorescent quantum yields among others around 0.053. In the presence of additional iodine atoms at position 2 and 6, the intersystem crossing will more likely occurred due to the interaction between f-block atom and excited electron. This effect will enhancing the energy transfer processes between chromophore and the ground state oxygen to generate more singlet oxygen molecules. In case of iodine atom at position 8, the heavy atom effect seems not occurred because the out-of-plane resonance

system between BODIPY core and *para*-phenyl substituent. Such species would act as the oxidizing agent in photooxidation which make our BODIPYs as photocatalysts under visible light.

Table 3.2 Photophysical properties of iodo-BODIPY derivatives

BODIPYs		I-GB[b]	3I-GB[b]	I-RB[b]	3I-RB[b]
Color of solutions	Ambient light				
	Fluorescent black light				
λ_{max}^{abs} (nm)		502	535	557	573
λ_{max}^{em} (nm)		513	554	592	604
ε ($M^{-1}cm^{-1}$)		91127	84461	69300	65490
Φ^a		0.377	0.054	0.104	0.053

[a]in isopropanol, [b] in THF, $\varepsilon_{rose\ bengal}$ 102616 $M^{-1}cm^{-1}$

3.4 Determination of singlet oxygen on photooxidation

From mechanism of photooxidation reaction using BODIPY as photocatalyst (scheme 1.16), [38] the singlet oxygen was produced during the irradiation of BODIPY. Therefore, it is important to us to determine the amount of singlet oxygen in each BODIPY catalyst. This information would allow us to grade the catalytic performance of BODIPYs and can compare with the well-known dye, rose bengal. To do so, the generated singlet oxygen quantity could be detected by trapping process using anthracene-9,10-dipropionic acid disodium salt (ADPA) in 10% water in THF as shown in scheme 3.8. [46] When a singlet oxygen is generated, ADPA will undergo cycloaddition with the singlet oxygen and form endoperoxide derivative (**14**). We can quantify the production of singlet oxygen by monitoring the loss of ADPA using UV-vis spectroscopy. The absorption maximum of ADPA at around 381 nm will decrease upon reacting with generated singlet oxygens. In our experiment, the UV-Vis spectrum of a

mixture containing ADPA and BODIPY catalysts as well as rose bengal will be recorded every 10 seconds under irradiation with various light sources. The collected absorbance values will be plotted as normalized absorption intensity *versus* reaction time for all catalysts. These will allow us to compare the ability to generate singlet oxygens among all catalysts.
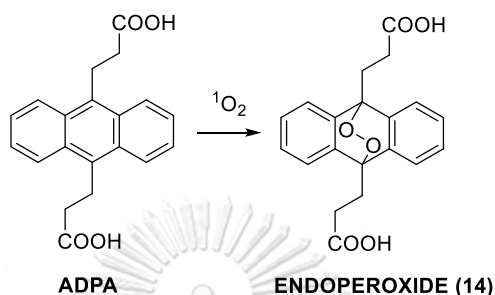
Scheme 3.8 Trapping mechanism of singlet oxygen by ADPA

The solution mixtures were irradiated under four light sources, white LED, red LED, blue LED, and green LED. When the five catalysts including rose bengal were irradiated under white LED or red LED or blue LED in the presence of ADPA as a trapping agent, the results showed that the absorbance of ADPA at 381 nm were not significantly decreased over time as seen in figure 3.14a-c. In case of **I-GB** and **I-RB**, there were also no change in absorbance during the irradiation under all light sources at the same condition (figure 3.14a-d). It indicates that no singlet oxygen was generated under those conditions. Therefore, we conclude that the introduction of iodine atom at phenyl group substituted at C8 on BODIPY do not enhance the release of singlet oxygen which is in agreement with relatively high quantum yield of **I-GB** and **I-RB** catalysts. On the contrary, when we used rose Bengal, **3I-GB**, and **3I-RB** as catalysts, the absorbance of ADPA decreased slightly over the light irradiation indicating the low generation of singlet oxygen as seen in figure 3.14a-c. These results might be caused by the mismatching between absorption maxima of catalysts and emissions of the light sources (white LED, blue LED, and red LED) as seen in figure 3.14e-g. [47] For white LED, the emission bands were between 440-550 and 610-660 nm which was partially match absorption wavelength of **3I-GB**, **3I-RB**, and rose bengal as seen in figure 3.14e. While emission spectrum of red LED was around 610-660 nm which was not overlap

with the absorption of all catalysts. Similarly, the mismatch between blue LED emission and absorption of **3I-GB**, **3I-RB**, and rose bengal were responded for low singlet oxygen generation as seen in figure 3.14g. When **3I-GB**, rose bengal, and **3I-RB** irradiated under green LED, the normalized absorption of ADPA significantly reduced to 0.3, 0.4, and 0.6, respectively, over 200 seconds (figure 3.14d). These results indicated that those catalysts give highest amount of singlet oxygens compared to **I-GB** and **I-RB** catalysts. The order of ability to generate singlet oxygens among three catalysts were **3I-GB** > rose bengal > **3I-RB**. These again can be explained by the strong overlap of emission of green LED and absorption of **3I-GB** and rose bengal, while only partial overlap was observed in case of **3I-RB** (figure 3.14h). Moreover, the introduction of iodine atoms that directly attached to the core structure in **3I-GB**, **3I-RB** and rose bengal can affect the singlet oxygen generation efficiency of the molecules comparing with the **I-GB** and **I-RB** that has out-of-plane iodine atom in C8 position.
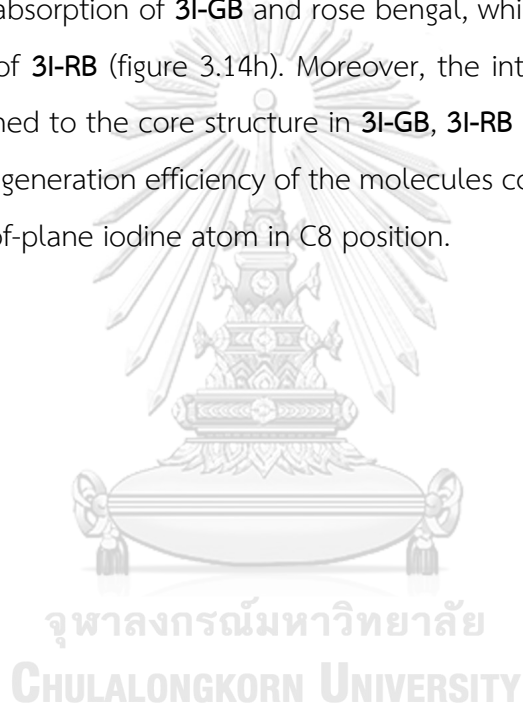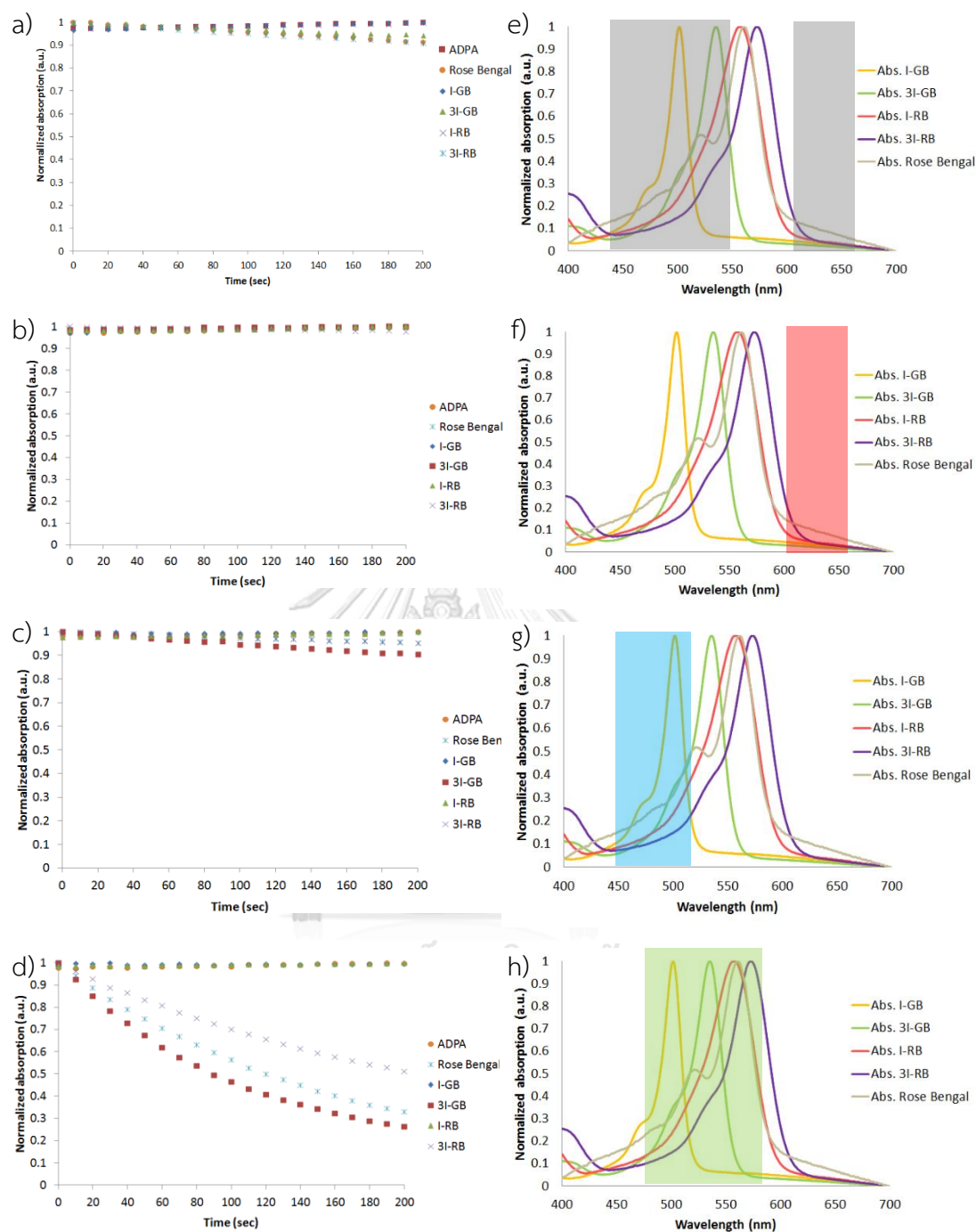
Figure 3.14 The change of absorbance of ADPA at 381 nm in the presence of photocatalyst in H$_2$O:THF (1:9) under a) white LED b) red LED c) blue LED d) green LED overtime and the overlap between absorption of photocatalysts and emission of e) white LED (white band) f) red LED (red band) g) blue LED (blue band) h) green LED (green band)

3.5 Optimization condition for photooxidation of organosulfur compounds

After we completed the synthesis of four iodo-BODIPY derivatives, the catalytic activity of all catalysts was tested in two different photooxidations as seen in scheme 3.9. The first reaction is the photooxidation of thiols into disulfides, while the second reaction is photooxidation of sulfide substrates into sulfoxide products. The optimized parameters are light source, amount of catalysts and reaction times. We will try various light sources such as white LED, red LED, blue LED and green LED and set the reaction in 1000 mL beaker wrapped with LED belts (SMD 5050 LED, 12 V) equipped with fan in order to maintain the reaction temperature at 36 °C as seen in figure 3.15. Then, the reaction will be evaluated using NMR spectroscopy and reported as %NMR yield as described in chapter 2 (figure 2.2 and figure 2.3).
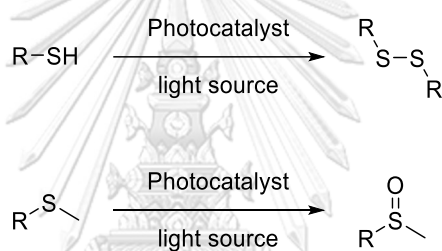
Scheme 3.9 photooxidation of a) thiol into disulfide and b) sulfide substrate into sulfoxide product

Figure 3.15 the four light sources in the reaction

3.5.1 The photooxidation of thiol into disulfide

Based on previous work from our group [34], we selected 4-chlorothiophenol as a model substrate for study catalytic activities of all prepared BODIPY dyes. This is due to the convenient to differentiate the pattern of proton NMR in aromatic ring between 4-chlorothiophenol (**15**) starting material and the corresponding disulfide product (**16**) as shown in figure 2.2.

3.5.1.1 Light source screening for the photooxidation of 4-chlorothiophenol (15)

To evaluate the effect of light sources for photooxidation, 4-chlorothiophenol (**15**) were dissolved in THF in the presence of 1 mol% of photocatalysts including rose bengal, **I-GB**, **I-RB**, **3I-RB**, and **3I-GB** and irradiated with four types of the light sources which are white LED, blue LED, red LED, and green LED. The percent NMR yields were summarized in figure 3.16. In the absence of catalysts, we detected the slight formation of disulfide **16** around 5-7% yield under irradiation with various light sources for 24 hours. When **I-GB** and **I-RB** were used as photocatalysts, poor yields of compound **16** (4-21%) were observed in every LED sources indicating that the photocatalysts are not involve in reactions as the yields are similar to the reaction without the use of catalysts. These results are consistent to the singlet oxygen generation efficiency described in topic 3.4 where **I-GB** and **I-RB** show relatively low efficiency in singlet oxygen generation. In case of rose bengal as photocatalyst, the reaction gave disulfides (**16**) more than 80% yield under white LED, while irradiation under blue LED, red LED, and green LED, 50% yield of compound **16** was obtained within 24 hours. For **3I-RB** and **3I-GB**, the results showed that green LED was the best light source giving product (**16**) in 100% NMR yield at 24 hours. In case of rose bengal catalyst, we would like to note that the reaction proceeded fastest in white LED even though the singlet oxygen generation was more efficiency in green LED (figure 3.14d). We therefore suspected that the singlet oxygen may not act as main oxidizing agent in this reaction. On the other hand, **3I-GB** and **3I-RB** performed well in green LED which corresponded to the singlet oxygen generation results (figure 3.14). So, the reaction might proceed through singlet oxygen, in case of **3I-GB** and **3I-RB**. The plausible mechanism of this reaction will be explained in the next section. From above results, we chose green LED as the light source for further optimization study.
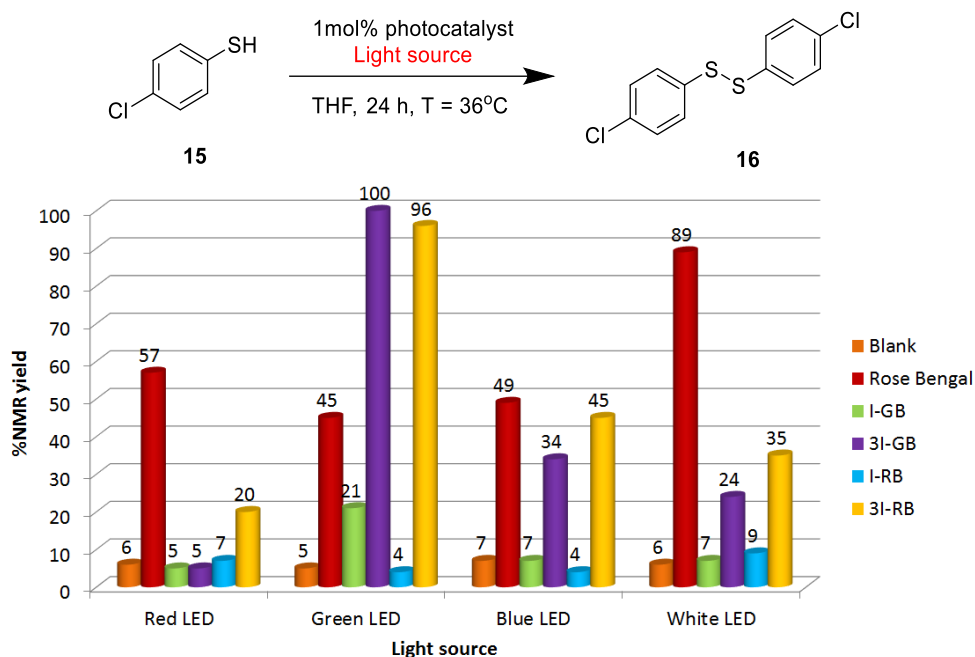
Figure 3.16 Effect of light source on the photooxidation of 4-chlorothiophenol (**15**). Reaction condition: 4-chlorothiophenol (0.3 mmol), THF (3.5 mL), photocatalyst (1 mol%), rt, 24 h.

3.5.1.2 Effect of photocatalyst loading on the oxidation of 4-chlorothiophenol (15)

We increased the amount of photocatalyst from 1 to 5 mol% in order to drive the reaction completely and the result was displayed in figure 3.17. According to NMR analysis, the result showed that **3I-GB** and **3I-RB** gave %NMR yield to nearly quantitative while for other catalysts, **I-GB**, **I-RB**, and rose bengal, yields were increased up to only 50%. Therefore, 5 mol% photocatalyst will be used in the reaction under green LED for further study to ensure the complete conversion.
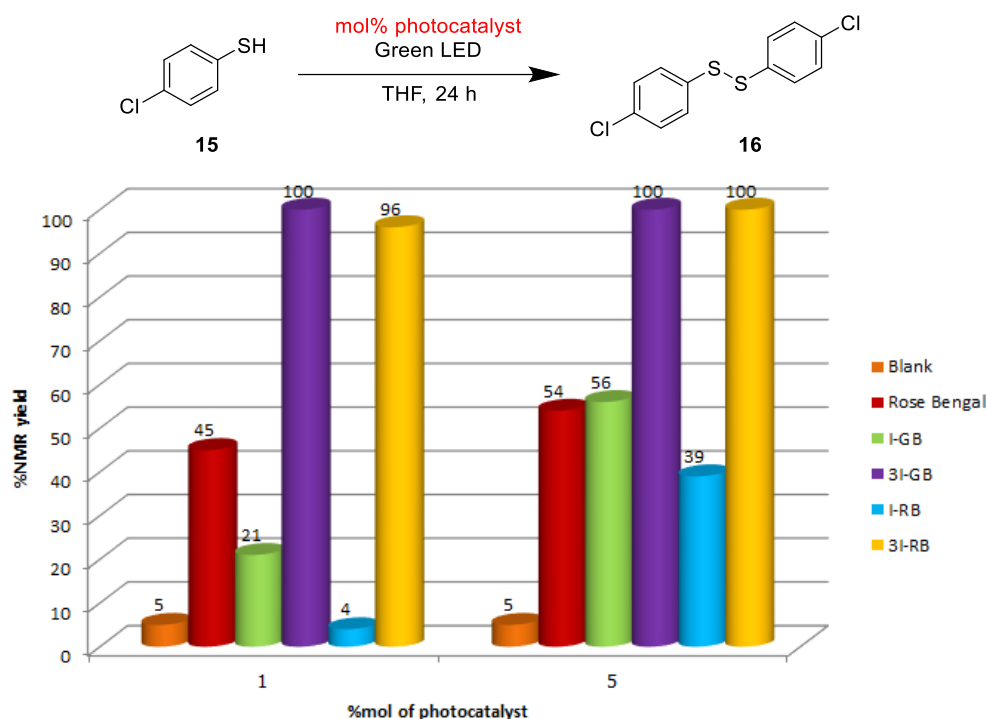
Figure 3.17 Effect of photocatalyst loading on the photooxidation of 4-chlorothiophenol (**15**). Reaction condition: 4-chlorothiophenol (0.3 mmol), THF (3.5 mL), green LED, rt, 24 h.

3.5.1.3 Kinetic study of photooxidation of 4-chlorothiophenol (15)

Then, we examined the reaction rate of photooxidation of 4-chlorothiophenol (**15**) using prepared BODIPY catalysts and rose bengal as a comparison (figure 3.18). In the absence of catalyst, only small amount of disulfide product **16** (4-5% yield) were observed. In case of BODIPY catalysts, when we perform the reaction for 6 hours under green LED, **3I-RB** and **3I-GB** gave quantitative yields of product **16** while **I-GB**, **I-RB**, and rose bengal provide only 30-50% yields of disulfide **16**. Even though the reactions were irradiated for 24 hours, the yield of product **16** slightly increased in case of **I-GB**, **I-RB**, and rose bengal. These results confirmed that under green LED, **3I-GB** and **3I-RB** are proven to be the best catalysts among the others for oxidation of 4-chlorothiophenol (**15**).
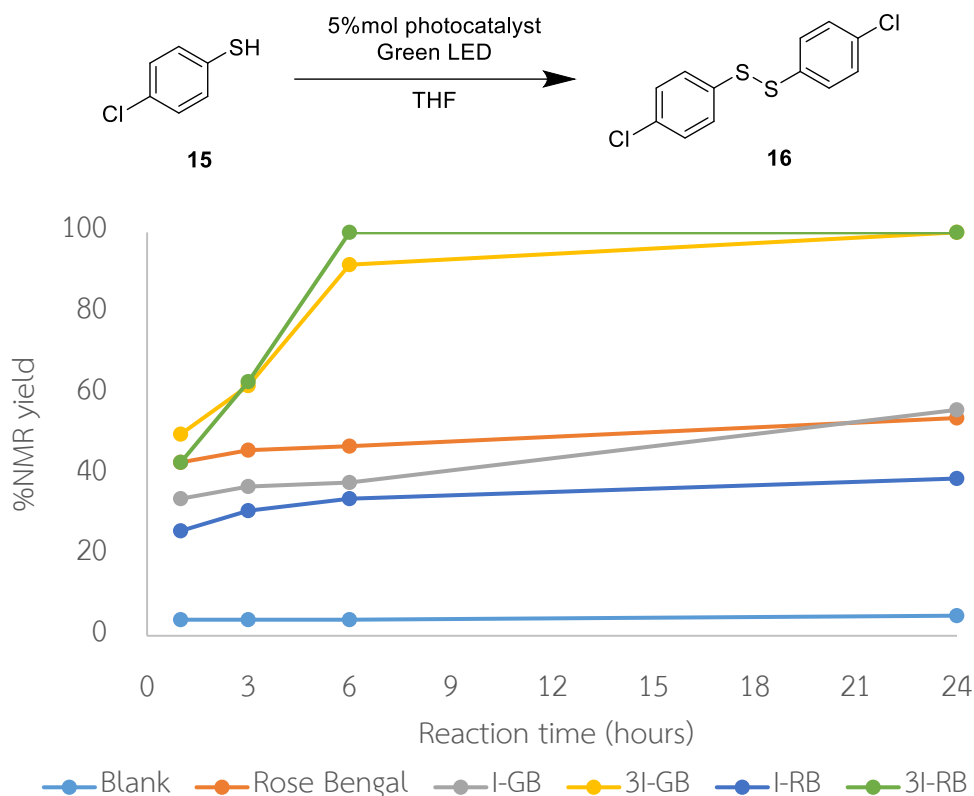
Figure 3.18 Time effect on NMR yield for photooxidation of 4-chlorothiophenol (**15**) under green LED. Reaction condition: 4-chlorothiophenol (0.3 mmol), THF (3.5 mL), photocatalyst (5 mol%), green LED, rt.
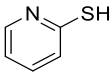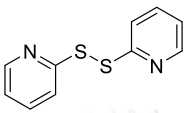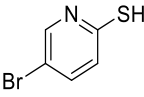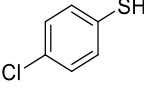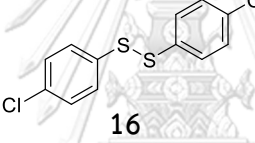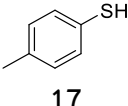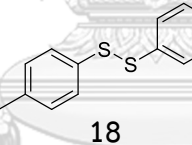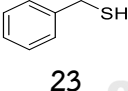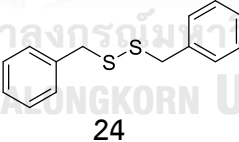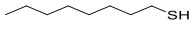
3.5.1.4 Substrate scope of photooxidation of thiol

Next, we investigated the scope of substrates by testing the reaction with aromatic thiol, heterocyclic thiol, and aliphatic thiol as starting materials as shown in Table 3.3. 2-Mercaptopyridine (**19**) and 4-bromo-2-mercaptopyridine (**21**) were examined as representative heterocyclic thiols. The reactions were carried in the presence of **3I-GB** and **3I-RB** as catalysts. We monitored reactions using TLC and found that starting material were completely consumed within 3.5 hours providing disulfide products (**20**, **22**) in 79-83% (table 3.3, entry 1) and 83-85% (table 3.3, entry 2) yields, respectively. For aromatic thiols, 4-chlorothiophenol (**15**) and 4-methylthiophenol (**17**), they required at least 6 hours to complete the reactions. In **3I-GB**, products **16** and **18** were isolated in 90% (table 3.3, entry 3) and 71% (table 3.3, entry 4) yields, respectively. **3I-RB** also provided disulfide **16** and **18** in excellent yields (table 3.3,

entry 3-4). In case of benzylic thiol, benzyl mercaptan (**23**), both catalysts gave disulfide (**24**) in quantitative yields (table 3.3, entry 5) when the reaction were irradiated for 12 hours. On the other hand, for aliphatic thiol oxidation, octane thiol (**25**), it gave no reaction (table 3.3, entry 6) even though the reaction were conducted for 24 hours and most of remaining starting material was observed in NMR of crude products. We would like to note that, the reactivities of thiol substrates follow the sequence: heterocyclic > aromatic > benzylic > aliphatic thiols. We hypothesize that the reaction may involve the formation of thiol radical followed by homocoupling reaction. According to above hypothesis, these trend are caused by higher stability of thiol radical in heterocyclic and aromatic thiols comparing to benzylic and aliphatic substrate due to their resonance effect and N heteroatom substituent. [34]

$$R\text{--}SH \xrightarrow[\text{THF}]{\substack{\text{Green LED,} \\ \text{5\%mol Photocatalyst}}} R^{\diagdown}{}_S{}^{\diagup}{}^S{}^{\diagdown}R$$
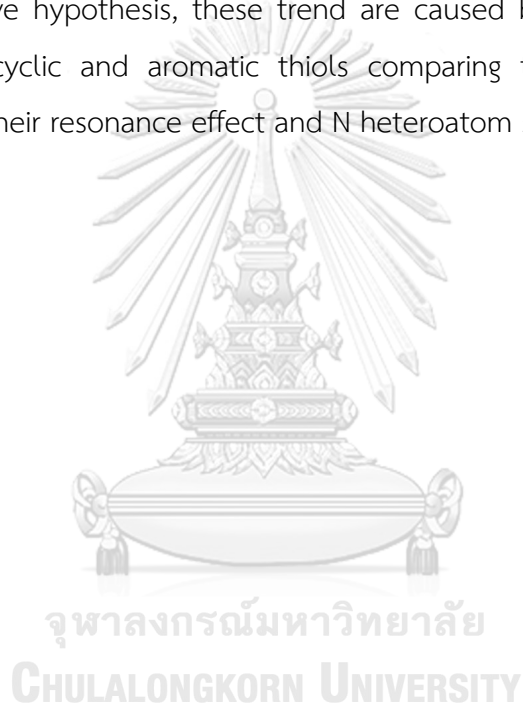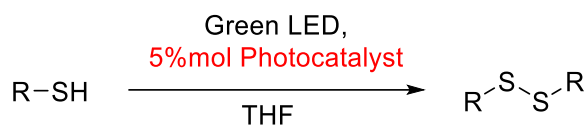
Table 3.3 Photooxidation of thiols under green LED

Entry	Substrate	Product	Reaction time (hours)	%isolated yields	
				3I-GB	3I-RB
1	**19**	**20**	3.5	79	83
2	**21**	**22**	3.5	83[a]	85[a]
3	**15**	**16**	6	90	68
4	**17**	**18**	6	71	100
5	**23**	**24**	12	100	100
6	**25**	**26**	24	N.R.	N.R.

[a] %NMR yield, N.R. = no reaction

3.5.1.5 Proposed mechanisms for photooxidation of thiols

According to the results from singlet oxygen generation efficiency (topic 3.4) and optimization study (topic 3.5), the trend of catalytic activities of BODIPY was corresponded with the singlet oxygen generation which we hypothesized that singlet oxygen is the key oxidizing agent in this reaction. Therefore, we proposed the main

mechanism for photooxidation of thiols into disulfide product using BODIPY derivatives as catalysts (scheme 3.10). [34] The ground state BODIPY is first excited by appropriate light source to be singlet excited state BODIPY (^{1}BODIPY*) and converts to triplet excited state (^{3}BODIPY*) through intersystem crossing (ISC) process. The energy can be transferred from triplet excited state BODIPY to triplet state oxygen molecule ($^3O_2$) and create singlet excited state oxygen molecules ($^1O_2$) in return. Subsequently, thiol compounds (RSH) are oxidized by such singlet excited state oxygen molecules to generate thiol radical (RS$^•$) along with hydroperoxyl radical (HO$_2^•$). The hydroperoxyl radical reacts with thiol substrate into thiol radical and provides hydrogen peroxide (H_2O_2) as byproduct. Then, homocoupling reaction between thiols give desired disulfide product (RSSR).
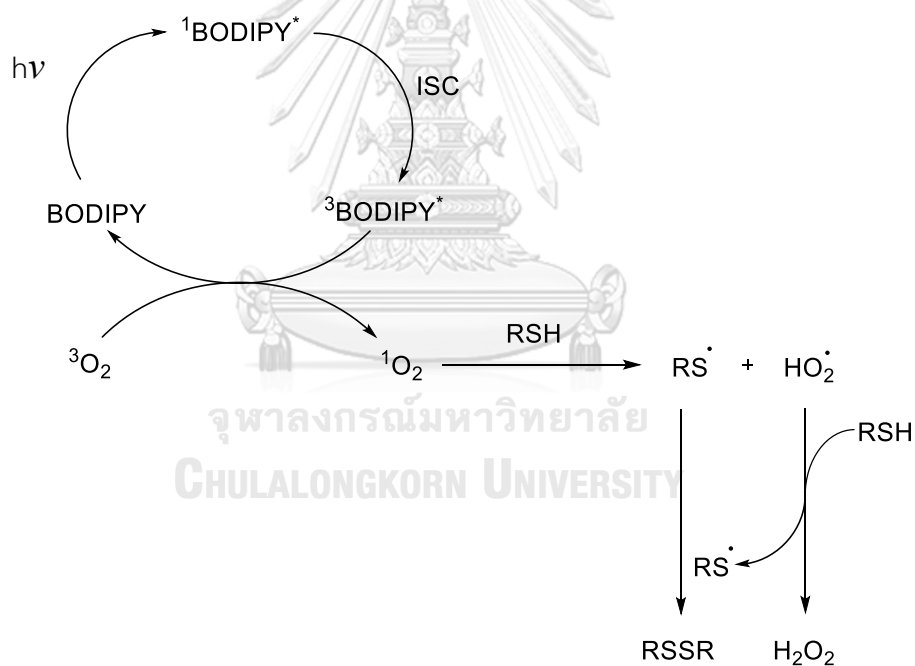
Scheme 3.10 The plausible mechanism for photocatalytic oxidation of thiols catalyzed by BODIPY

Unlike BODIPY catalysts, rose bengal might proceed via different mechanism. Based on investigation in singlet oxygen generation (topic 3.3) and optimization study (topic 3.4), the rose bengal favor a green LED for singlet oxygen generation as seen in figure 3.14d while a white LED proven to be the suitable light source for the oxidation

of 4-chlorothiophenol (**15**) as shown in figure 3.16. Therefore, the singlet oxygen generation might not be the main mechanism and another competitive mechanism involving electron transfer process might occur as proposed in scheme 3.11. [33, 48] Initially, excited state rose bengal (Rose Bengal[*]) is generated by irradiation of rose bengal with proper light source, and then react with thiol compounds to give thiol radical species and rose bengal radical anion (Rose Bengal[•−]) in return. Then, thiol radicals undergo homocoupling reaction to give disulfide product. Then, rose bengal radical anion transfers the electron to oxygen molecule to generate oxygen radical anion ($O_2^{•−}$) and return to ground state rose bengal. Such process also provide thiol radical leading to the formation of disulfide product.
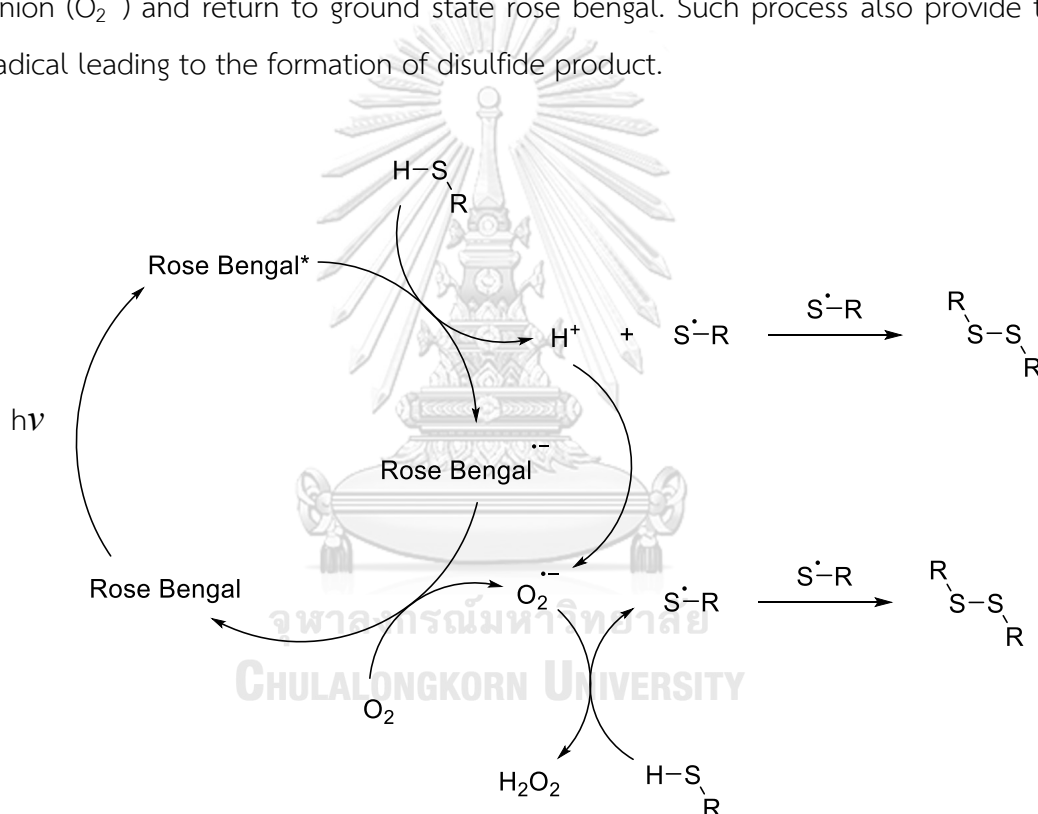
Scheme 3.11 The plausible mechanism for photocatalytic oxidation of thiols catalyzed by rose bengal

3.5.2 The photooxidation of sulfide substrate into sulfoxide product

Next, we would like to extend the scope of photooxidation into other organosulfur. In this section, we will use our prepared catalysts to oxidize methyl thioether into the corresponding sulfoxide which is considered as significant

intermediates for various pharmaceutical compound. [49] In this study, thioanisole (**27**) was chosen as a model substrate to study catalytic activity of our prepared BODIPYs in photooxidation (scheme 3.12). This is due to the differentiation of methyl thioether between starting (**27**) and product (**28**) in ^{1}H-NMR. The chemical shift of methyl thioether in **27** appear around 2.4 ppm as a singlet peak while, in case of **28,** methyl peak show at 2.8 ppm (for more detail please see figure 2.3). These will allow us to determine the yield of our reactions.
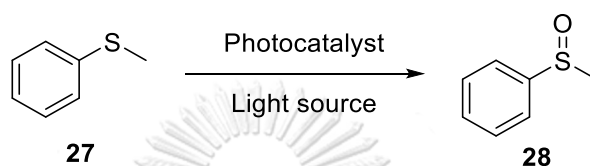
Scheme 3.12 Photooxidation of thioanisole into sulfoxide product

3.5.2.1 Screening light source on the photooxidation of thioanisole (27)

To find the appropriate light source for photooxidation of thioanisole (**27**) in THF, reactions were irradiated by four different light sources which are white LED, blue LED, red LED, and green LED in the presence of 1 mol% photocatalysts and the reactions were monitored using NMR as seen in figure 3.19. From the results, when **I-GB** and **I-RB** were used as photocatalysts, the reactions displayed low yields (0-2%) under various light sources. These results indicated that those catalysts are not involved in the reactions as the reaction yields are similar to that of the control reaction. For **3I-RB**, moderate yield (32%yield) of sulfoxide (**28**) was observed under green LED, while the other light sources showed lower efficiency (3-14%yield). Similarly, for **3I-GB**, the reaction that irradiated under green LED gave the highest yield (71%yield), while the reaction irradiated under white LED, blue LED, and red LED obtained significant lower yields (2-27%yield). These results might be caused by the matching of the absorption wavelength of photocatalysts and range of emission wavelength of light source as seen in figure 3.14e-h. In case of rose bengal, the reactions provided 50% and 59% NMR yields of sulfoxide (**28**) when irradiated under blue and white LED, respectively, while under red and green LED, reaction provided lower yields of desired product. As expected, the high efficiency of rose bengal in white

LED is not corresponded with the results from singlet oxygen generation study (figure 3.14). These results might be caused by the difference in reaction mechanism which will be discussed in the next part. Therefore, green LED was chosen to use as a light source for further study.
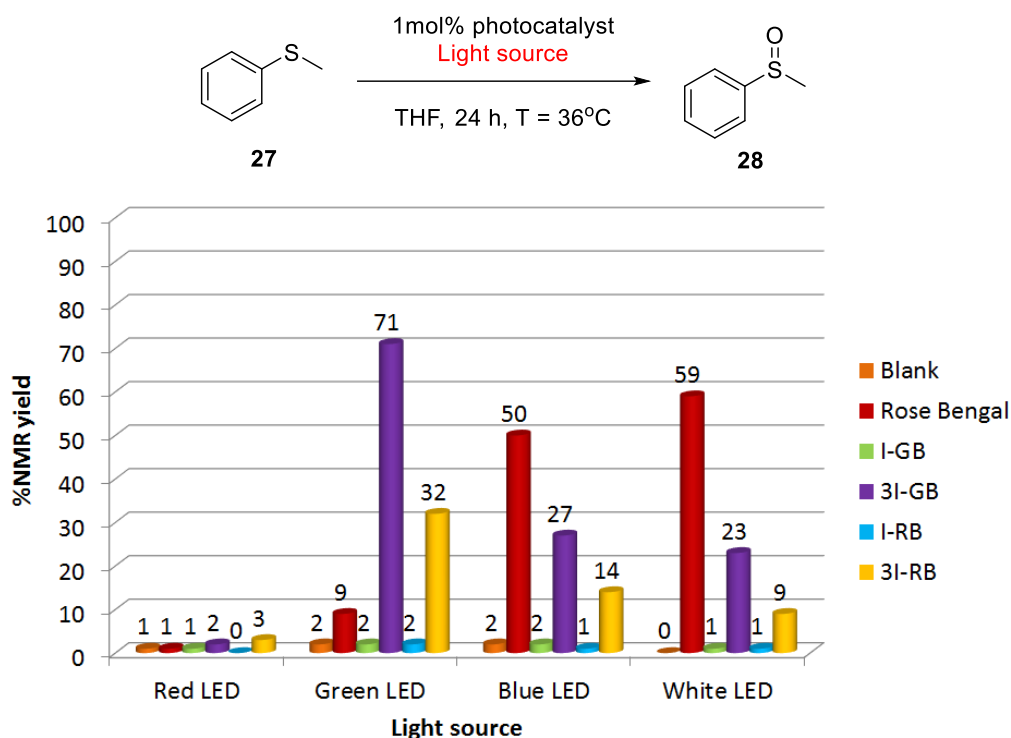
Figure 3.19 Effect of light source on the photooxidation of thioanisole. Reaction condition: thioanisole (0.3 mmol), THF (3.5 mL), photocatalyst (1 mol%), rt, 24 h.
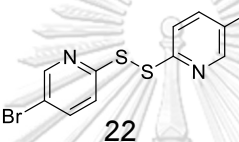
3.5.2.2 Screening amount of photocatalyst on the photooxidation of thioanisole

Based on above results, using the green LED with **3I-GB** and **3I-RB** catalysts gave the promising results for the oxidation of thioanisole. In order to enhance the reaction efficiency, the amount of catalysts was increased from 1 to 5 mol% and the comparison among each dye was investigated as seen in figure 3.20. In case of **I-GB** and **I-RB**, less than 5% yields of **28** were observed. On the other hand, increasing amount of **3I-GB**, **3I-RB**, and rose bengal lead to a significant improve photooxidation efficiency. The reaction using 5 mol% **3I-RB** and **3I-GB** under green LED gave 77 and 90% NMR yields, respectively, while rose bengal provided only 48% NMR yield of

sulfoxide (**28**). Therefore, 5 mol% photocatalyst was chosen as a condition for the photooxidation of the other thioethers under green LED.
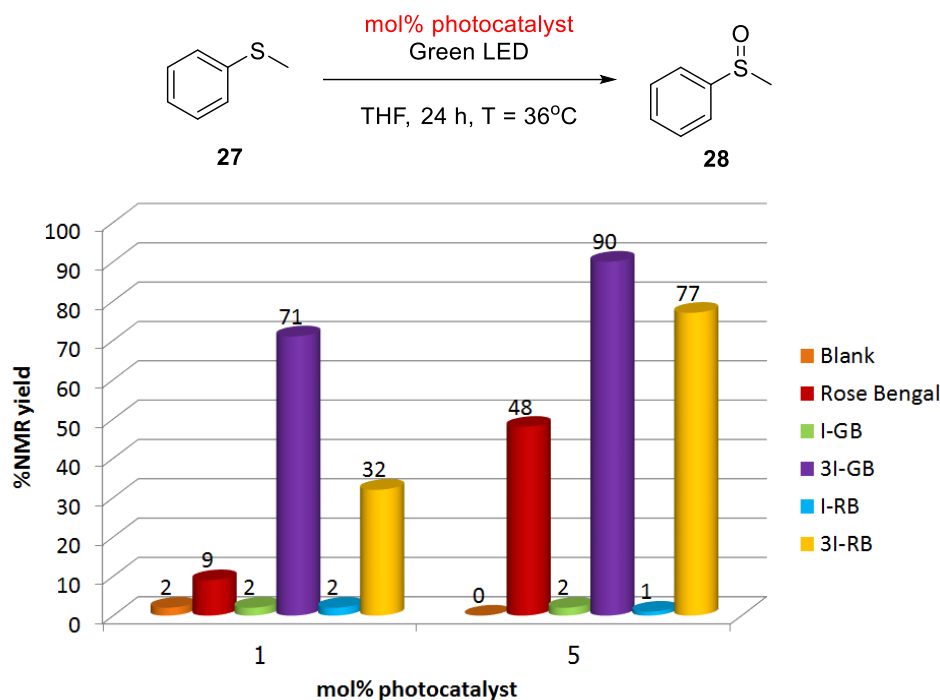
Figure 3.20 Effect of photocatalyst loading on the photooxidation of thioanisole. Reaction condition: thioanisole (0.3 mmol), THF (3.5 mL), green LED, rt, 24 h.

3.5.2.3 Preparation of other sulfur substrates for photooxidation

We planned to test the photooxidation using BODIPY catalysts to oxidize various thioether substrates such as aromatic, heterocyclic, and aliphatic substrates. To do so, we first prepared thioether substrates from the corresponding thiols as seen in scheme 3.13. [50] The metalation of thioethers (**15** and **19**) with methyl iodide in the presence of sodium hydroxide at room temperature gave the desired products, 4-chlorothioanisole (**29**) and 2-(methylthio)pyridine (**30**) in excellent yields. In case of aliphatic thioether (**23**), stronger base is required due to the higher pKa (9.43) of the corresponding acidic proton. The use of sodium-*t*-butoxide as base to perform methylation of thioether (**23**) was successful and provided product (**31**) in 80% yield. All prepared thioethers were characterized using ^{1}H-NMR (figure A.28-A.30) which are corresponded with the known literatures. [51]

R–SH $\xrightarrow[\text{EtOAc, rt, 1 h}]{\text{1 eq. MeI, 1 eq. NaOH or }t\text{-BuONa}}$ R–SMe

15, 19, 23   **29, 30, 31**

29	**30**	**31**
86 %yield	95 %yield	80 %yield
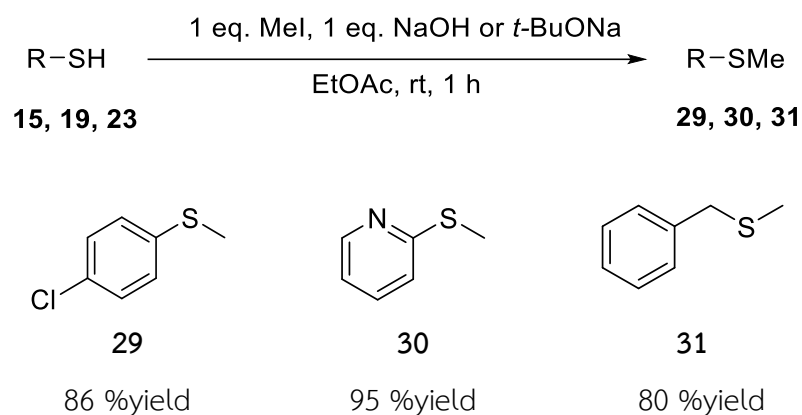
Scheme 3.13 Synthesis of 4-chlorothioanisole (**29**), 2-(methylthio)pyridine (**30**), and benzyl methyl sulfide (**31**)

3.5.2.4 Substrate scope of photooxidation for sulfoxide product

With the aromatic (**29**), heterocyclic (**30**), and aliphatic (**31**) thioethers in hand, we began the photooxidation of those substrates using **3I-GB** or **3I-RB** as photocatalysts as seen in table 3.4. Unfortunately, oxidation of 4-chlorothioanisole (**29**) in the presence of **3I-GB** or **3I-RB** using green LED as a light source gave the product (**32**) only 18-19% yield. Moreover, oxidation of **30** and **31** under the same condition lead to almost no reaction and only trace amount of sulfoxide products (**33, 34**) were detected in NMR of crude products (figure A.33-A.36). We hypothesized that low yields from those substrates caused by the poor nucleophile of sulfur atom from those substrates. The strong electron withdrawing group from chlorine in **29** and nitrogen atom in **30**, lower the nucleophilicity of sulfur atom during the reaction between substrates and electrophilic singlet oxygen. The mechanism of this formation will be further explained in the next section.

$$R-S \xrightarrow[\text{THF, 24 h}]{\substack{\text{Green LED,} \\ \text{5\%mol Photocatalyst}}} R-S=O$$
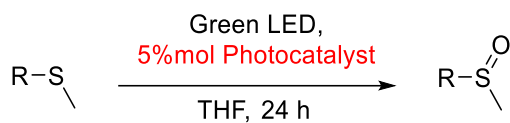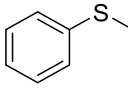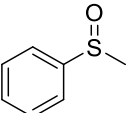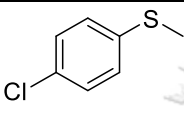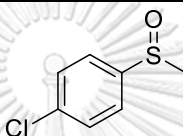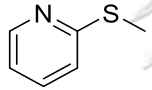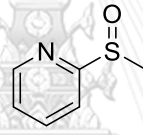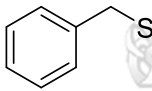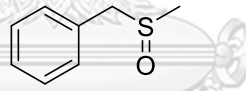
Table 3.4 Photooxidation of thioethers under green LED

Entry	Substrate	Product	%NMR yield	
			3I-GB	3I-RB
1	**27**	**28**	90	77
2	**29**	**32**	19	18
3	**30**	**33**	3	3
4	**31**	**34**	Complex mixtures	Complex mixtures

3.5.2.5 Proposed mechanism for photooxidation of thioanisole

From the investigation in section 3.5.2.1, the use of BODIPY, **3I-GB** and **3I-RB**, in green LED gave the best yield of sulfoxide product (**28**). These results corresponded to the singlet oxygen generation experiment in section 3.4 (figure 3.14e) where **3I-GB** and **3I-RB** gave the best singlet oxygen production when green LED were used as a light source. Therefore, when BODIPYs are used as catalysts, the main mechanism for photooxidation of thioanisole to sulfoxide product may involve singlet oxygen as proposed in scheme 3.14. [38, 45] The singlet excited state BODIPY (^{1}BODIPY*) is generated by excite the ground state BODIPY via light source and change to triplet excited state (^{3}BODIPY*) through intersystem crossing (ISC) process. The triplet excited

state BODIPY transfers energy to triplet state oxygen molecules ($^3O_2$) and generates singlet excited state oxygen molecules ($^1O_2$). Then, the nucleophilic addition from thioanisole to singlet excited state oxygen give the reactive intermediate (**35**). The abstraction of oxygen in intermediate (**35**) by water occurs, producing cation intermediate (**36**) along with peroxide anion as a byproduct. Finally, the proton abstraction of intermediate **36** provides the sulfoxide product.
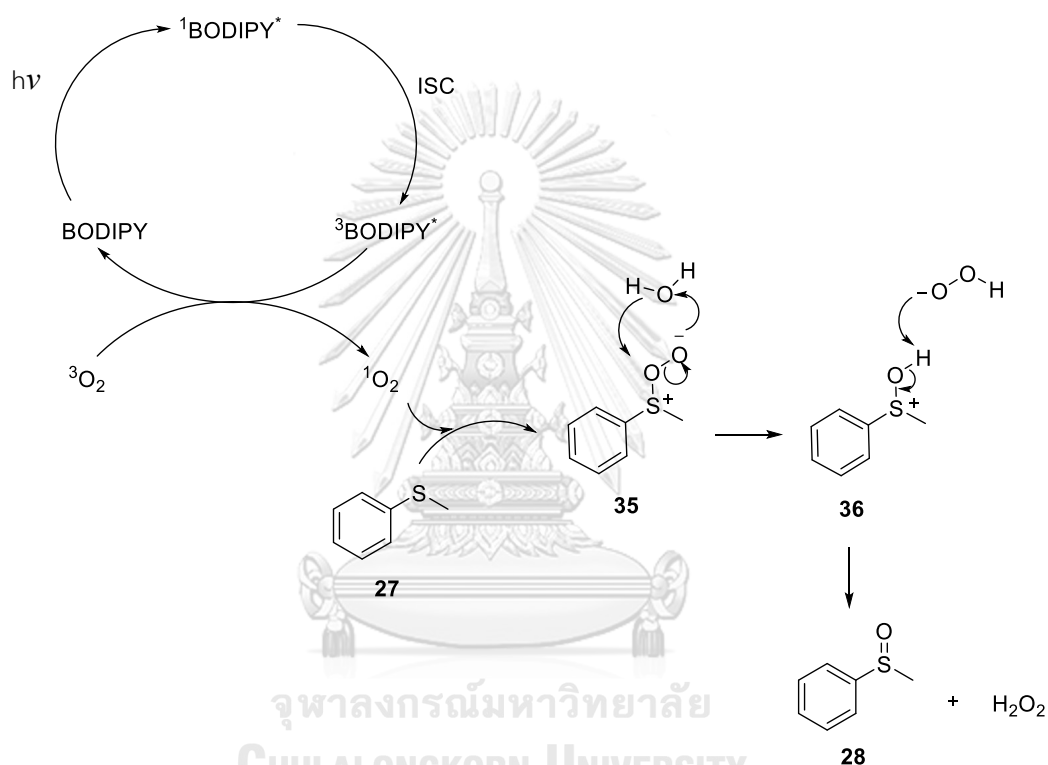
Scheme 3.14 The plausible mechanism for photocatalytic oxidation of thioanisole catalyzed by BODIPY

Unlike BODIPY catalysts, when rose bengal were used as catalyst, white LED irradiation provided better yield of sulfoxide (**28**) comparing to other light sources in figure 3.19. This observation differs from the singlet oxygen generation results in figure 3.14. Therefore, we hypothesized that the mechanism of thioanisole oxidation catalyzed by rose bengal may proceed through another mechanism involving the electron transfer process which is different from the BODIPYs. The plausible mechanism for oxidation of thioanisole catalyzed by rose bengal were demonstrated

in scheme 3.15. [33, 48] The mechanism starts with the excitation process of ground state rose bengal to give excited state rose bengal (Rose Bengal*) under visible light irradiation. The reactive rose bengal species (Rose Bengal*) accept electron from thioanisole and convert to radical anion (Rose Bengal$^{\bullet-}$) which consequently react with oxygen molecule generating oxygen radical anion ($O_2^{\bullet-}$). Then, radical anion (Rose Bengal$^{\bullet-}$) goes back to its original ground state. Meanwhile, the thioanisole is converted into radical cation (**37**) and react with oxygen radical anion to generate intermediate (**35**). Therefore, the reaction is driven as same as scheme 3.15 to give desired product, sulfoxide with hydrogen peroxide as byproduct.
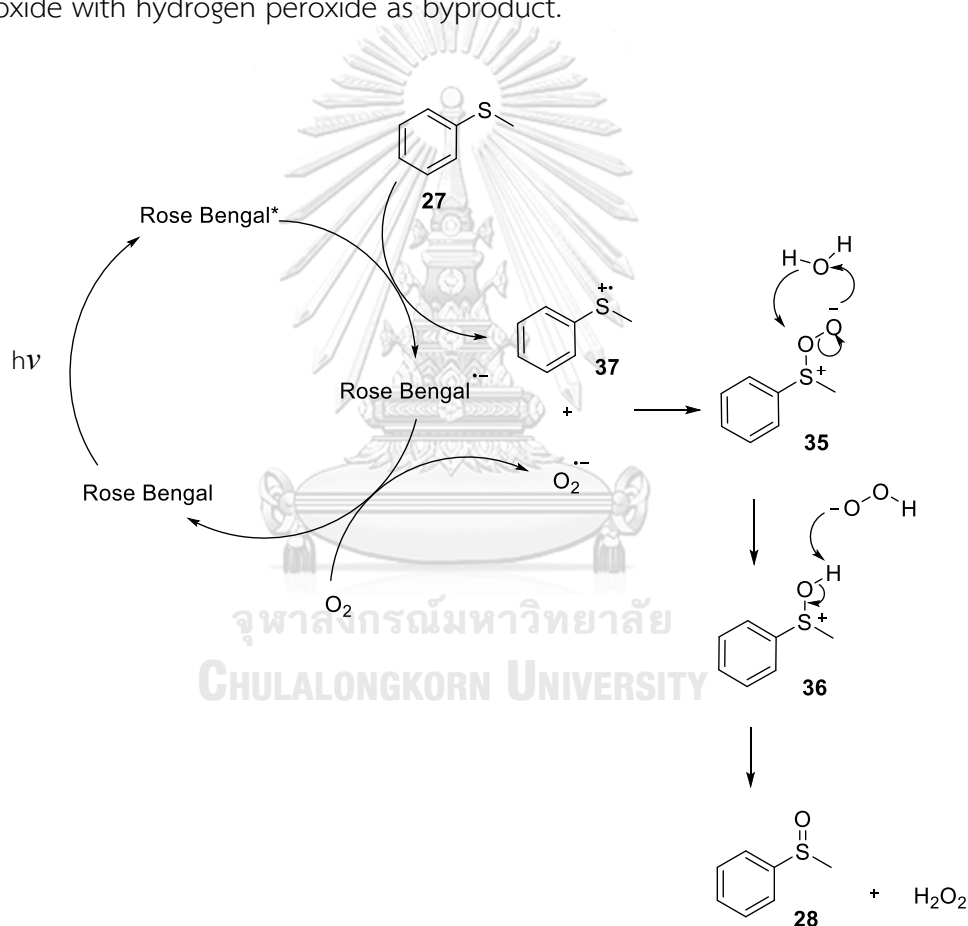
Scheme 3.15 The plausible mechanism for photocatalytic oxidation of sulfur substrate catalyzed by rose bengal

CHAPTER 4

CONCLUSIONS

In summary, iodo-BODIPY derivatives, **I-GB**, **3I-GB**, **I-RB**, and **3I-RB** were successfully synthesized and compared their photocatalytic activity in oxidation of organosulfurs with benchmark rose bengal catalyst. Among all BODIPY catalysts, the results from singlet oxygen generation revealed that **3I-GB**, **3I-RB** are the best catalyst under green LED irradiation caused by the incorporation of heavy atom effect from iodine atoms at C2 and C6 positions of BODIPY core. Under green LED, **3I-GB** and **3I-RB** showed better catalytic activity than other prepared catalysts and benchmark rose bengal in both oxidation of thiols and thioethers. For oxidation of thiols under green LED, **3I-GB** and **3I-RB** is proven to be a good photocatalysts for oxidation of heterocyclic, aromatic, and benzylic thiol substrates into the corresponding disulfides. Moreover, these iodo-BODIPYs were able to catalyze aromatic thioethers into sulfoxides in moderate to good yields. Based on our investigation, we proposed that the photocatalyst using BODIPY may proceed via energy transfer process involving the formation of singlet oxygen while the photoreaction using benchmark rose bengal catalyst may undergo via electron transfer process. These findings provide the new knowledges for photo catalyst design and alternative green process for organosulfur oxidation.

REFERENCES

[1] Amit, D., Nityananda, N., and Kumar, B.D. Thiophosphoryl disulfides as crosslinking agents for chloroprene rubber. Journal of Applied Polymer Science 91(3) (2004): 1913-1919.

[2] Hidaka, Y. and Shimamoto, S. Folding of peptides and proteins: role of disulfide bonds, recent developments. in BioMolecular Concepts. 2013. 597.

[3] Saito, G., Swanson, J.A., and Lee, K.-D. Drug delivery strategy utilizing conjugation via reversible disulfide linkages: role and site of cellular reducing activities. Advanced Drug Delivery Reviews 55(2) (2003): 199-215.

[4] Ge, W. and Wei, Y. Iodine-catalyzed oxidative system for 3-sulfenylation of indoles with disulfides using DMSO as oxidant under ambient conditions in dimethyl carbonate. Green Chemistry 14(7) (2012): 2066-2070.

[5] Zottola, M.A., Beigel, K., Soni, S.-D., and Lawrence, R. Disulfides as Cyanide Antidotes: Evidence for a New In Vivo Oxidative Pathway for Cyanide Detoxification. Chemical Research in Toxicology 22(12) (2009): 1948-1953.

[6] Chauhan, D., Kumar, P., Joshi, C., Labhsetwar, N., Ganguly, S.K., and Jain, S.L. Photo-assisted oxidation of thiols to disulfides using cobalt "Nanorust" under visible light. New Journal of Chemistry 39(8) (2015): 6193-6200.

[7] Shakeel, M., Jabeen, F., Shabbir, S., Asghar, M.S., Khan, M.S., and Chaudhry, A.S. Toxicity of Nano-Titanium Dioxide (TiO2-NP) Through Various Routes of Exposure: a Review. Biological Trace Element Research 172(1) (2016): 1-36.

[8] Neumann, M., Füldner, S., König, B., and Zeitler, K. Metal‐Free, Cooperative Asymmetric Organophotoredox Catalysis with Visible Light. Angewandte Chemie International Edition 50(4) (2011): 951-954.

[9] Zhao, Q., Huang, C., and Li, F. Phosphorescent heavy-metal complexes for bioimaging. Chemical Society Reviews 40(5) (2011): 2508-2524.

[10] Xie, F., et al. Thioanisole oxidation with hydrogen peroxide catalyzed by hexadentate 8-quinolinolato manganese(III) complexes. Journal of Molecular Catalysis A: Chemical 307(1) (2009): 93-97.

[11]   Mba, M., Prins, L.J., and Licini, G. C3-Symmetric Ti(IV) Triphenolate Amino Complexes as Sulfoxidation Catalysts with Aqueous Hydrogen Peroxide. Organic Letters 9(1) (2007): 21-24.

[12]   Liu, H., et al. Organic dye photocatalyzed [small alpha]-oxyamination through irradiation with visible light. Green Chemistry 12(6) (2010): 953-956.

[13]   Rosenthal, J., Pistorio, B.J., Chng, L.L., and Nocera, D.G. Aerobic Catalytic Photooxidation of Olefins by an Electron-Deficient Pacman Bisiron(III) μ-Oxo Porphyrin. The Journal of Organic Chemistry 70(5) (2005): 1885-1888.

[14]   Sideri, I.K., Voutyritsa, E., and Kokotos, C.G. Photoorganocatalysis, small organic molecules and light in the service of organic synthesis: the awakening of a sleeping giant. Organic & Biomolecular Chemistry (2018).

[15]   Caron, S., Dugger, R.W., Ruggeri, S.G., Ragan, J.A., and Ripin, D.H.B. Large-Scale Oxidations in the Pharmaceutical Industry. Chemical Reviews 106(7) (2006): 2943-2989.

[16]   Cambié, D., Bottecchia, C., Straathof, N.J.W., Hessel, V., and Noël, T. Applications of Continuous-Flow Photochemistry in Organic Synthesis, Material Science, and Water Treatment. Chemical Reviews 116(17) (2016): 10276-10341.

[17]   Shimada, Y., Hattori, K., Tada, N., Miura, T., and Itoh, A. Facile Aerobic Photooxidation of Alcohols Using 2-Chloroanthraquinone under Visible Light Irradiation. Synthesis 45(19) (2013): 2684-2688.

[18]   Liu, W., Wang, C., Huang, Y., Chen, Q., Wang, L., and He, M. Visible-light-mediated facile synthesis of disulfides using reusable TiO2/MoS2 nanocomposite photocatalyst. Synthetic Communications 46(15) (2016): 1268-1274.

[19]   Hari, D.P. and König, B. Eosin Y Catalyzed Visible Light Oxidative C–C and C–P bond Formation. Organic Letters 13(15) (2011): 3852-3855.

[20]   Alfred, T. and Franz-Heinrich, K. Difluorboryl-Komplexe von Di- und Tripyrrylmethenen. Justus Liebigs Annalen der Chemie 718(1) (1968): 208-223.

[21]   Yogo, T., Urano, Y., Ishitsuka, Y., Maniwa, F., and Nagano, T. Highly Efficient and Photostable Photosensitizer Based on BODIPY Chromophore. Journal of the American Chemical Society 127(35) (2005): 12162-12163.

[22]   Boens, N., et al. Visible Absorption and Fluorescence Spectroscopy of Conformationally Constrained, Annulated BODIPY Dyes. The Journal of Physical Chemistry A 116(39) (2012): 9621-9631.

[23]   Huang, L., Zhao, J., Guo, S., Zhang, C., and Ma, J. Bodipy Derivatives as Organic Triplet Photosensitizers for Aerobic Photoorganocatalytic Oxidative Coupling of Amines and Photooxidation of Dihydroxylnaphthalenes. The Journal of Organic Chemistry 78(11) (2013): 5627-5637.

[24]   Quan, L., Lin, W., Sun, T., Xie, Z., Huang, Y., and Jing, X. Green Photocatalysis with Oxygen Sensitive BODIPYs under Visible Light. Catalysis Letters 144(2) (2014): 308-313.

[25]   Li, Z., Li, L.-J., Sun, T., Liu, L., and Xie, Z. Benzimidazole-BODIPY as optical and fluorometric pH sensor. Dyes and Pigments 128 (2016): 165-169.

[26]   Foissner, I. Fluorescent phosphocholine-a specific marker for the endoplasmic reticulum and for lipid droplets in Chara internodal cells. Vol. 238, 2009.

[27]   Wang, Z., Hong, X., Zong, S., Tang, C., Cui, Y., and Zheng, Q. BODIPY-doped silica nanoparticles with reduced dye leakage and enhanced singlet oxygen generation. Scientific Reports 5 (2015): 12602.

[28]   Kazem, M.M., Shahriare, G., Soroush, Z., Hossein, F.M., and Behrang, S. Tributylammonium Halochromates/silica Gel: Simple Reagents for Oxidative Coupling of Thiols to Symmetrical Disulfides. Chinese Journal of Chemistry 28(11) (2010): 2199-2203.

[29]   Oba, M., Tanaka, K., Nishiyama, K., and Ando, W. Aerobic Oxidation of Thiols to Disulfides Catalyzed by Diaryl Tellurides under Photosensitized Conditions. The Journal of Organic Chemistry 76(10) (2011): 4173-4177.

[30]   Dharmarathna, S., King'ondu, C.K., Pahalagedara, L., Kuo, C.-H., Zhang, Y., and Suib, S.L. Manganese octahedral molecular sieve (OMS-2) catalysts for selective aerobic oxidation of thiols to disulfides. Applied Catalysis B: Environmental 147 (2014): 124-131.

[31]   Abdel-Mohsen, H.T., Sudheendran, K., Conrad, J., and Beifuss, U. Synthesis of disulfides by laccase-catalyzed oxidative coupling of heterocyclic thiols. Green Chemistry 15(6) (2013): 1490-1495.

[32] Hattori, K., Nakadate, K., Morii, A., Noguchi, T., Ogasawara, Y., and Ishii, K. Exposure to nano-size titanium dioxide causes oxidative damages in human mesothelial cells: The crystal form rather than size of particle contributes to cytotoxicity. Biochemical and Biophysical Research Communications 492(2) (2017): 218-223.

[33] Ali, T., et al. Metal-Free Photocatalytic Aerobic Oxidation of Thiols to Disulfides in Batch and Continuous-Flow. Advanced Synthesis & Catalysis 357(10) (2015): 2180-2186.

[34] Tankam, T., Poochampa, K., Vilaivan, T., Sukwattanasinitt, M., and Wacharasindhu, S. Organocatalytic visible light induced S–S bond formation for oxidative coupling of thiols to disulfides. Tetrahedron 72(6) (2016): 788-793.

[35] Yang, C., et al. Tetra-(tetraalkylammonium)octamolybdate catalysts for selective oxidation of sulfides to sulfoxides with hydrogen peroxide. Green Chemistry 11(9) (2009): 1401-1405.

[36] Das, R. and Chakraborty, D. Cu(II)-catalyzed oxidation of sulfides. Tetrahedron Letters 51(48) (2010): 6255-6258.

[37] Gu, X., Li, X., Chai, Y., Yang, Q., Li, P., and Yao, Y. A simple metal-free catalytic sulfoxidation under visible light and air. Green Chemistry 15(2) (2013): 357-361.

[38] Li, W., et al. Iodo-BODIPY: a visible-light-driven, highly efficient and photostable metal-free organic photocatalyst. RSC Advances 3(32) (2013): 13417-13421.

[39] Yuan, Y., Shi, X., and Liu, W. Transition-Metal-Free, Chemoselective Aerobic Oxidations of Sulfides and Alcohols with Potassium Nitrate and Pyridinium Tribromide or Bromine. Synlett 2011(04) (2011): 559-564.

[40] Kang, H., et al. Photophysical/Chemistry Properties of Distyryl-BODIPY Derivatives: An Experimental and Density Functional Theoretical Study. The Journal of Physical Chemistry A (2018).

[41] Kaewchangwat, N., Sukato, R., V., chirawongkwin, V., Vilaivan, T., Sukwattanasinitt, M., and Wacharasindhu, S. Direct synthesis of aryl substituted pyrroles from calcium carbide: an underestimated chemical feedstock. Green Chemistry 17(1) (2015): 460-465.

[42]   Singh-Rachford, T.N., Haefele, A., Ziessel, R., and Castellano, F.N. Boron Dipyrromethene Chromophores: Next Generation Triplet Acceptors/Annihilators for Low Power Upconversion Schemes. Journal of the American Chemical Society 130(48) (2008): 16164-16165.

[43]   Lim, S.H., et al. In Vitro and In Vivo Photocytotoxicity of Boron Dipyrromethene Derivatives for Photodynamic Therapy. Journal of Medicinal Chemistry 53(7) (2010): 2865-2874.

[44]   Burghart, A., et al. 3,5-Diaryl-4,4-difluoro-4-bora-3a,4a-diaza-s-indacene (BODIPY) Dyes: Synthesis, Spectroscopic, Electrochemical, and Structural Properties. The Journal of Organic Chemistry 64(21) (1999): 7813-7819.

[45]   Wang, L., Cao, J., Wang, J.-w., Chen, Q., Cui, A.-j., and He, M.-y. Facile synthesis of dimeric BODIPY and its catalytic activity for sulfide oxidation under visible light. RSC Advances 4(28) (2014): 14786-14790.

[46]   Wang, Z., Hong, X., Zong, S., Tang, C., Cui, Y., and Zheng, Q. BODIPY-doped silica nanoparticles with reduced dye leakage and enhanced singlet oxygen generation. Vol. 5, 2015.

[47]   Böhner, N., Danzl, W., and Rieblinger, K. INFLUENCE OF LED-ILLUMINATION ON DISCOLOURATION AND OXYGEN UPTAKE ON CURED BOILED SAUSAGE. 2013.

[48]   Liu, Q. and Wu, L.-Z. Recent advances in visible-light-driven organic reactions. National Science Review 4(3) (2017): 359-380.

[49]   Fernández, I. and Khiar, N. Recent Developments in the Synthesis and Utilization of Chiral Sulfoxides. Chemical Reviews 103(9) (2003): 3651-3706.

[50]   Xing, H., Chen, L., Jia, Y., Jiang, Z., and Yang, Z. Fe2O3-catalyzed Pummerer rearrangement of acyl chlorides and sulfoxides: Facile synthesis of alkylthiomethyl ester. Tetrahedron Letters 58(23) (2017): 2199-2202.

[51]   Xie, J., Wu, C., Christopher, B.W., Quan, J., and Zhu, L. Ionic Liquids—Promoted S-Methylation of Thiols Utilizing Dimethyl Carbonate. Phosphorus, Sulfur, and Silicon and the Related Elements 186(1) (2010): 31-37.

APPENDIX

จุฬาลงกรณ์มหาวิทยาลัย

CHULALONGKORN UNIVERSITY
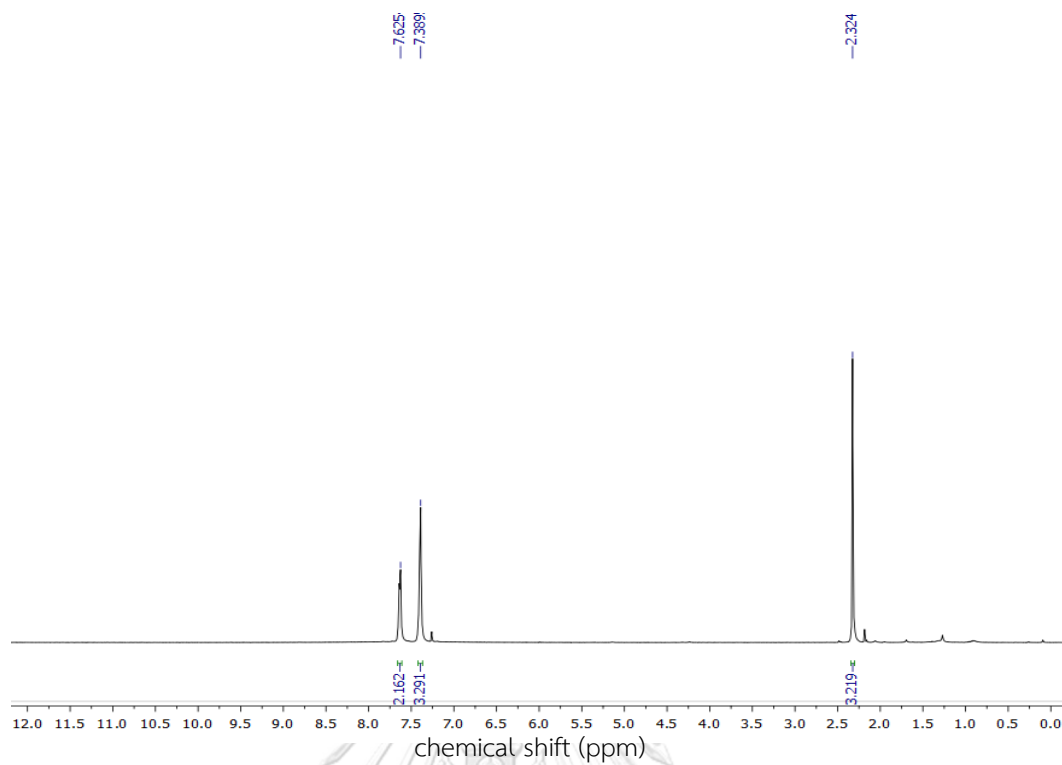
Figure A.1 ^{1}H-NMR spectrum of oxime (CDCl$_3$, 400 MHz)
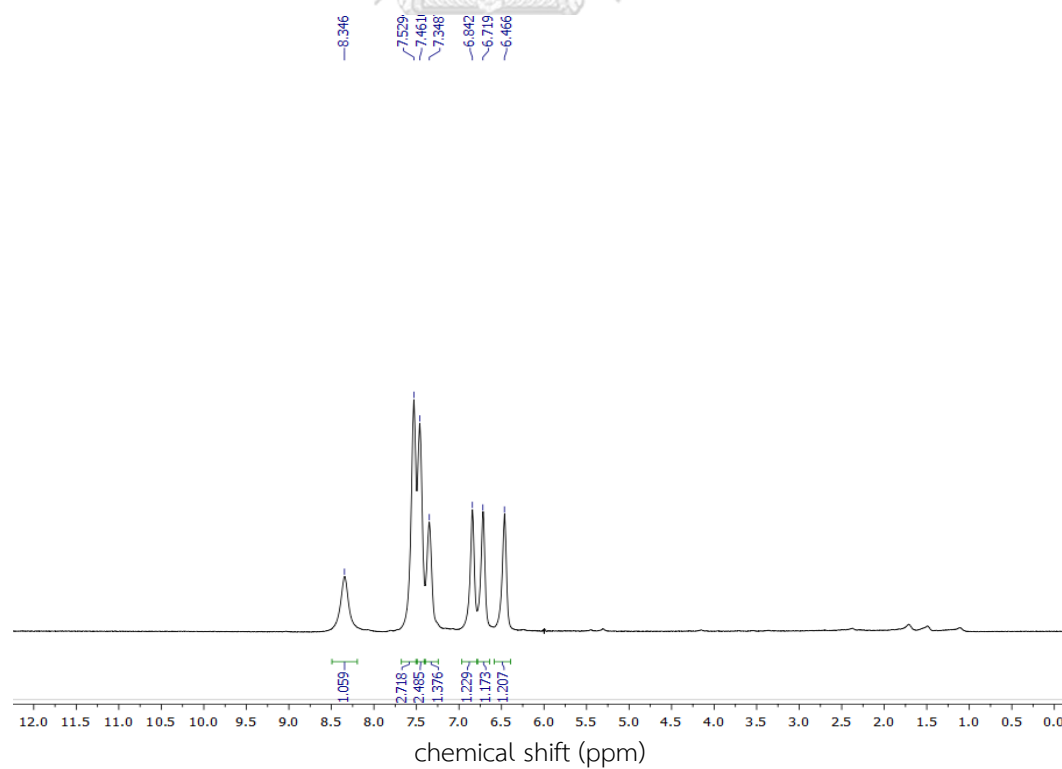
Figure A.2 ^{1}H-NMR spectrum of 2-phenyl pyrrole (CDCl$_3$, 400 MHz)

Figure A.3 ^{1}H-NMR spectrum of **I-GB** (CDCl$_3$, 400 MHz)

Figure A.4 ^{13}C-NMR spectrum of **I-GB** (CDCl$_3$, 100 MHz)

Mass Spectrum List Report

Analysis Info

Analysis Name	OSCUSJ590824002_2.d	Acquisition Date	8/24/2016 12:51:37 PM
Method	Tune_wide_POS_Tawatchai_05Feb2016.m	Operator	Administrator
Sample Name	I-GB ASO OSO52 Exact Mass	Instrument	micrOTOF 72
	24-08-2016		

Acquisition Parameter

Source Type	ESI	Ion Polarity	Positive	Set Corrector Fill	50 V
Scan Range	n/a	Capillary Exit	150.0 V	Set Pulsar Pull	337 V
Scan Begin	50 m/z	Hexapole RF	400.0 V	Set Pulsar Push	337 V
Scan End	3000 m/z	Skimmer 1	70.0 V	Set Reflector	1300 V
		Hexapole 1	25.0 V	Set Flight Tube	9000 V
				Set Detector TOF	2295 V

Intens. x10^6

+MS, 0.1-0.1min #(5-8)

451.0654

#	m/z	I	I %	S/N	FWHM	Res.
1	403.0667	20660	1.3	45.8	0.0784	5141
2	413.2654	49606	3.0	111.0	0.0870	4751
3	414.2697	14226	0.9	30.9	0.0843	4912
4	430.0613	117246	7.2	261.9	0.0853	5041
5	431.0586	504729	31.0	1131.6	0.0860	5015 ~f
6	432.0603	104316	6.4	232.7	0.0848	5097
7	433.0647	11341	0.7	24.1	0.0884	4898
8	449.0530	14580	0.9	31.0	0.1083	4147
9	449.3530	14514	0.9	30.8	0.1136	3956
10	450.0671	416713	25.6	926.3	0.0898	5010
11	450.7648	10526	0.6	21.9	0.2811	1604
12	451.0654	1630154	100.0	3626.3	0.0955	4725
13	452.0668	346517	21.3	769.3	0.0902	5013
14	453.0691	37066	2.3	80.9	0.0873	5187
15	472.0488	143133	8.8	314.1	0.0921	5125
16	473.0462	629782	38.6	1386.8	0.0938	5042 +Na
17	474.0483	128254	7.9	281.0	0.0945	5019
18	475.0525	13977	0.9	29.1	0.0944	5033
19	488.0230	23618	1.4	50.0	0.0956	5105
20	489.0204	94439	5.8	205.1	0.0951	5144
21	490.0251	23914	1.5	50.6	0.0947	5177
22	491.0257	10911	0.7	22.1	0.1030	4766
23	814.5487	17733	1.1	44.4	0.1628	5003
24	815.5492	11155	0.7	27.2	0.1789	4559
25	921.1027	23264	1.4	65.5	0.1795	5132
26	922.0988	188065	11.5	547.6	0.1781	5176
27	923.0981	431772	26.5	1261.9	0.1789	5160
28	924.0995	166334	10.2	485.1	0.1788	5167
29	925.1014	34638	2.1	99.2	0.1791	5166
30	1373.1466	10598	0.7	31.6	0.2621	5239

Bruker Daltonics DataAnalysis 3.3   printed: 8/25/2016 9:10:04 AM   Page 1 of 1
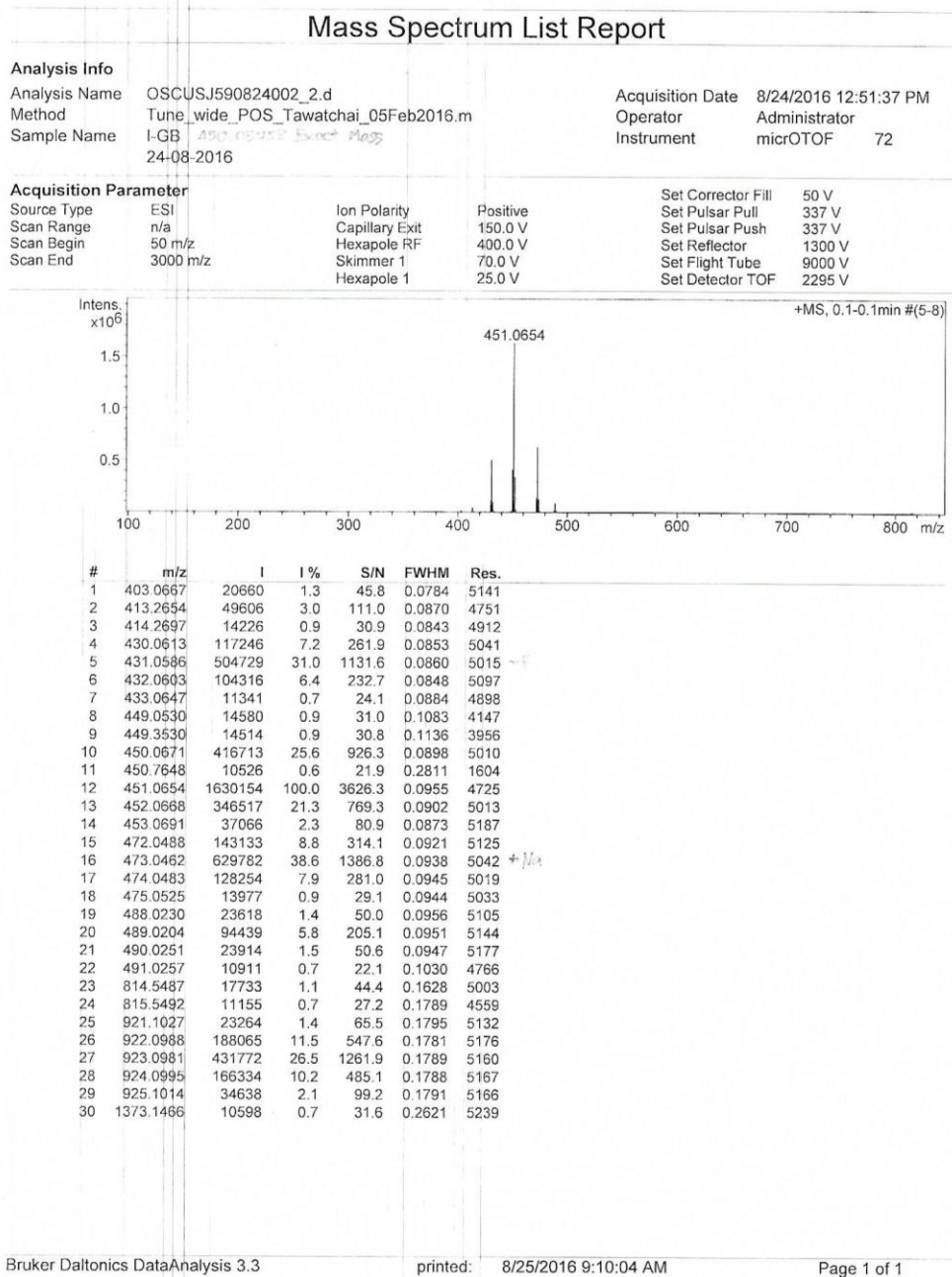
Figure A.5 High resolution mass spectrum of **I-GB**
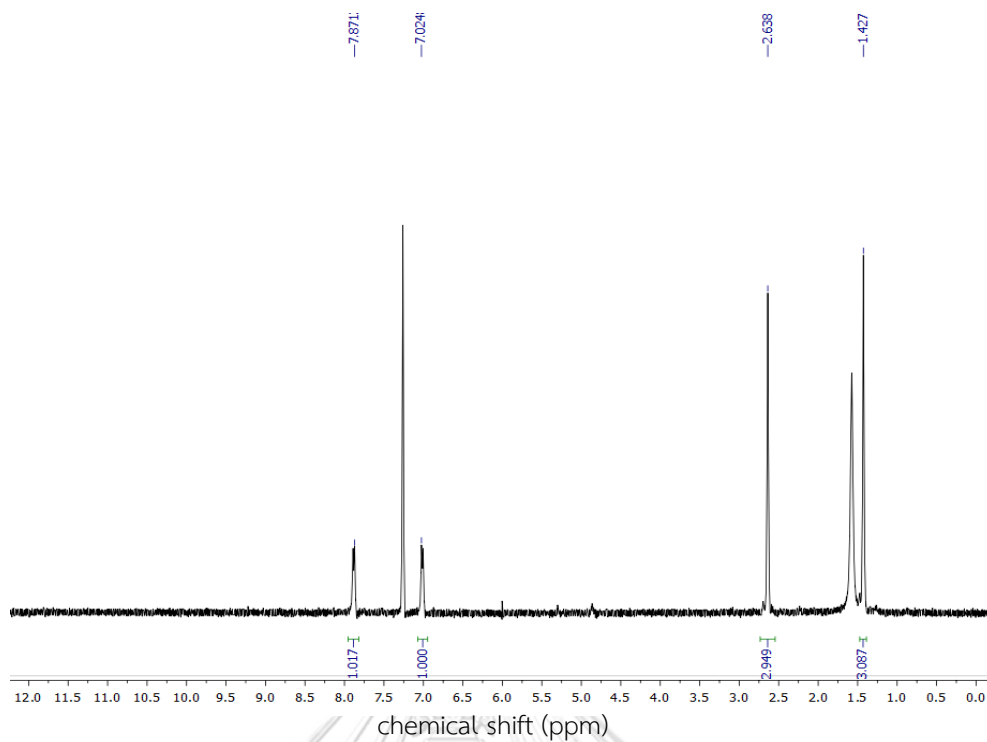
Figure A.6 ^{1}H-NMR spectrum of **3I-GB** (CDCl$_3$, 400 MHz)

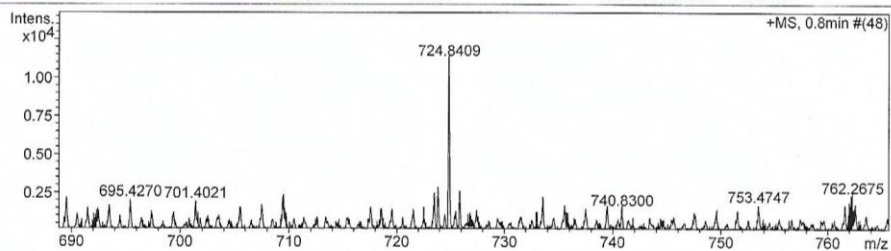**Figure A.7** ^{13}C-NMR spectrum sof **3I-GB** (CDCl$_3$, 100 MHz)

Mass Spectrum List Report

Analysis Info

Analysis Name	OSPT20170906001.d	Acquisition Date	9/6/2017 11:08:11 AM
Method	Tune_wide_POS_Natee20130403.m	Operator	Administrator
Sample Name	3IGB	Instrument	micrOTOF 72
	3IGB exact mass 701.8509		

Acquisition Parameter

Source Type	ESI	Ion Polarity	Positive	Set Corrector Fill	50 V
Scan Range	n/a	Capillary Exit	200.0 V	Set Pulsar Pull	337 V
Scan Begin	50 m/z	Hexapole RF	600.0 V	Set Pulsar Push	337 V
Scan End	3000 m/z	Skimmer 1	70.0 V	Set Reflector	1300 V
		Hexapole 1	25.0 V	Set Flight Tube	9000 V
				Set Detector TOF	2295 V

+MS, 0.8min #(48)

#	m/z	I	I %	S/N	FWHM	Res.
1	691.4975	1241	11.1	5.0	0.1182	5850
2	692.4536	672	6.0	2.7	0.1108	6247
3	695.4270	1767	15.7	7.1	0.1234	5636
4	698.4286	343	3.1	1.4	0.0363	19220
5	701.4021	1658	14.8	6.6	0.1295	5416
6	705.5130	1309	11.7	5.2	0.1558	4529
7	709.4537	1239	11.0	5.0	0.2135	3323
8	712.5858	648	5.8	2.6	0.1165	6116
9	713.3860	630	5.6	2.5	0.1439	4958
10	715.3862	523	4.7	2.1	0.1820	3930
11	718.5402	1168	10.4	4.7	0.1499	4793
12	722.5104	1303	11.6	5.2	0.0458	15777
13	723.4750	2234	19.9	9.0	0.1205	6006
14	723.8411	2598	23.2	10.5	0.1099	6589
15	724.8409	11221	100.0	45.2	0.1192	6083
16	725.8451	2372	21.1	9.5	0.1172	6192
17	727.4052	1099	9.8	4.4	0.1289	5642
18	729.3831	544	4.8	2.2	0.1803	4046
19	733.0228	1008	9.0	4.1	0.0159	46102
20	734.5366	604	5.4	2.4	0.1907	3852
21	737.4854	1208	10.8	4.9	0.1497	4926
22	740.8300	1484	13.2	6.0	0.0851	8707
23	741.8242	638	5.7	2.6	0.0255	29074
24	745.5948	675	6.0	2.7	0.1480	5039
25	749.5432	943	8.4	3.8	0.1898	3949
26	753.4747	1457	13.0	6.0	0.1097	6869
27	757.4052	500	4.5	2.0	0.1858	4076
28	761.5765	1460	13.0	6.0	0.1271	5991
29	762.2675	2324	20.7	9.6	0.0190	40129

Figure A.8 High resolution mass spectrum of **3I-GB**
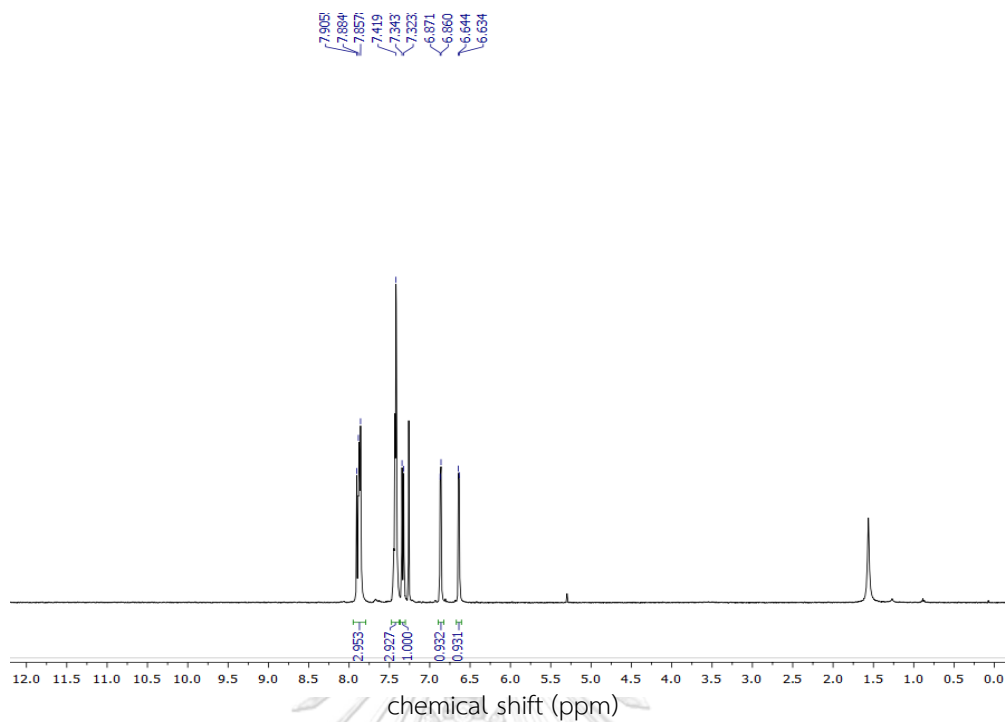
Figure A.9 ^{1}H-NMR spectrum of **I-RB** (CDCl$_3$, 400 MHz)
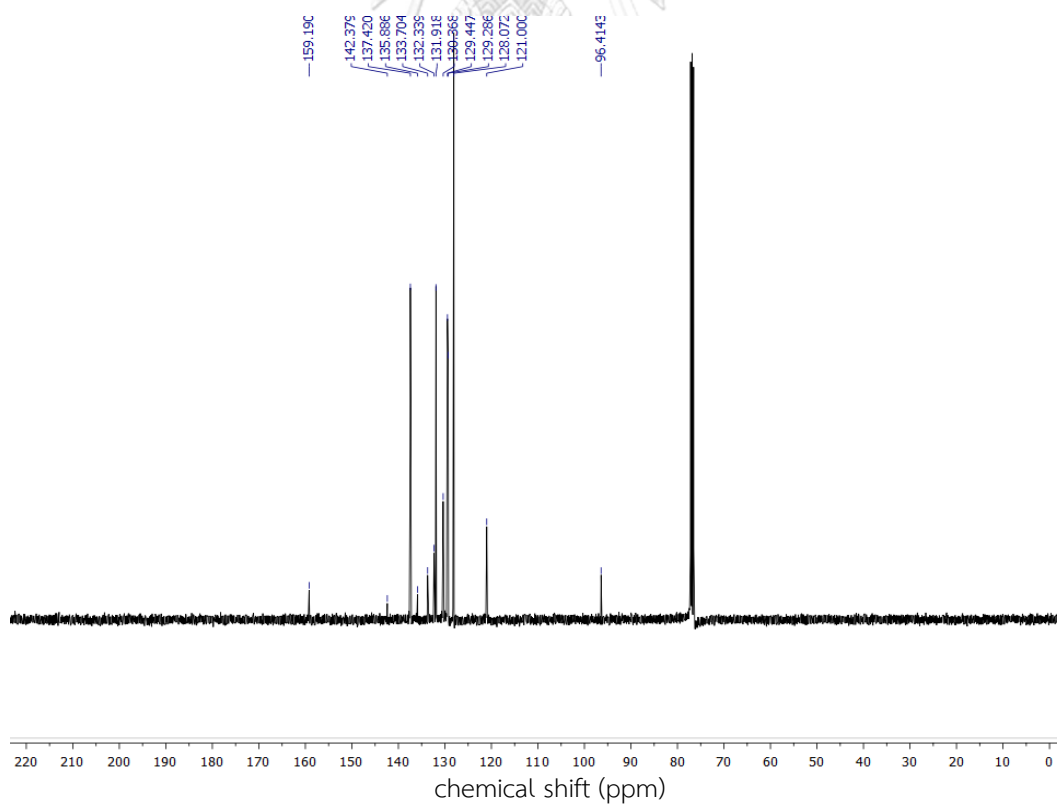
Figure A.10 ^{13}C-NMR spectrum of **I-RB** (CDCl$_3$, 100 MHz)

Mass Spectrum List Report

Analysis Info

Analysis Name	OSPT20170906003.d		Acquisition Date	9/6/2017 11:13:21 AM
Method	Tune_wide_POS_Natee20130403.m		Operator	Administrator
Sample Name	IRB		Instrument	micrOTOF 72
	IRB Exact mass 546.0976.			

Acquisition Parameter

Source Type	ESI	Ion Polarity	Positive	Set Corrector Fill	50 V
Scan Range	n/a	Capillary Exit	200.0 V	Set Pulsar Pull	337 V
Scan Begin	50 m/z	Hexapole RF	600.0 V	Set Pulsar Push	337 V
Scan End	3000 m/z	Skimmer 1	70.0 V	Set Reflector	1300 V
		Hexapole 1	25.0 V	Set Flight Tube	9000 V
				Set Detector TOF	2295 V

+MS, 0.3min #(19)

#	m/z	I	I %	S/N	FWHM	Res.
1	296.9161	3806	3.3	16.2	0.0319	9301
2	413.2636	7017	6.1	27.4	0.0772	5353
3	441.2941	4165	3.6	15.2	0.0843	5237
4	503.3510	3797	3.3	12.3	0.1083	4649
5	526.0611	8449	7.3	27.4	0.0895	5876
6	527.0574	36759	31.8	122.3	0.0882	5973
7	528.0613	11130	9.6	36.3	0.0836	6316
8	533.3579	3487	3.0	10.6	0.1328	4015
9	547.0629	4557	3.9	14.1	0.0859	6367
10	547.3726	4062	3.5	12.5	0.1382	3962
11	563.3641	3446	3.0	10.4	0.1830	3079
12	568.0494	26493	23.0	87.5	0.0922	6162
13	569.0466	115425	100.0	385.1	0.0951	5983
14	570.0490	34332	29.7	113.8	0.0935	6096
15	571.0512	5073	4.4	15.9	0.0916	6232
16	577.4046	3855	3.3	11.9	0.1763	3276
17	584.0250	9446	8.2	30.7	0.0943	6193
18	585.0201	40035	34.7	133.8	0.1009	5798
19	586.0241	13089	11.3	43.0	0.0981	5971
20	587.0208	4873	4.2	15.3	0.0973	6034
21	591.4202	4502	3.9	14.1	0.1739	3402
22	607.3825	3594	3.1	11.1	0.1505	4036
23	635.4347	4004	3.5	12.6	0.1291	4923
24	651.4071	3512	3.0	11.0	0.1296	5025
25	663.4643	3604	3.1	11.4	0.1403	4729
26	679.4539	4003	3.5	12.9	0.1391	4883
27	695.4319	3469	3.0	11.1	0.1289	5395
28	820.8396	4233	3.7	15.5	0.1395	5883
29	2339.1599	3915	3.4	20.1	0.0896	26099
30	2867.9978	3481	3.0	17.0	0.0937	30621

Figure A.11 High resolution mass spectrum of **I-RB**

e
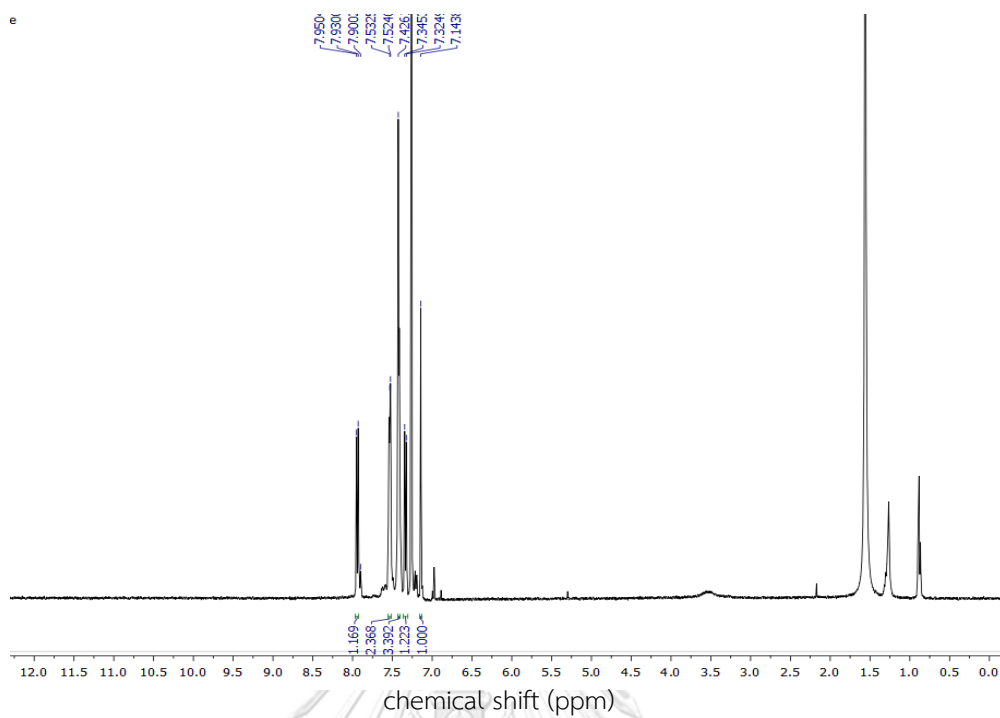
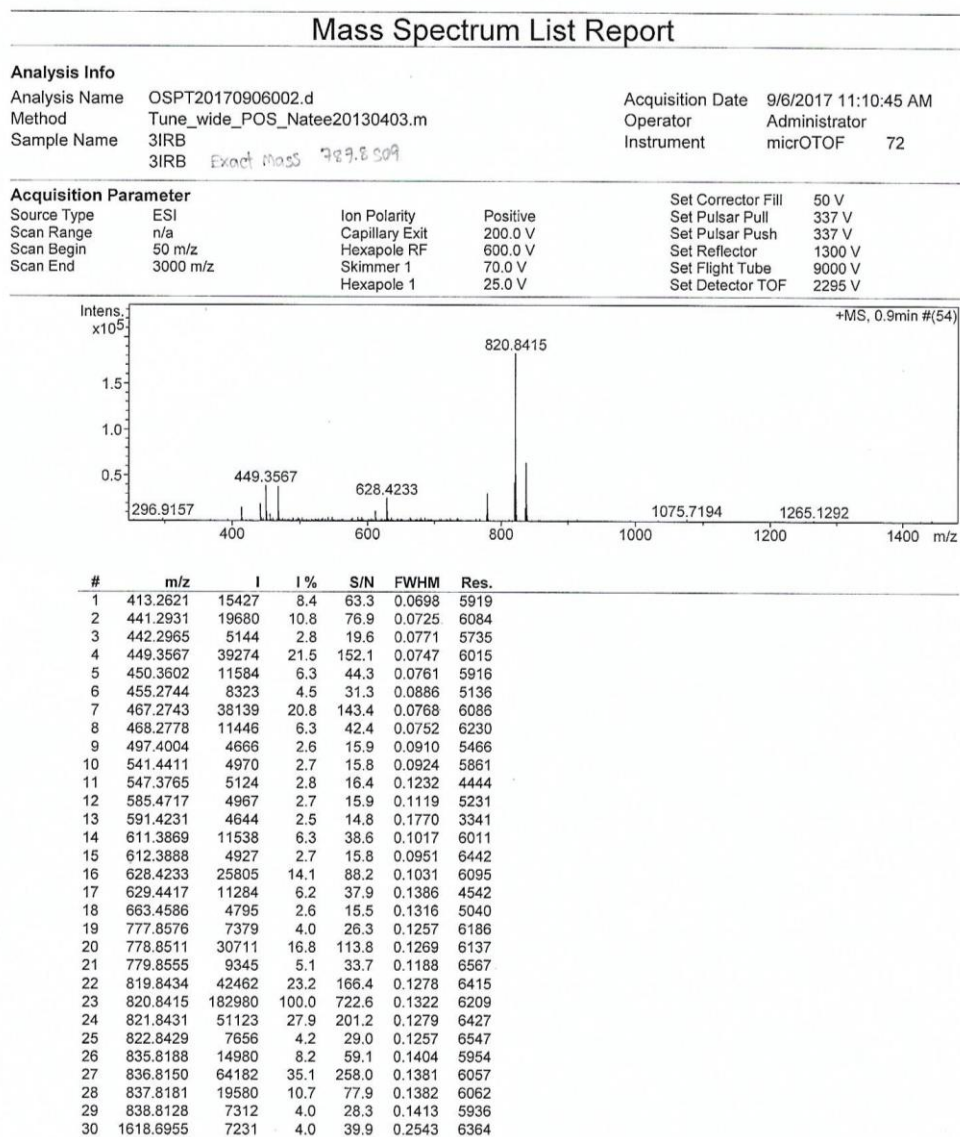**Figure A.12** ^{1}H-NMR spectrum of **3I-RB** (CDCl$_3$, 400 MHz)
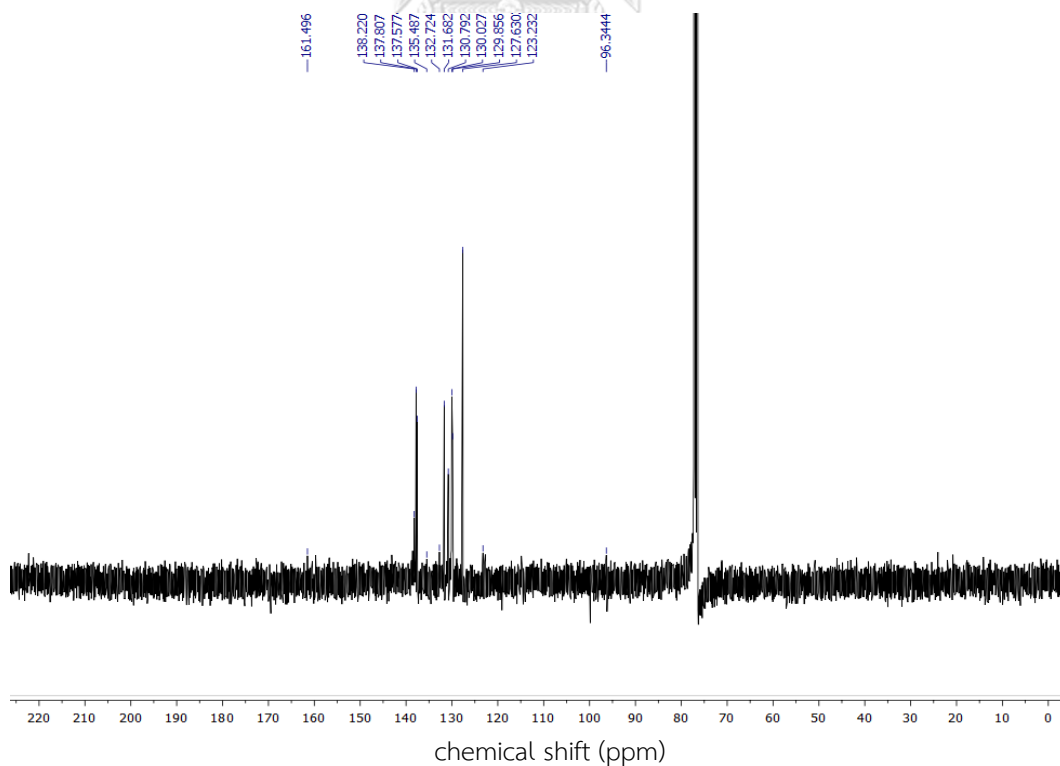
Figure A.13 ^{13}C-NMR spectrum of **3I-RB** (CDCl$_3$, 100 MHz)

Mass Spectrum List Report

Analysis Info

Analysis Name	OSPT20170906002.d	Acquisition Date	9/6/2017 11:10:45 AM
Method	Tune_wide_POS_Natee20130403.m	Operator	Administrator
Sample Name	3IRB	Instrument	micrOTOF 72
	3IRB Exact Mass 789.8 909		

Acquisition Parameter

Source Type	ESI	Ion Polarity	Positive	Set Corrector Fill	50 V	
Scan Range	n/a	Capillary Exit	200.0 V	Set Pulsar Pull	337 V	
Scan Begin	50 m/z	Hexapole RF	600.0 V	Set Pulsar Push	337 V	
Scan End	3000 m/z	Skimmer 1	70.0 V	Set Reflector	1300 V	
		Hexapole 1	25.0 V	Set Flight Tube	9000 V	
				Set Detector TOF	2295 V	

+MS, 0.9min #(54)

#	m/z	I	I %	S/N	FWHM	Res.
1	413.2621	15427	8.4	63.3	0.0698	5919
2	441.2931	19680	10.8	76.9	0.0725	6084
3	442.2965	5144	2.8	19.6	0.0771	5735
4	449.3567	39274	21.5	152.1	0.0747	6015
5	450.3602	11584	6.3	44.3	0.0761	5916
6	455.2744	8323	4.5	31.3	0.0886	5136
7	467.2743	38139	20.8	143.4	0.0768	6086
8	468.2778	11446	6.3	42.4	0.0752	6230
9	497.4004	4666	2.6	15.9	0.0910	5466
10	541.4411	4970	2.7	15.8	0.0924	5861
11	547.3765	5124	2.8	16.4	0.1232	4444
12	585.4717	4967	2.7	15.9	0.1119	5231
13	591.4231	4644	2.5	14.8	0.1770	3341
14	611.3869	11538	6.3	38.6	0.1017	6011
15	612.3888	4927	2.7	15.8	0.0951	6442
16	628.4233	25805	14.1	88.2	0.1031	6095
17	629.4417	11284	6.2	37.9	0.1386	4542
18	663.4586	4795	2.6	15.5	0.1316	5040
19	777.8576	7379	4.0	26.3	0.1257	6186
20	778.8511	30711	16.8	113.8	0.1269	6137
21	779.8555	9345	5.1	33.7	0.1188	6567
22	819.8434	42462	23.2	166.4	0.1278	6415
23	820.8415	182980	100.0	722.6	0.1322	6209
24	821.8431	51123	27.9	201.2	0.1279	6427
25	822.8429	7656	4.2	29.0	0.1257	6547
26	835.8188	14980	8.2	59.1	0.1404	5954
27	836.8150	64182	35.1	258.0	0.1381	6057
28	837.8181	19580	10.7	77.9	0.1382	6062
29	838.8128	7312	4.0	28.3	0.1413	5936
30	1618.6955	7231	4.0	39.9	0.2543	6364

Figure A.14 High resolution mass spectrum of **3I-RB**

Molar absorptivity of photocatalyst:
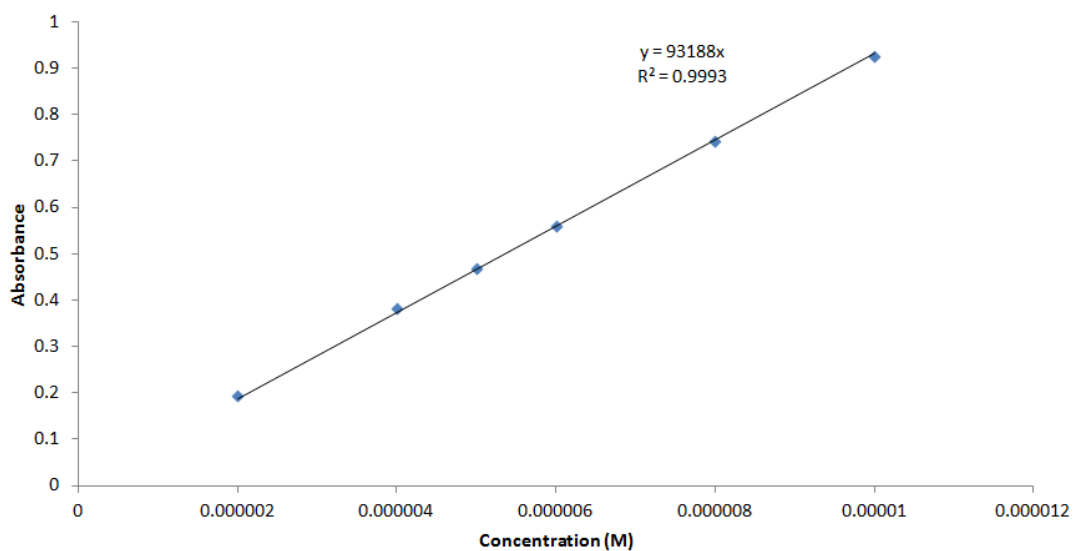
Figure A.15 Calibration curve for quantitative determination of **I-GB** in THF (λ_{max}^{abs} = 502 nm)
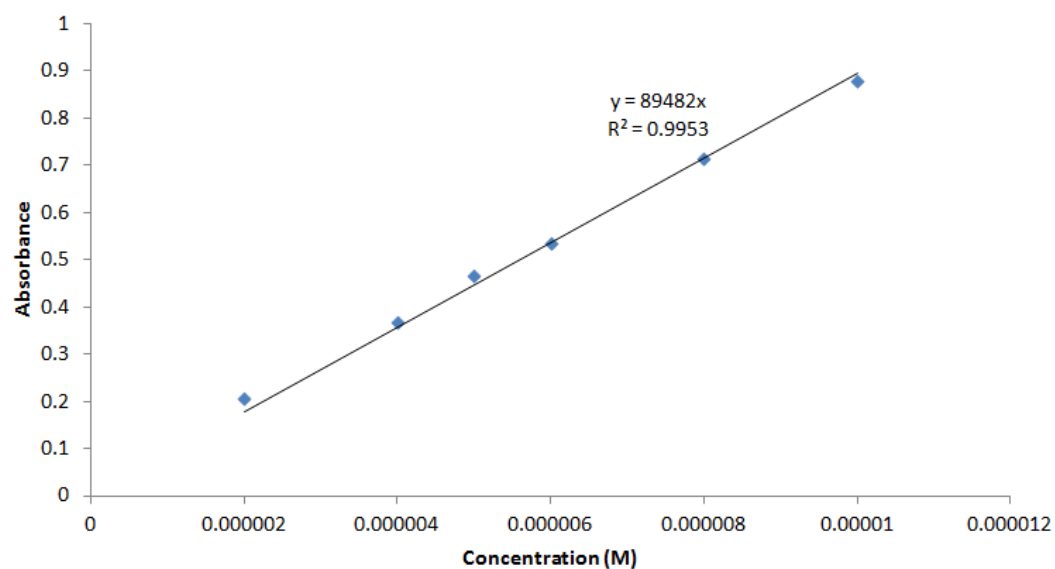
Figure A.16 Calibration curve for quantitative determination of **3I-GB** in THF (λ_{max}^{abs} = 535 nm)
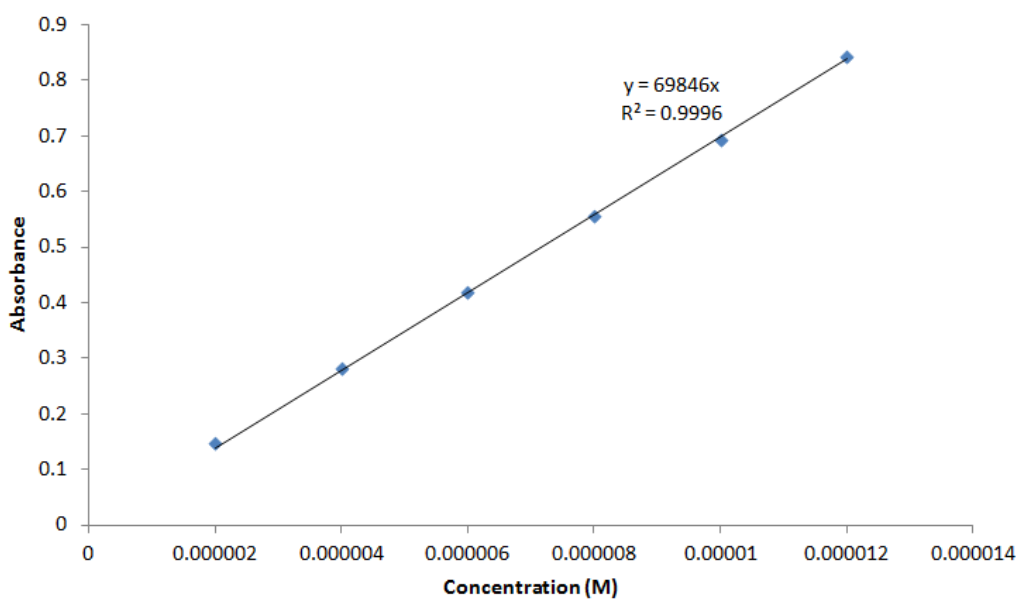
Figure A.17 Calibration curve for quantitative determination of **I-RB** in THF (λ_{max}^{abs} = 557 nm)
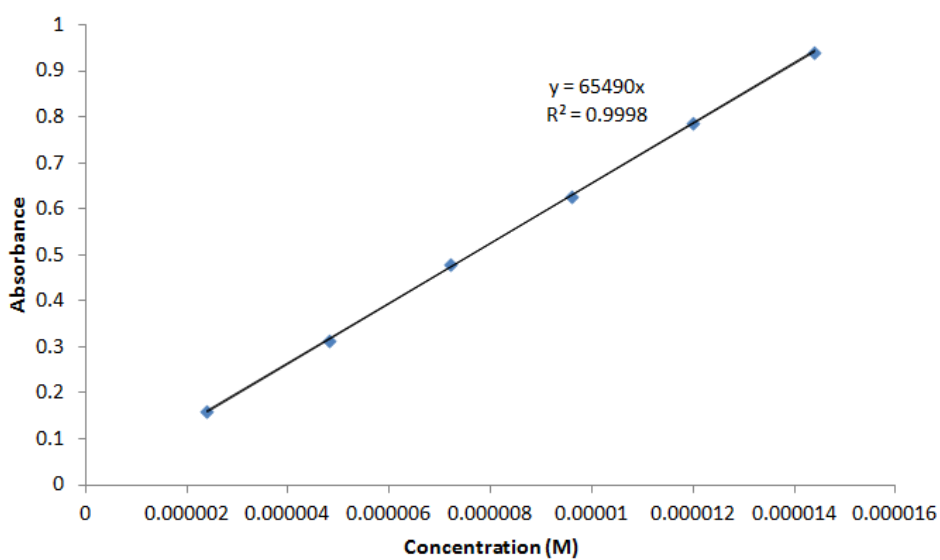
Figure A.18 Calibration curve for quantitative determination of **3I-RB** in THF (λ_{max}^{abs} = 573 nm)
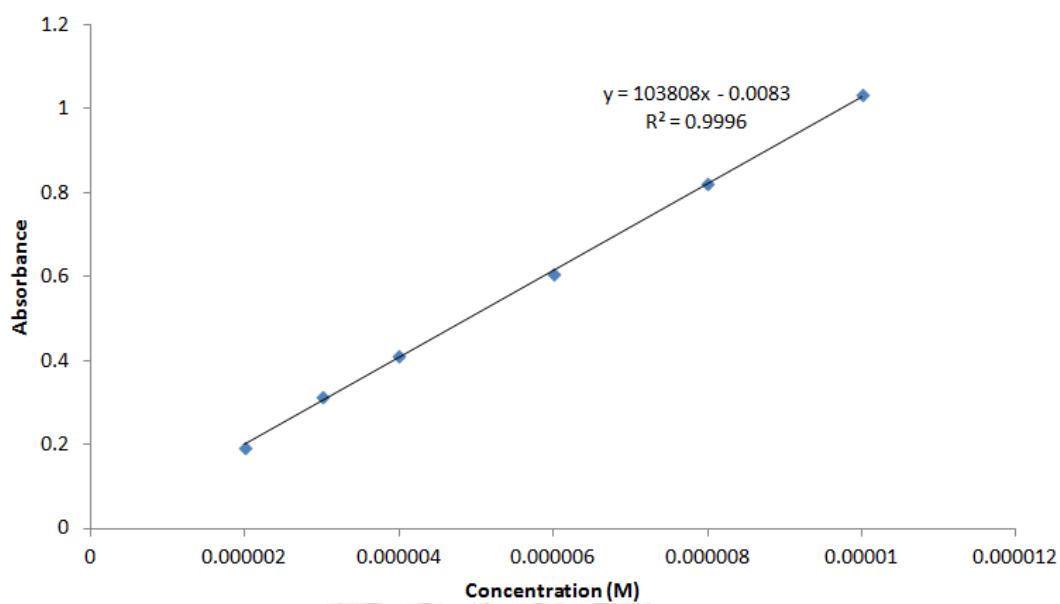
Figure A.19 Calibration curve for quantitative determination of rose bengal in THF (λ_{max}^{abs} = 561 nm)

จุฬาลงกรณ์มหาวิทยาลัย

CHULALONGKORN UNIVERSITY

Quantum yield of photocatalysts:

$y = 120835x + 359.38$
$R^2 = 0.9952$
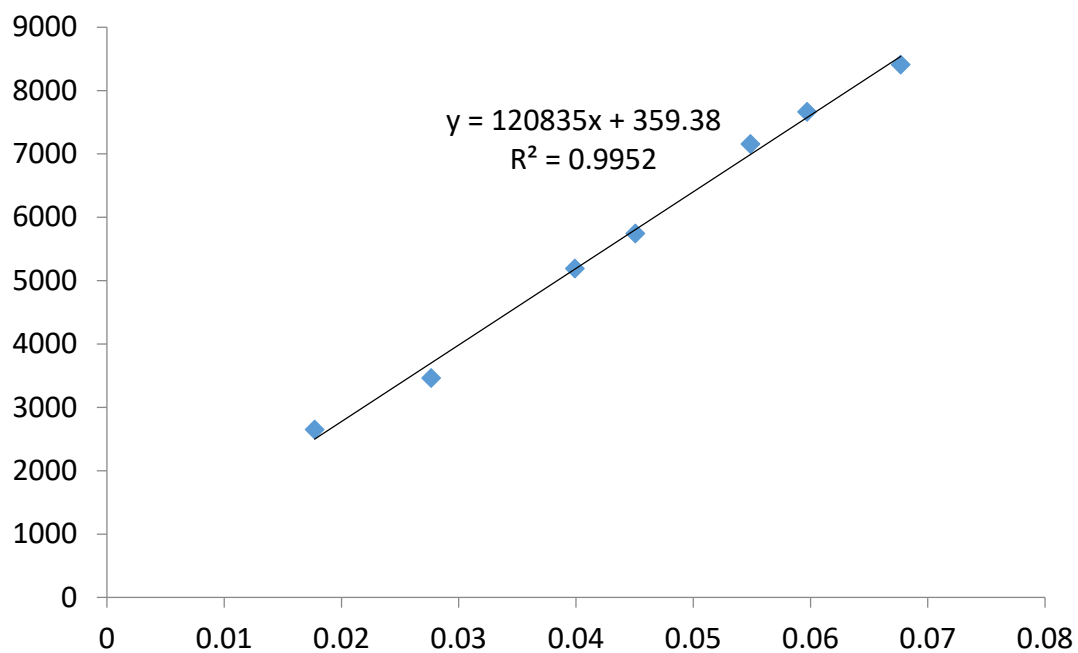
Figure A.20 Quantum yield of I-GB (exc 480) = 0.377, Std = fluorescene

$y = 324031x + 680.96$
$R^2 = 0.9977$
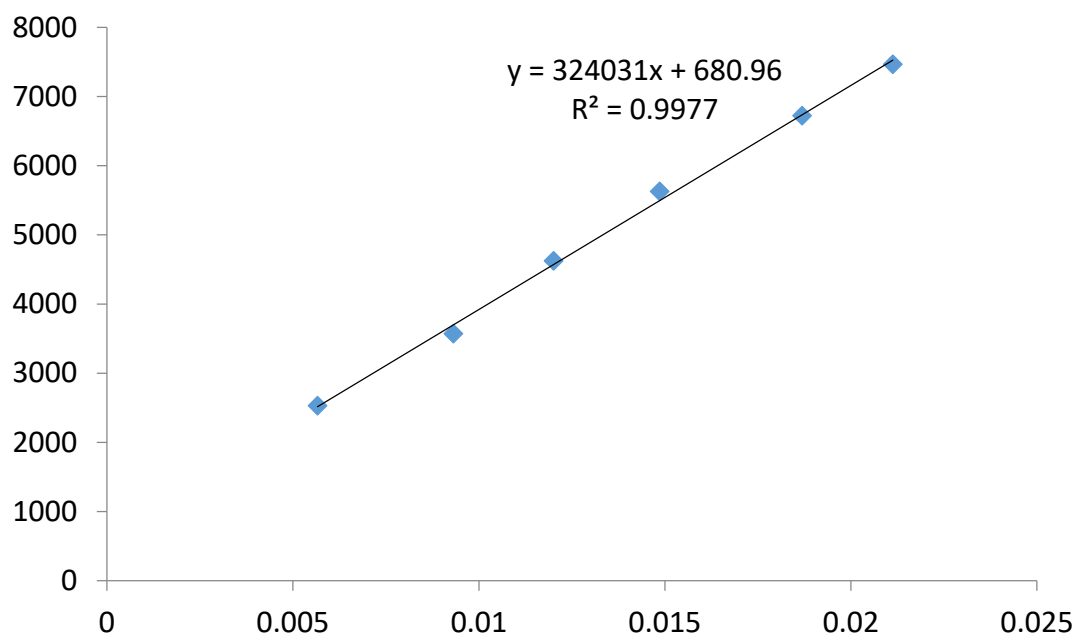
Figure A.21 Quantum yield of Fluorescene (exc 480) = 0.95
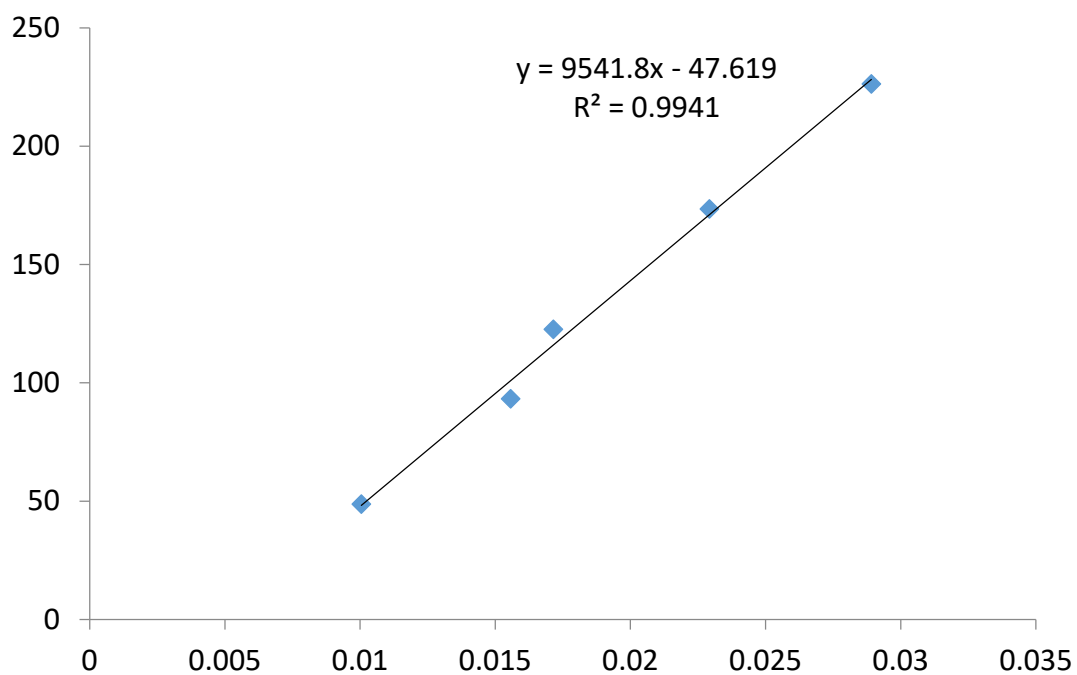
Figure A.22 Quantum yield of 3I-GB (exc 500) = 0.0540, Std = florescene
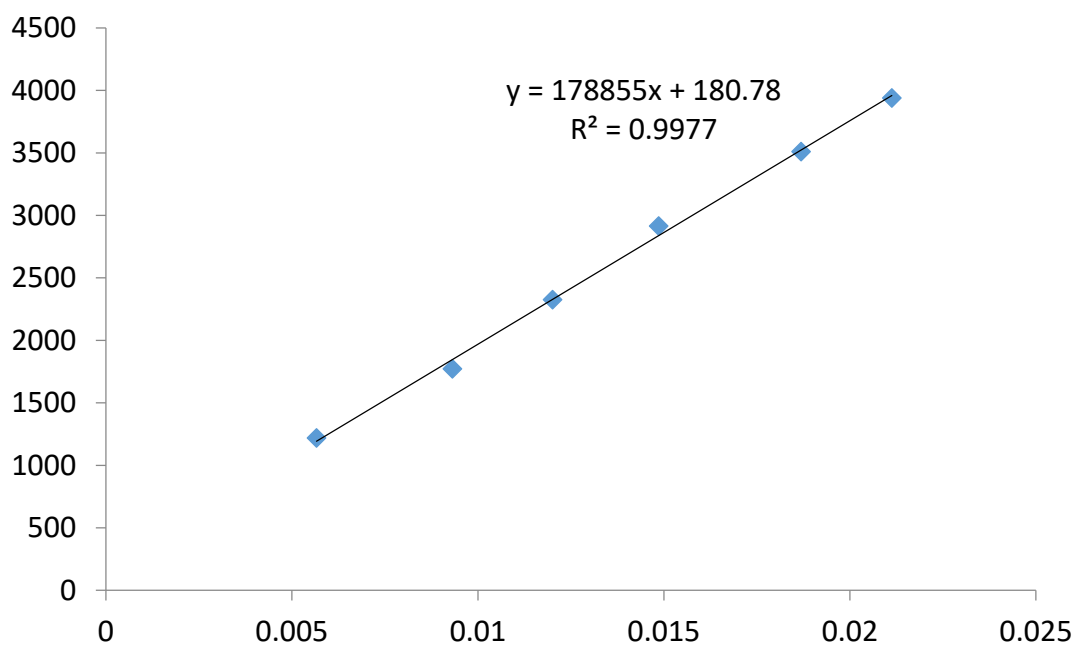
Figure A.23 Quantum yield of Fluorescene (exc 500) = 0.95
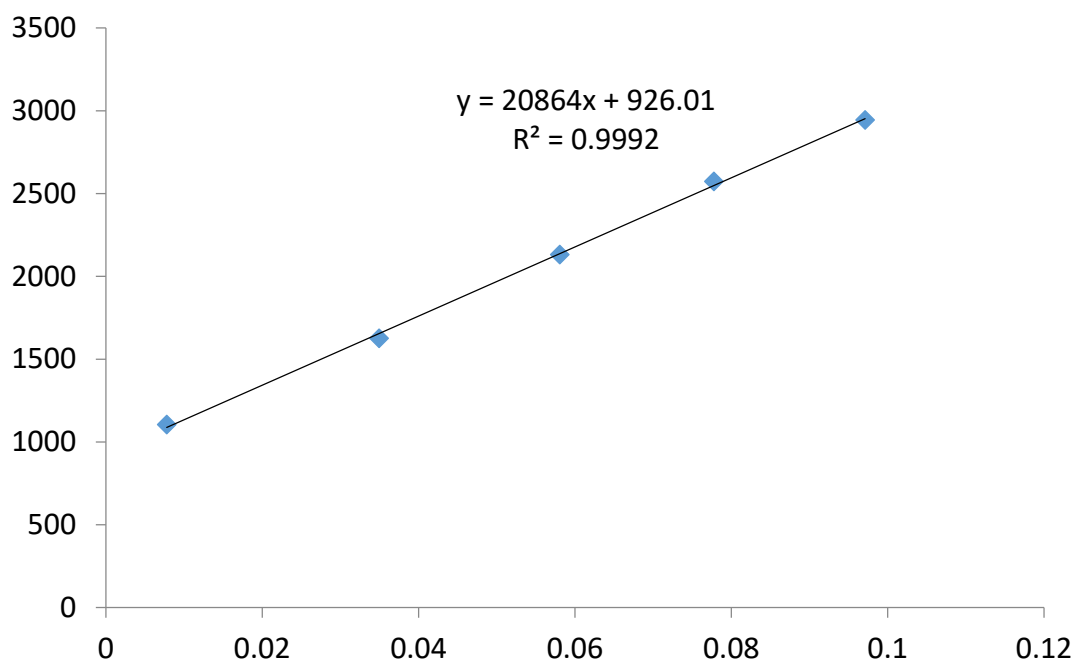
Figure A.24 Quantum yield of I-RB (exc 540) = 0.104, Std = Rhodamine B

Rhodamine B /H$_2$O exc 540
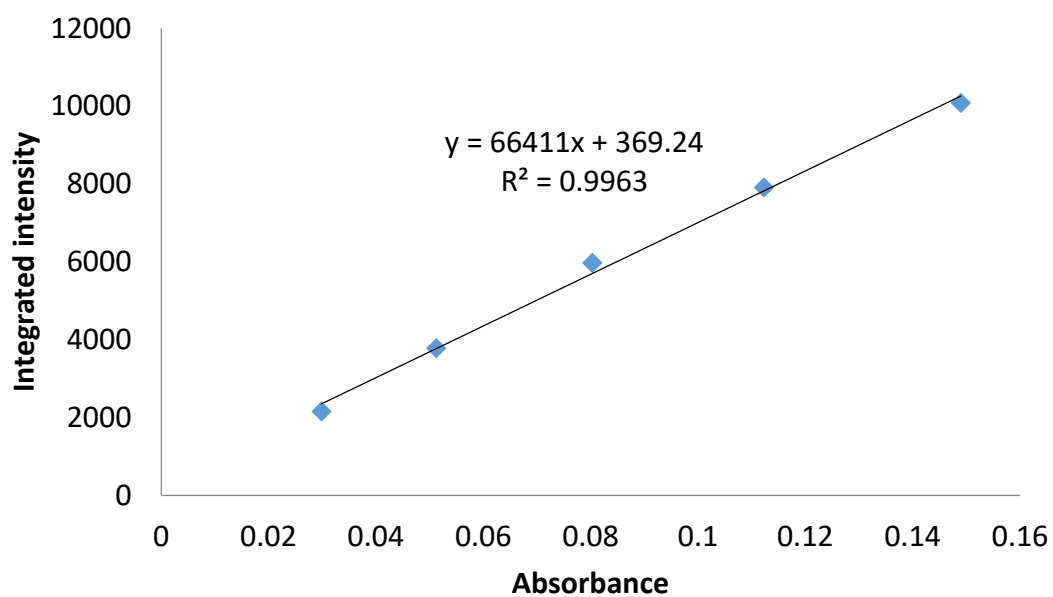
Figure A.25 Quantum yield of Rhodamine B=0.31
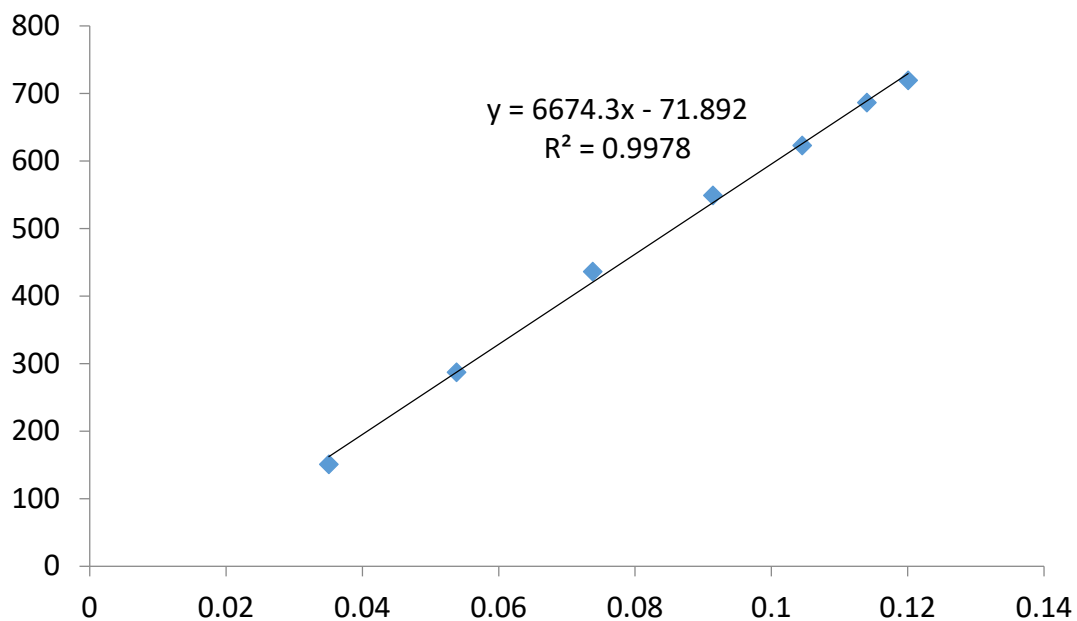
Figure A.26 Quantum yield of 3I-RB (exc 560) = 0.0532, Std = cresyl violet

Cresyl violet/MeOH exc 560
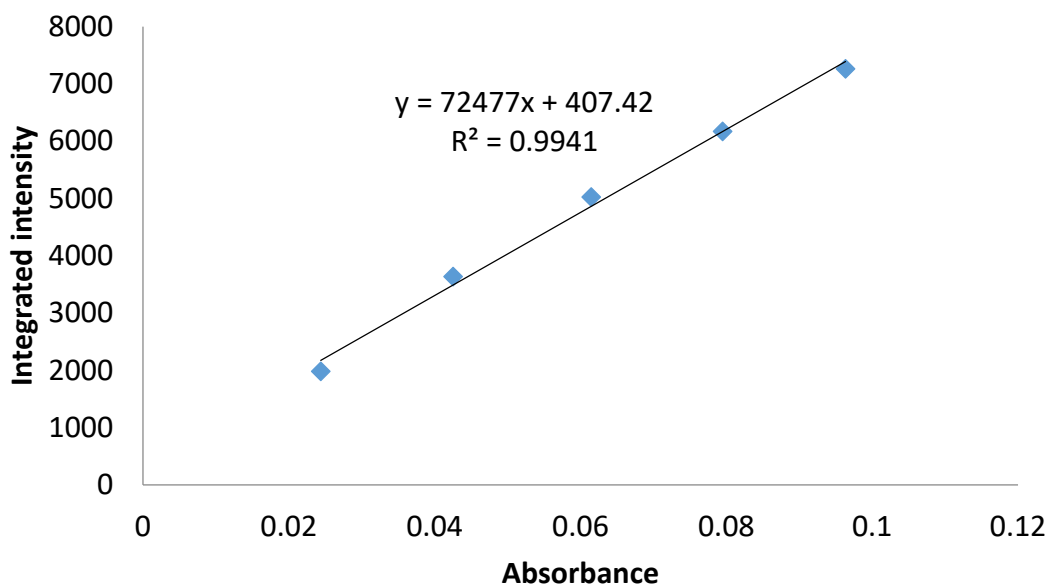
Figure A.27 Quantum yield of Cresyl violet=0.54
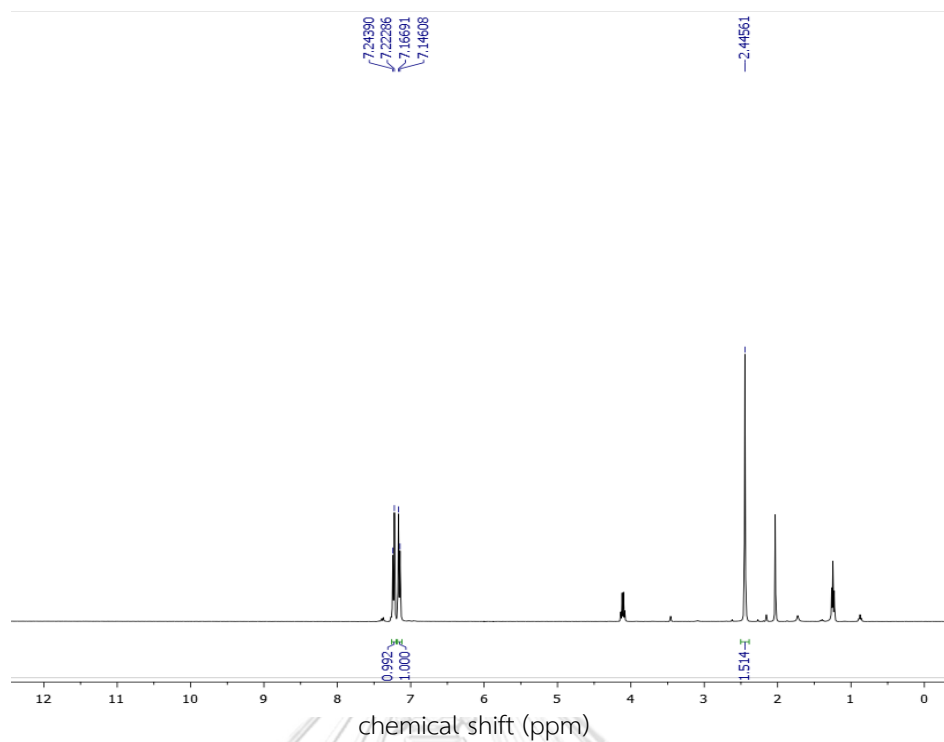
Figure A.28 ^{1}H-NMR spectrum of 4-chlorothioanisole (CDCl$_3$, 400 MHz)
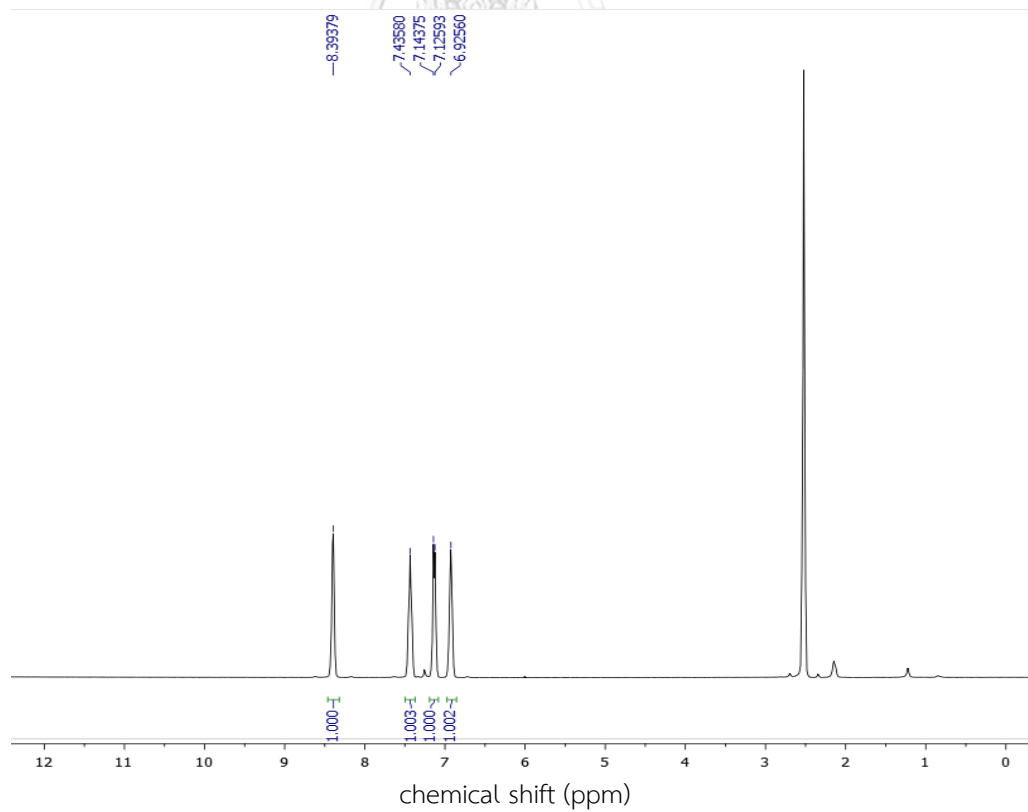
Figure A.29 ^{1}H-NMR spectrum of 2-(methylthio)pyridine (CDCl$_3$, 400 MHz)
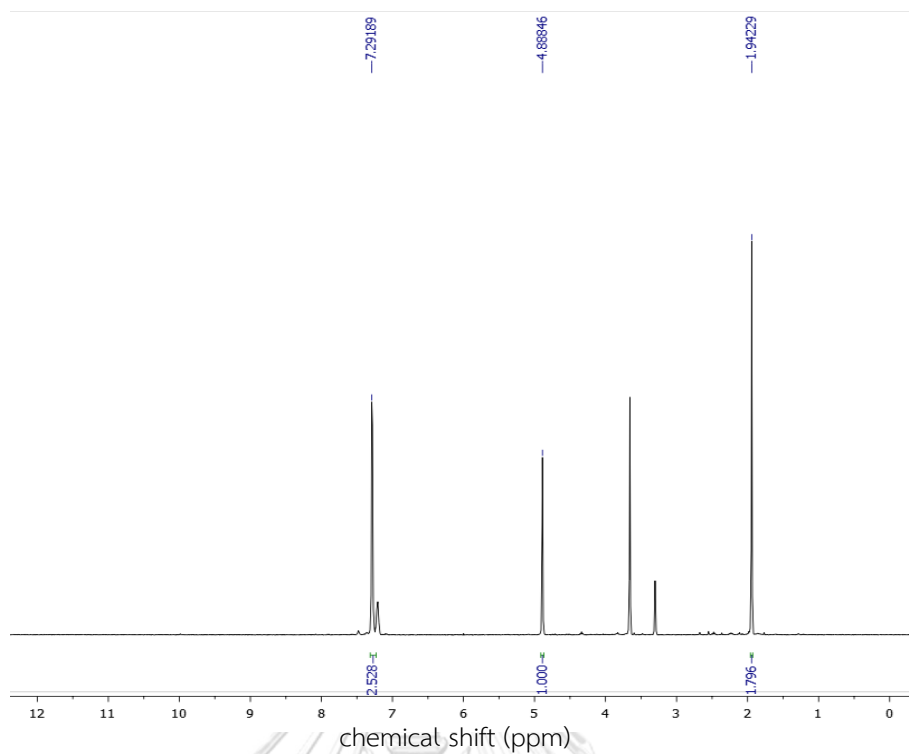
Figure A.30 ^{1}H-NMR spectrum of benzyl methyl sulfide (CDCl$_3$, 400 MHz)
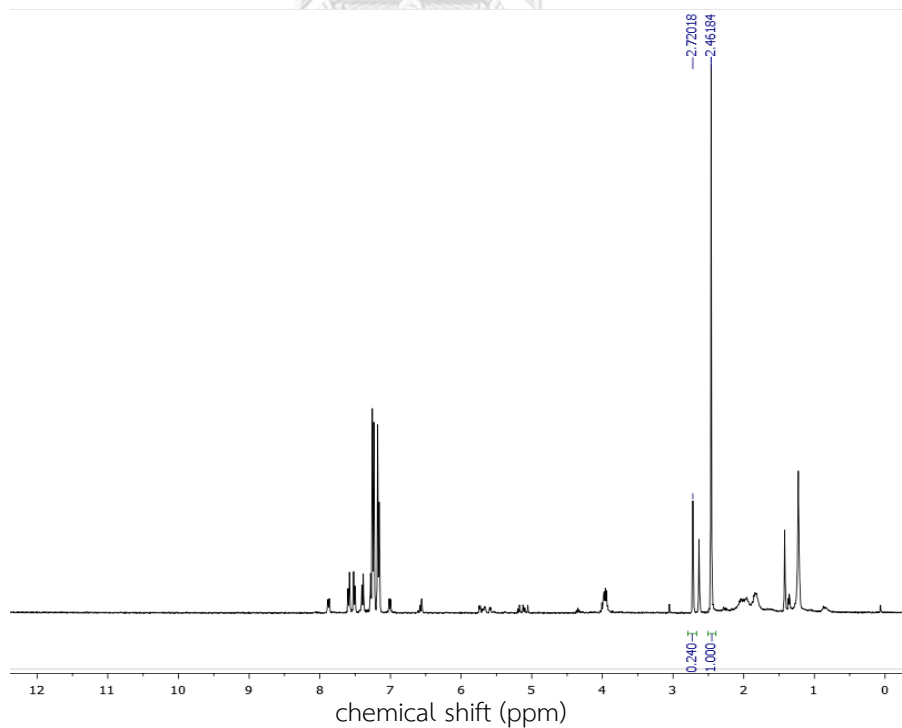
Figure A.31 ^{1}H-NMR spectrum of crude of 4-chlorothioanisole using **3I-GB** as photocatalyst (CDCl$_3$, 400 MHz)
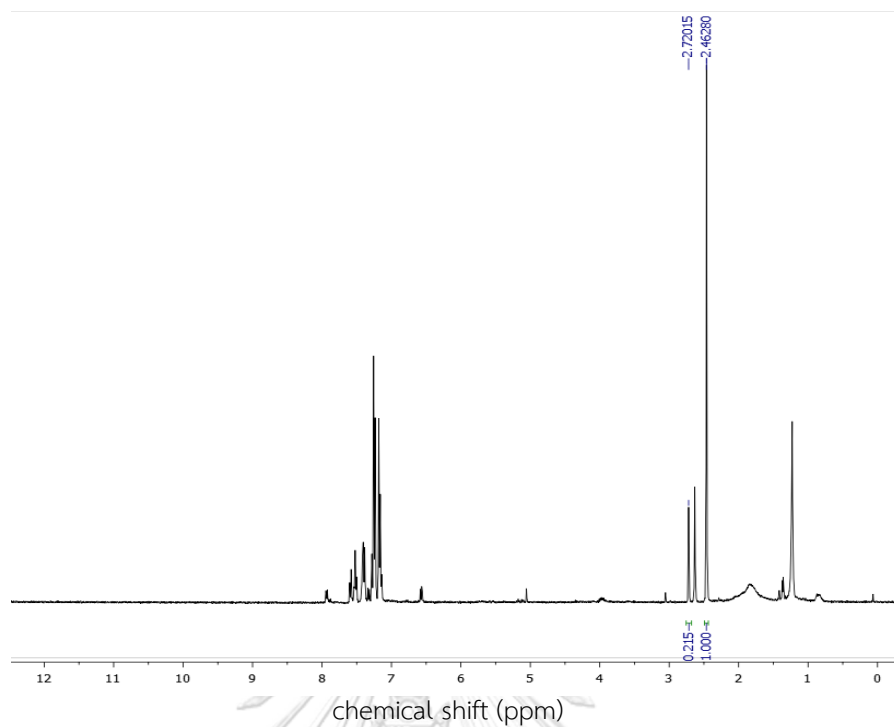
Figure A.32 ^{1}H-NMR spectrum of crude of 4-chlorothioanisole using **3I-RB** as photocatalyst (CDCl$_3$, 400 MHz)
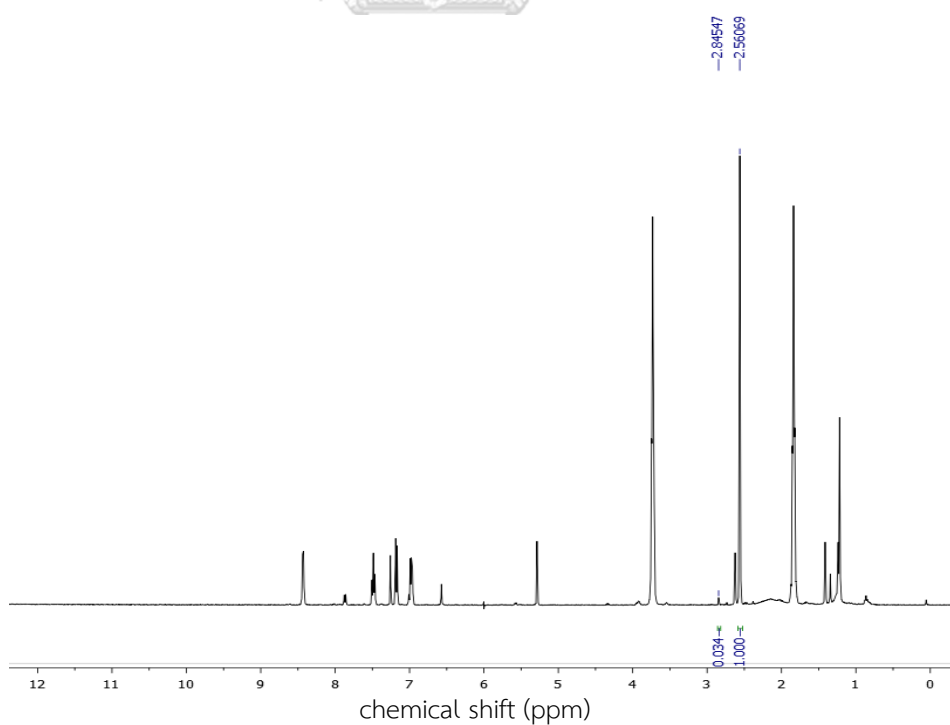
Figure A.33 ^{1}H-NMR spectrum of crude of 2-(methylthio)pyridine using **3I-GB** as photocatalyst (CDCl$_3$, 400 MHz)
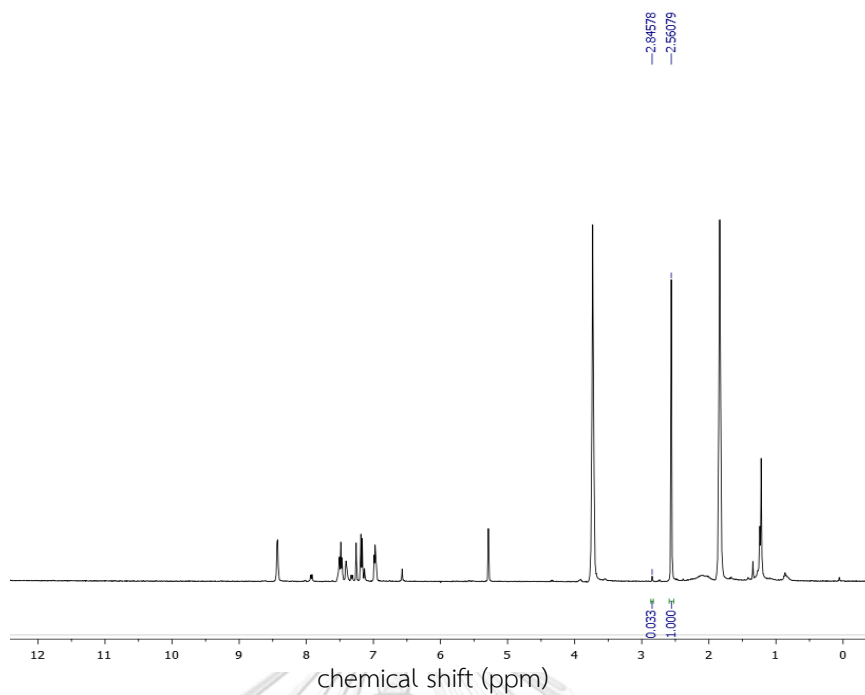
Figure A.34 ^{1}H-NMR spectrum of crude of 2-(methylthio)pyridine using **3I-RB** as photocatalyst (CDCl$_3$, 400 MHz)
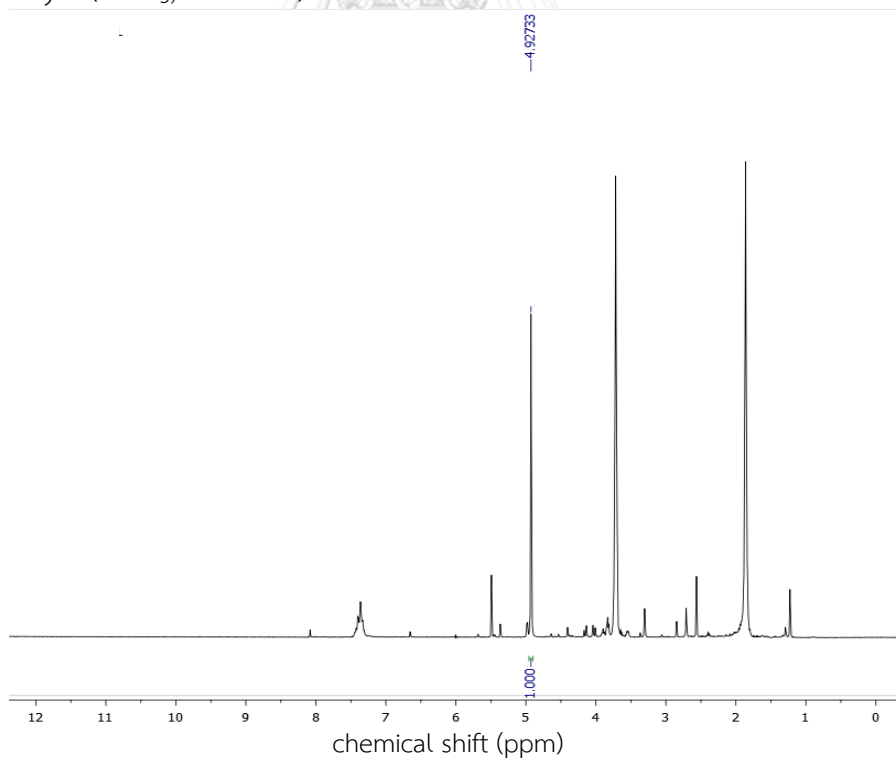
Figure A.35 ^{1}H-NMR spectrum of crude of benzyl methyl sulfide using **3I-GB** as photocatalyst (CDCl$_3$, 400 MHz)
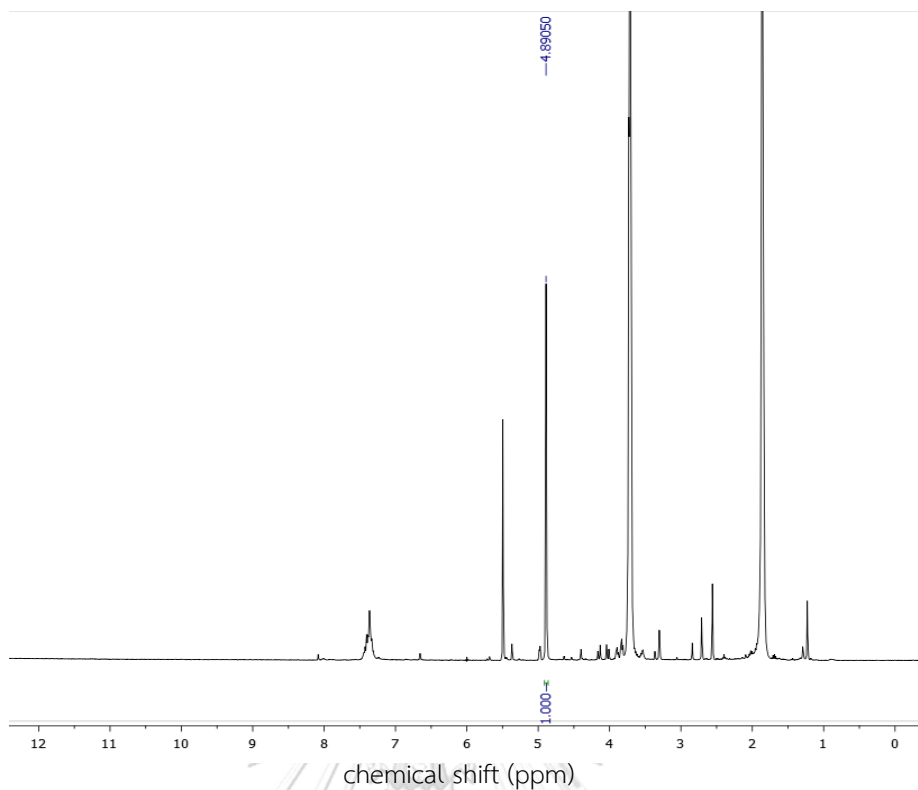
Figure A.36 ^{1}H-NMR spectrum of crude of benzyl methyl sulfide using **3I-RB** as photocatalyst (CDCl$_3$, 400 MHz)
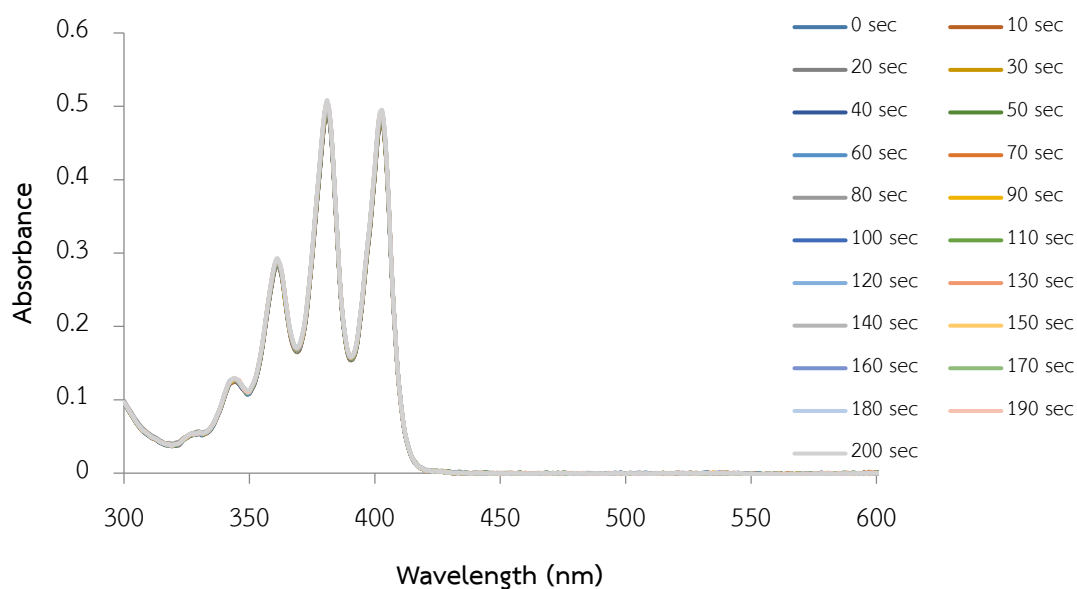
Figure A.37 The change of absorbance of ADPA at 381 nm in H$_2$O:THF (1:9) under white LED overtime
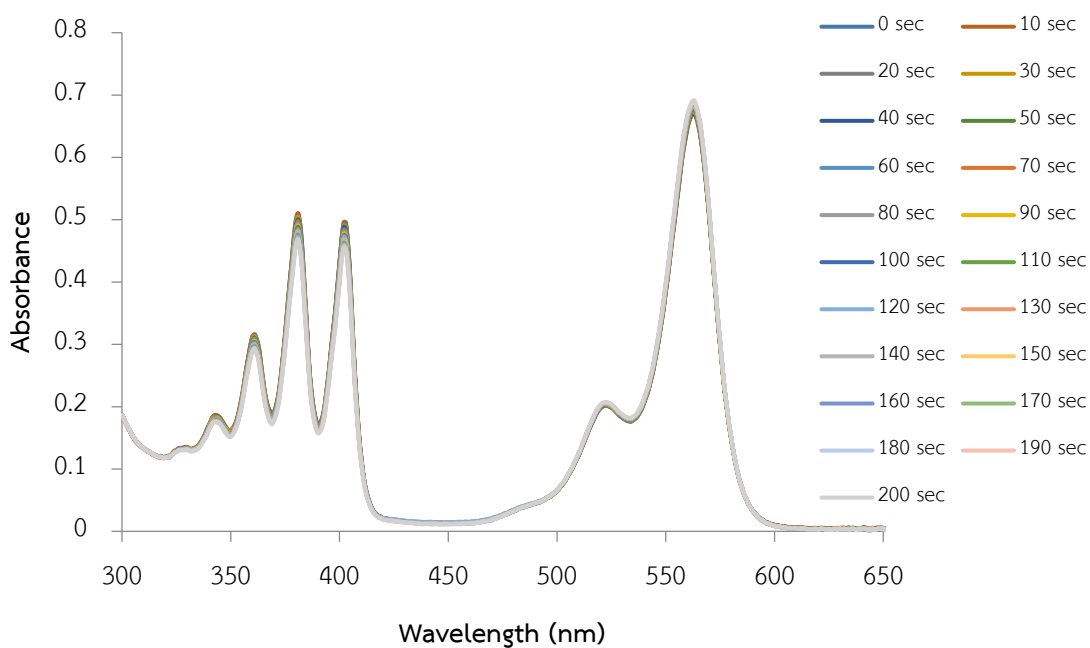
Figure A.38 The change of absorbance of ADPA at 381 nm in the presence of rose bengal in H_2O:THF (1:9) under white LED overtime
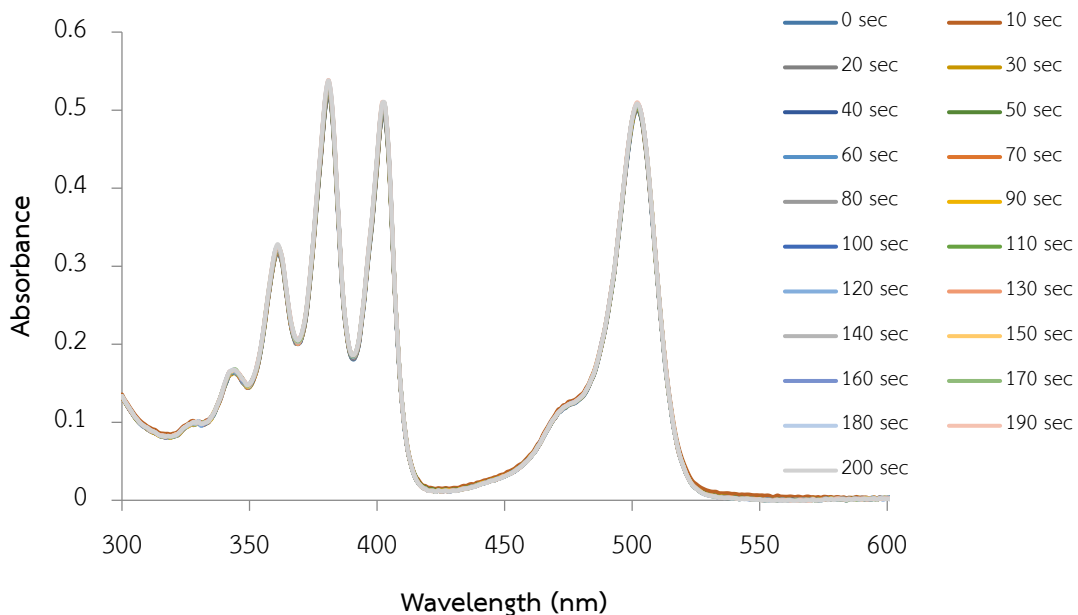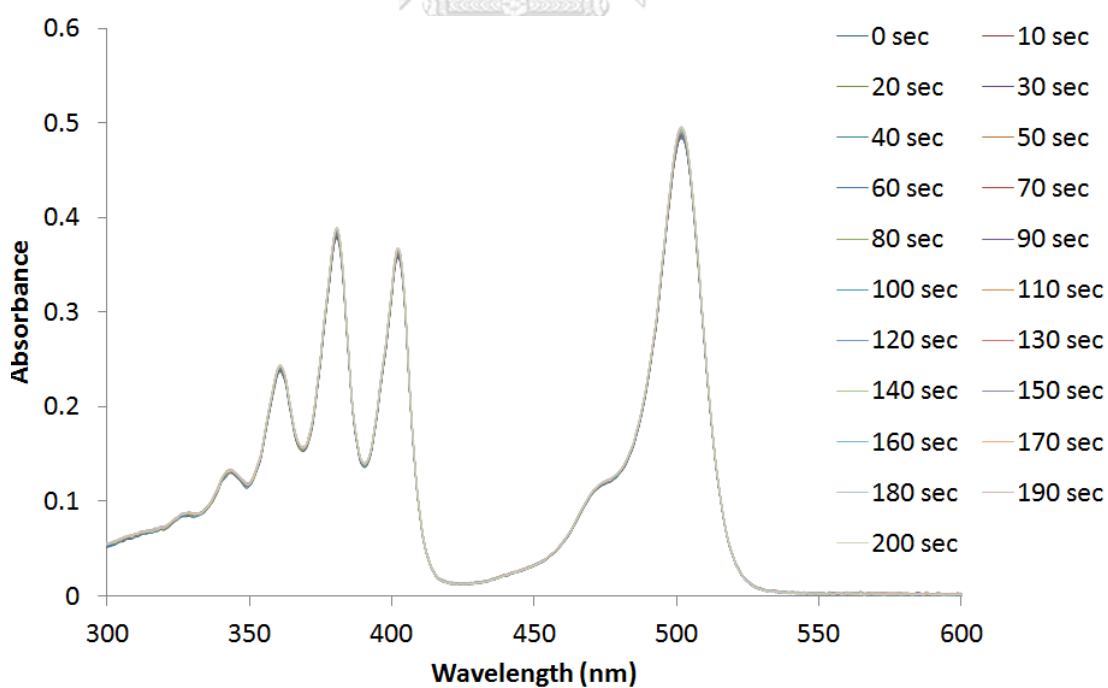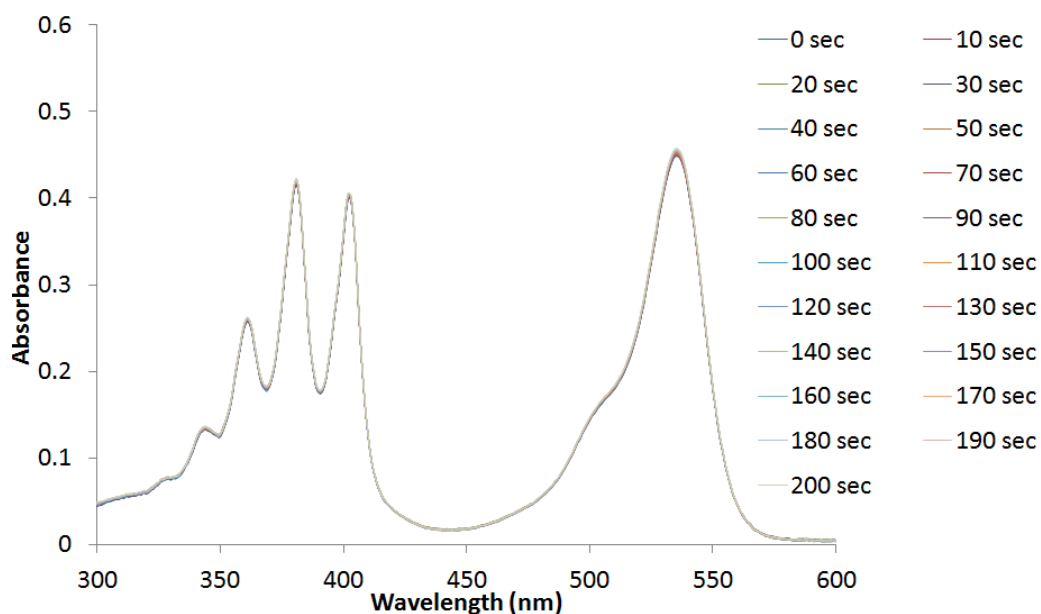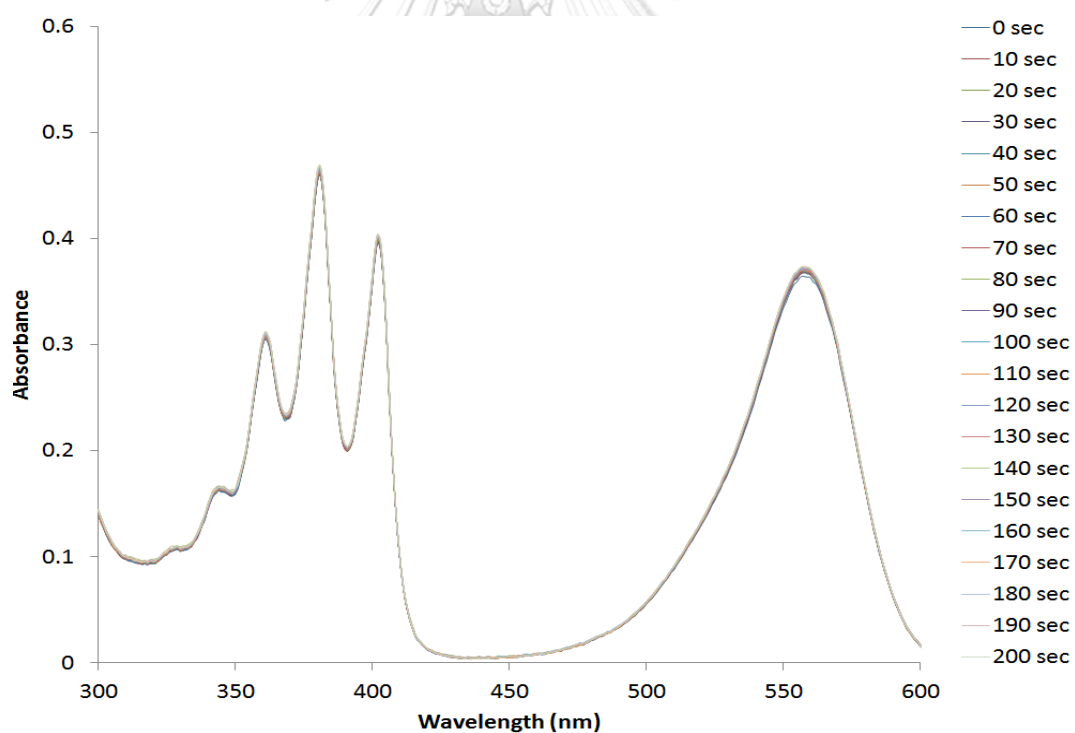

Figure A.39 The change of absorbance of ADPA at 381 nm in the presence of **I-GB** in H_2O:THF (1:9) under white LED overtime
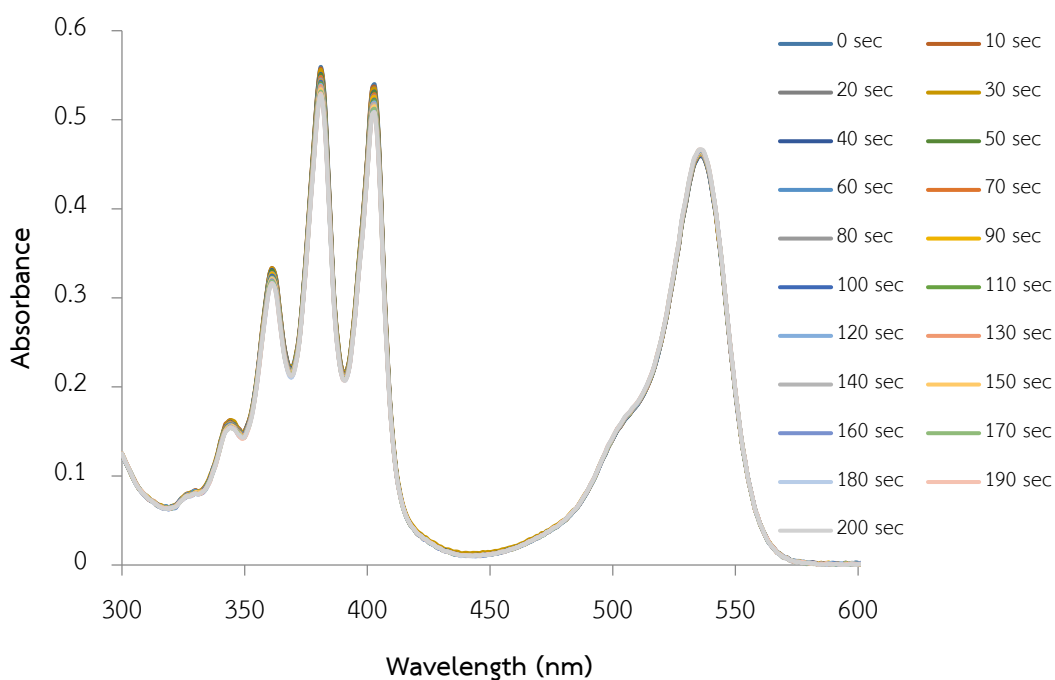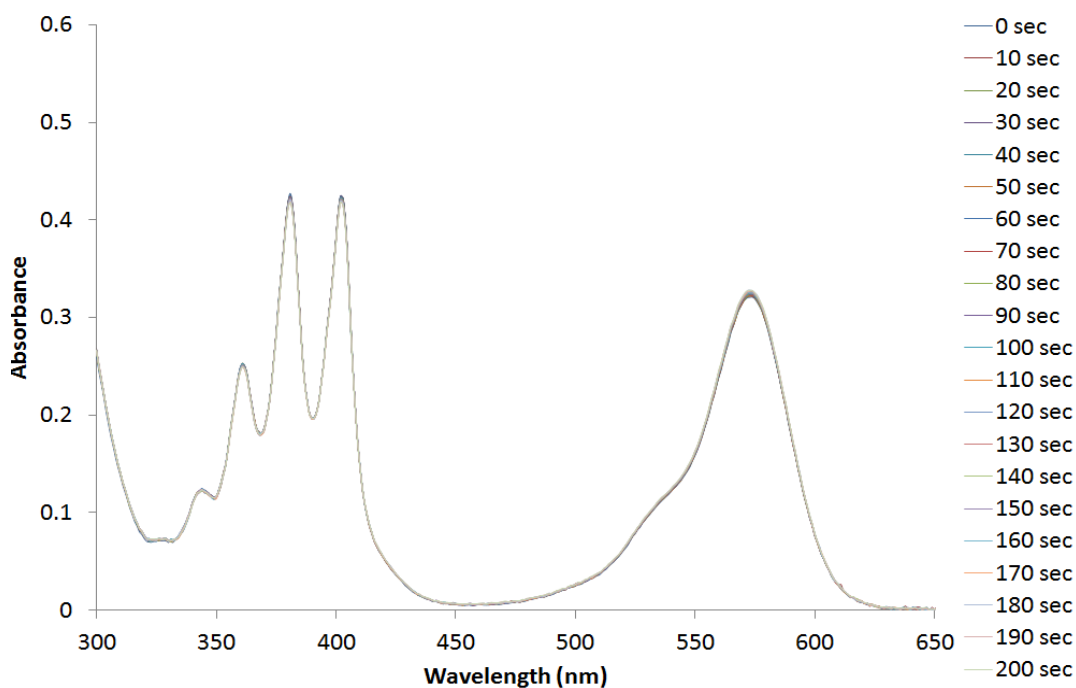
Figure A.40 The change of absorbance of ADPA at 381 nm in the presence of **3I-GB** in H_2O:THF (1:9) under white LED overtime
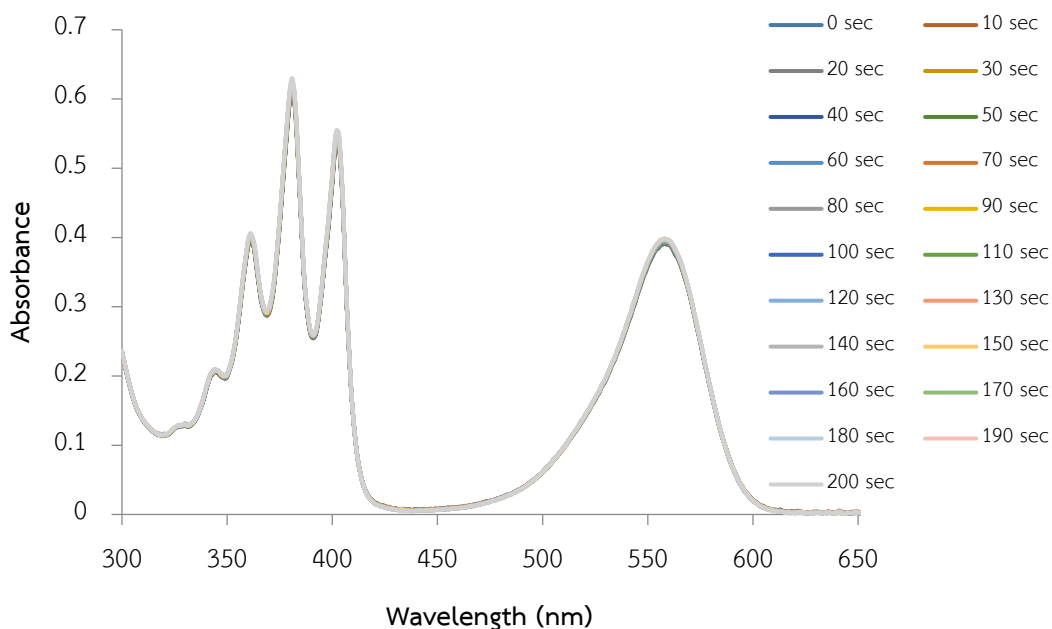
Figure A.41 The change of absorbance of ADPA at 381 nm in the presence of **I-RB** in H_2O:THF (1:9) under white LED overtime
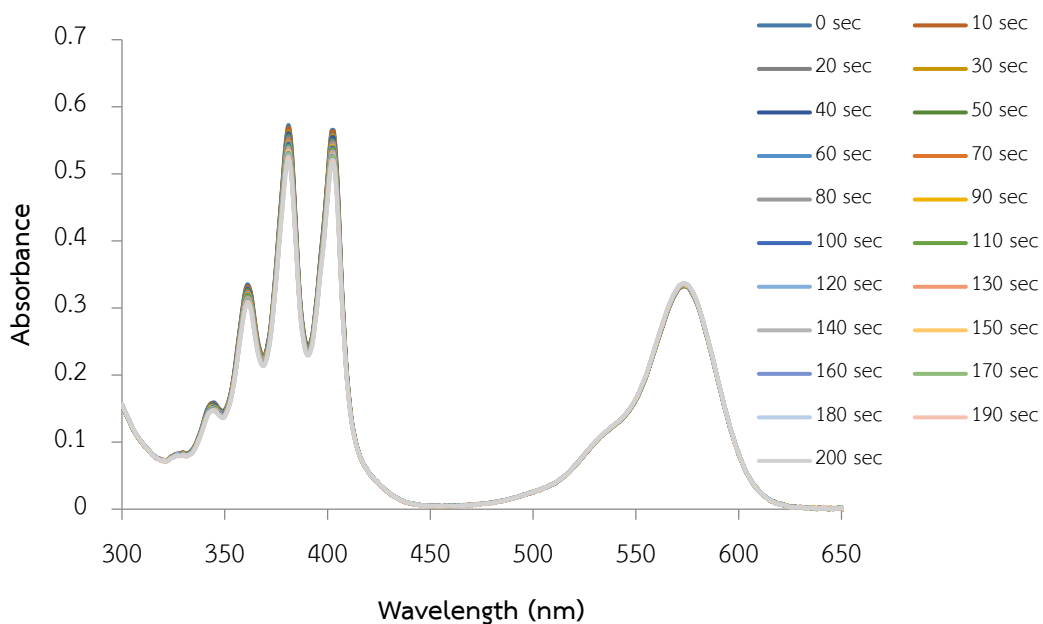
Figure A.42 The change of absorbance of ADPA at 381 nm in the presence of **3I-RB** in H$_2$O:THF (1:9) under white LED overtime
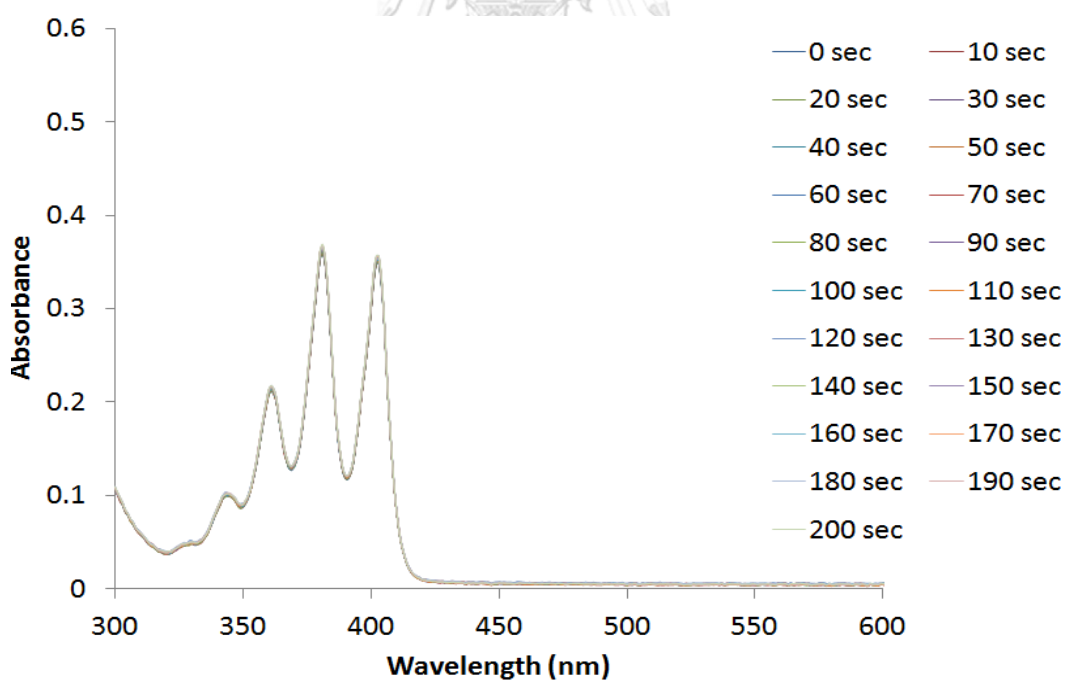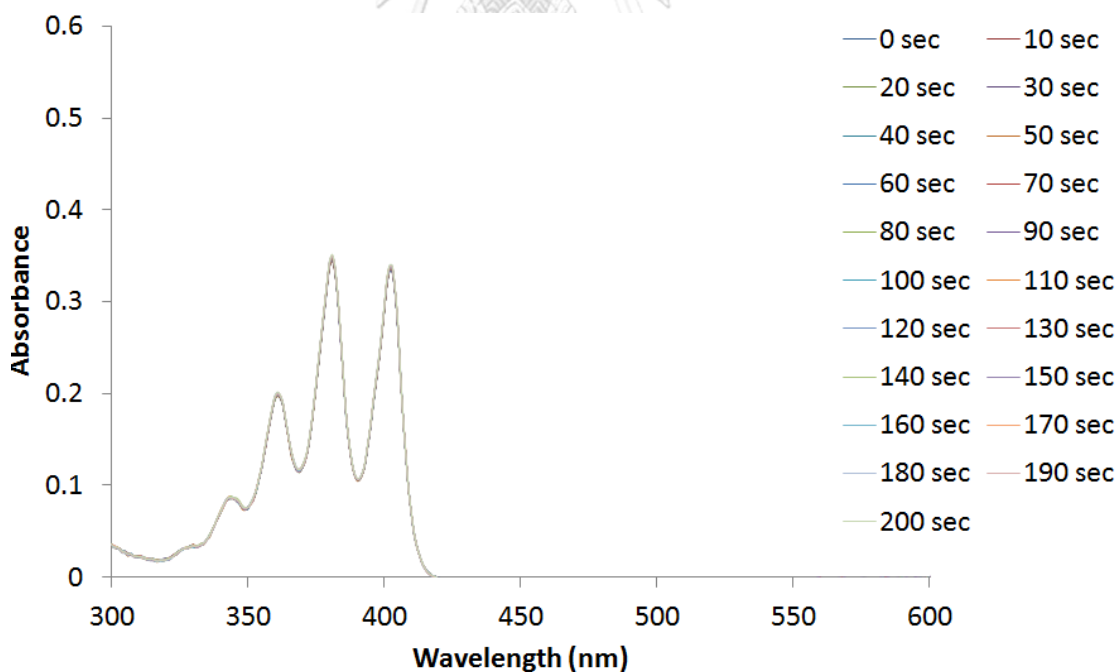

Figure A.43 The change of absorbance of ADPA at 381 nm in H$_2$O:THF (1:9) under red LED overtime
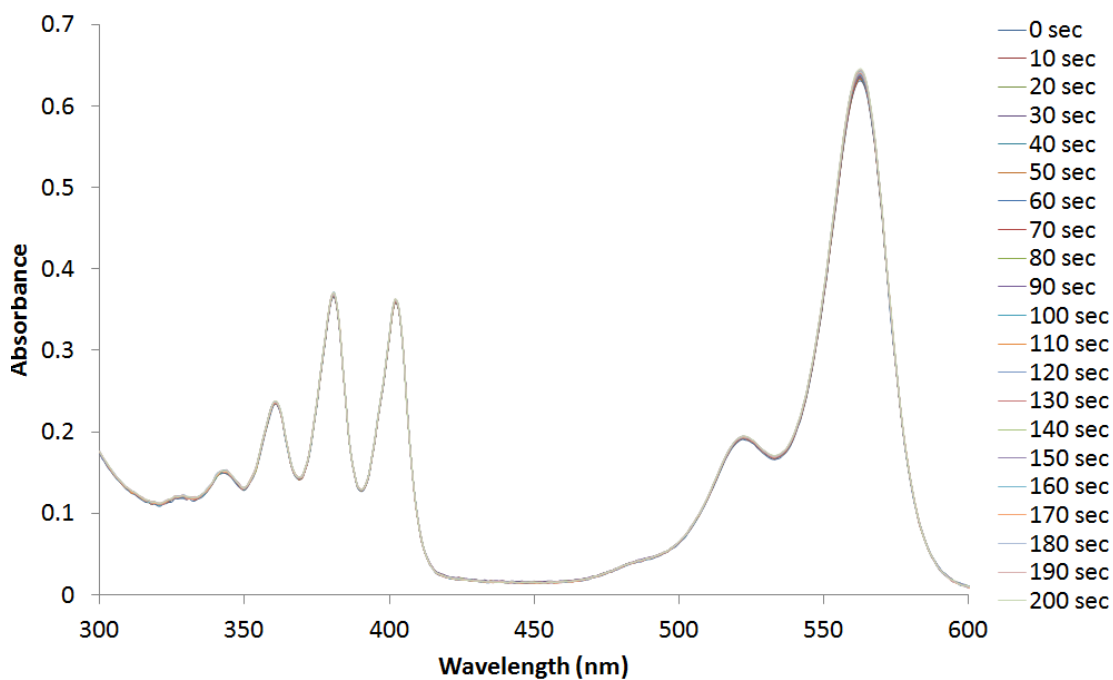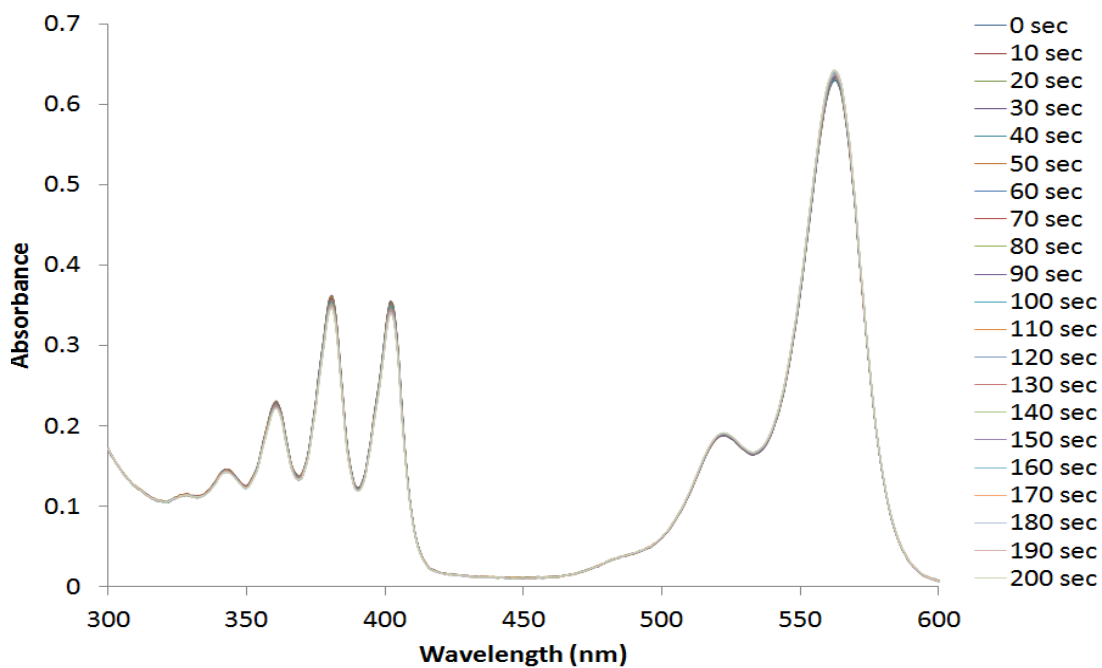
Figure A.44 The change of absorbance of ADPA at 381 nm in the presence of rose bengal in H_2O:THF (1:9) under red LED overtime
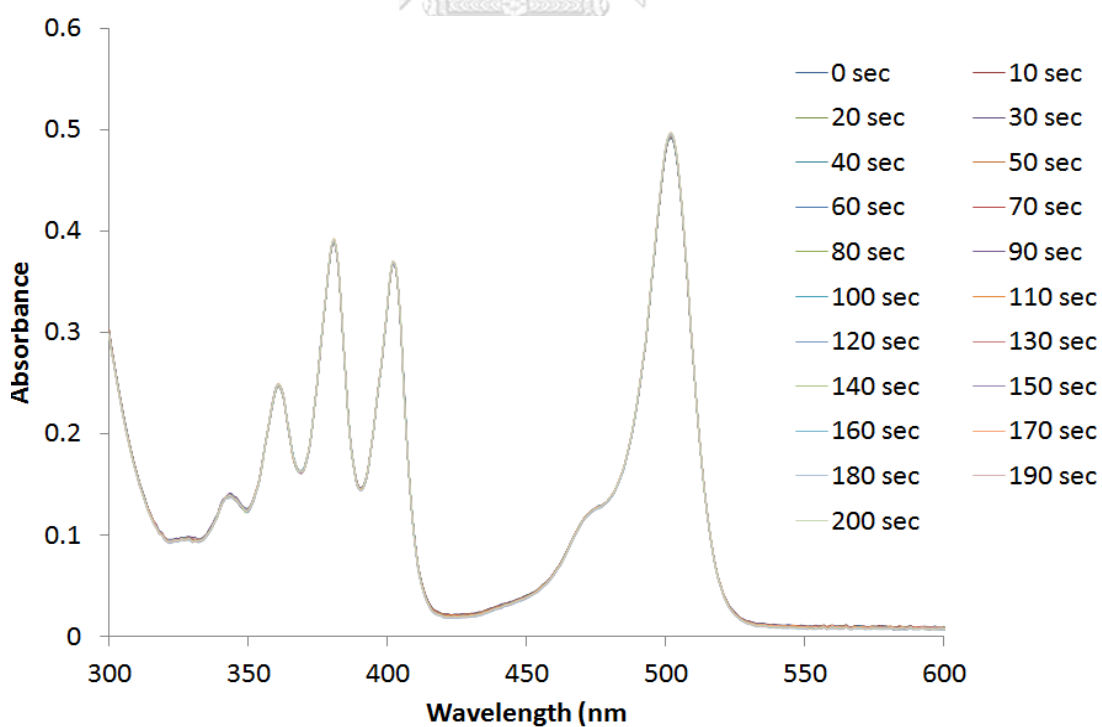

Figure A.45 The change of absorbance of ADPA at 381 nm in the presence of **I-GB** in H_2O:THF (1:9) under red LED overtime

Figure A.46 The change of absorbance of ADPA at 381 nm in the presence of **3I-GB** in H_2O:THF (1:9) under red LED overtime

Figure A.47 The change of absorbance of ADPA at 381 nm in the presence of **I-RB** in H_2O:THF (1:9) under red LED overtime
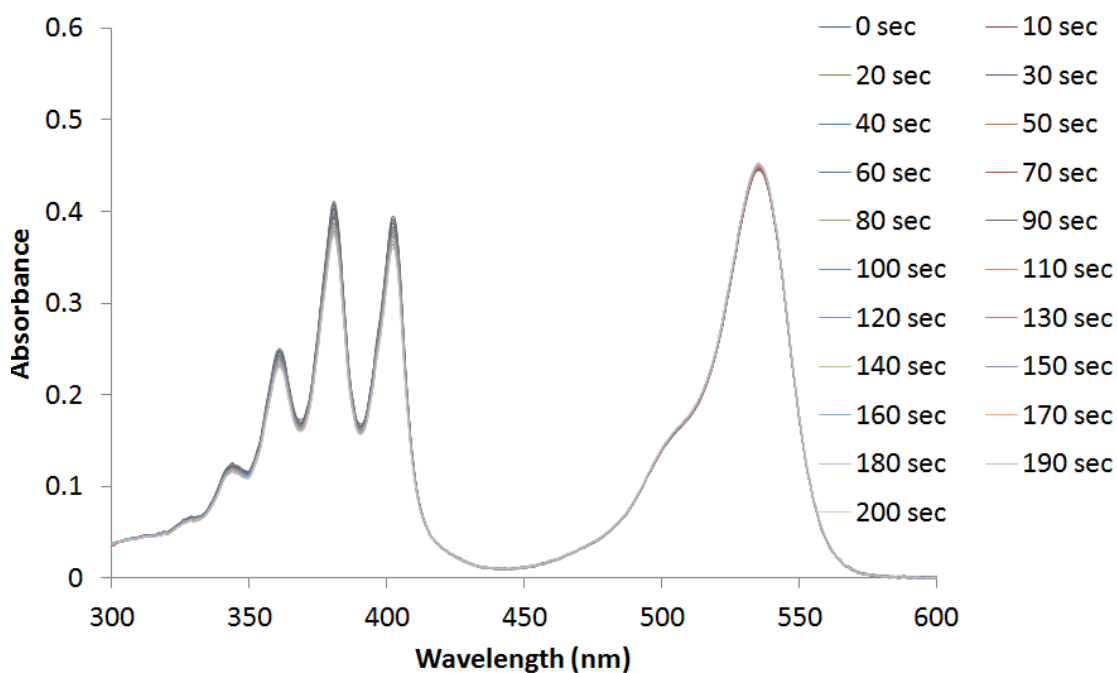
Figure A.48 The change of absorbance of ADPA at 381 nm in the presence of **3I-RB** in H$_2$O:THF (1:9) under red LED overtime

Figure A.49 The change of absorbance of ADPA at 381 nm in H$_2$O:THF (1:9) under blue LED overtime

Figure A.50 The change of absorbance of ADPA at 381 nm in the presence of rose bengal in H_2O:THF (1:9) under blue LED overtime

Figure A.51 The change of absorbance of ADPA at 381 nm in the presence of **I-GB** in H_2O:THF (1:9) under blue LED overtime

Figure A.52 The change of absorbance of ADPA at 381 nm in the presence of **3I-GB** in H$_2$O:THF (1:9) under blue LED overtime
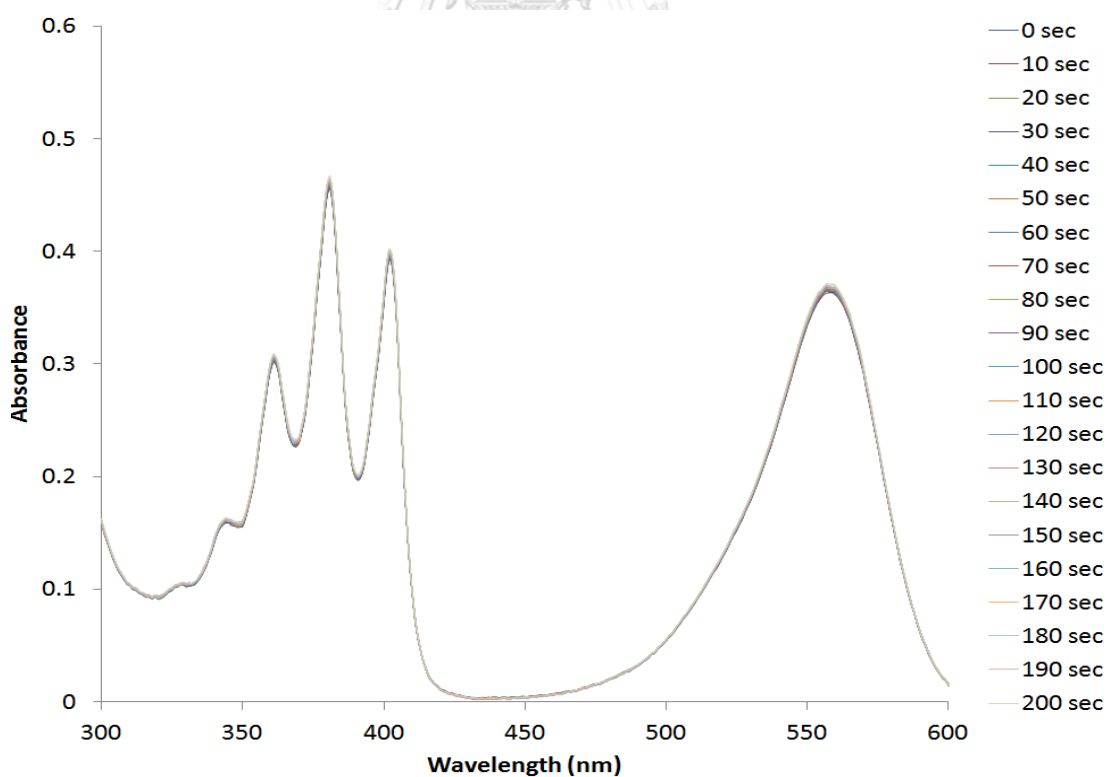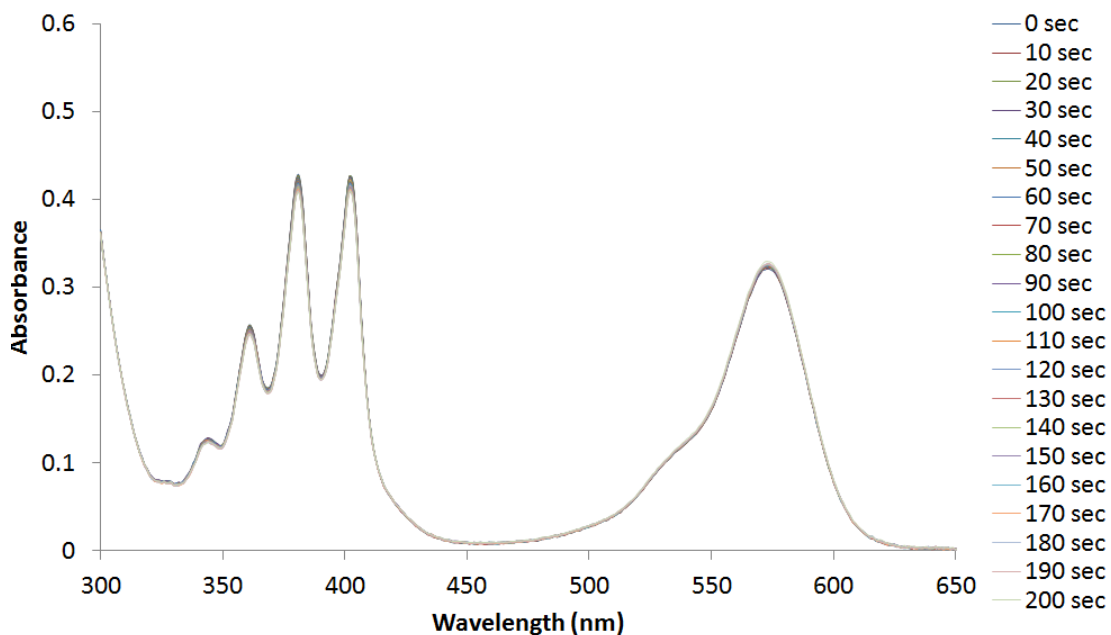

Figure A.53 The change of absorbance of ADPA at 381 nm in the presence of **I-RB** in H$_2$O:THF (1:9) under blue LED overtime

Figure A.54 The change of absorbance of ADPA at 381 nm in the presence of **3I-RB** in H_2O:THF (1:9) under blue LED overtime
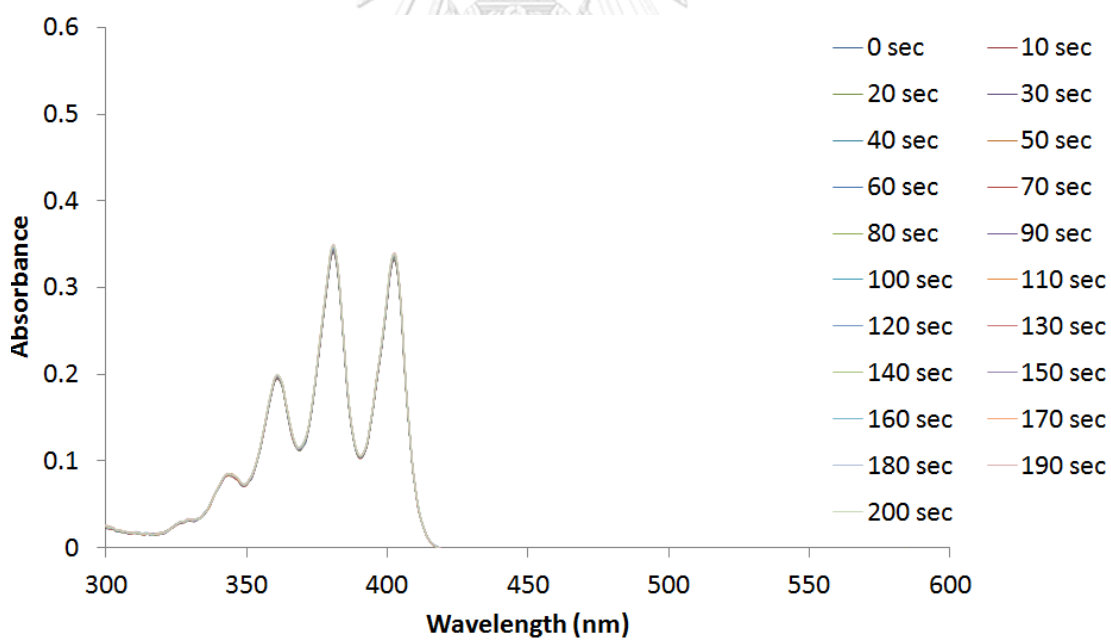

Figure A.55 The change of absorbance of ADPA at 381 nm in H_2O:THF (1:9) under green LED overtime
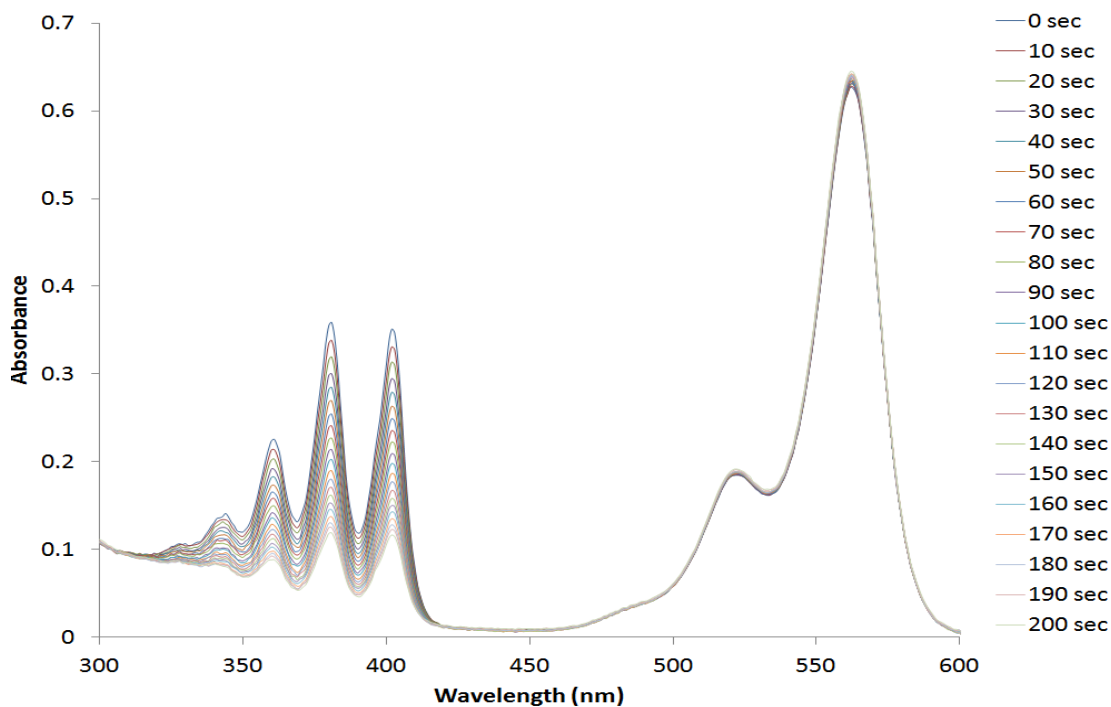
Figure A.56 The change of absorbance of ADPA at 381 nm in the presence of rose bengal in H_2O:THF (1:9) under green LED overtime
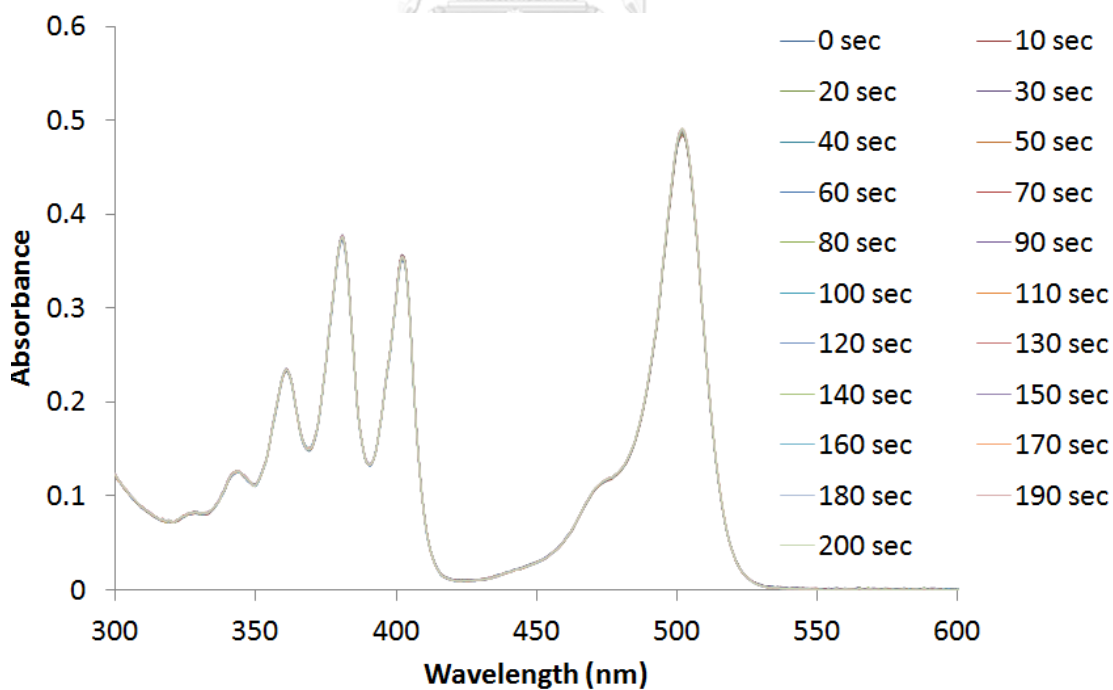

Figure A.57 The change of absorbance of ADPA at 381 nm in the presence of **I-GB** in H_2O:THF (1:9) under green LED overtime
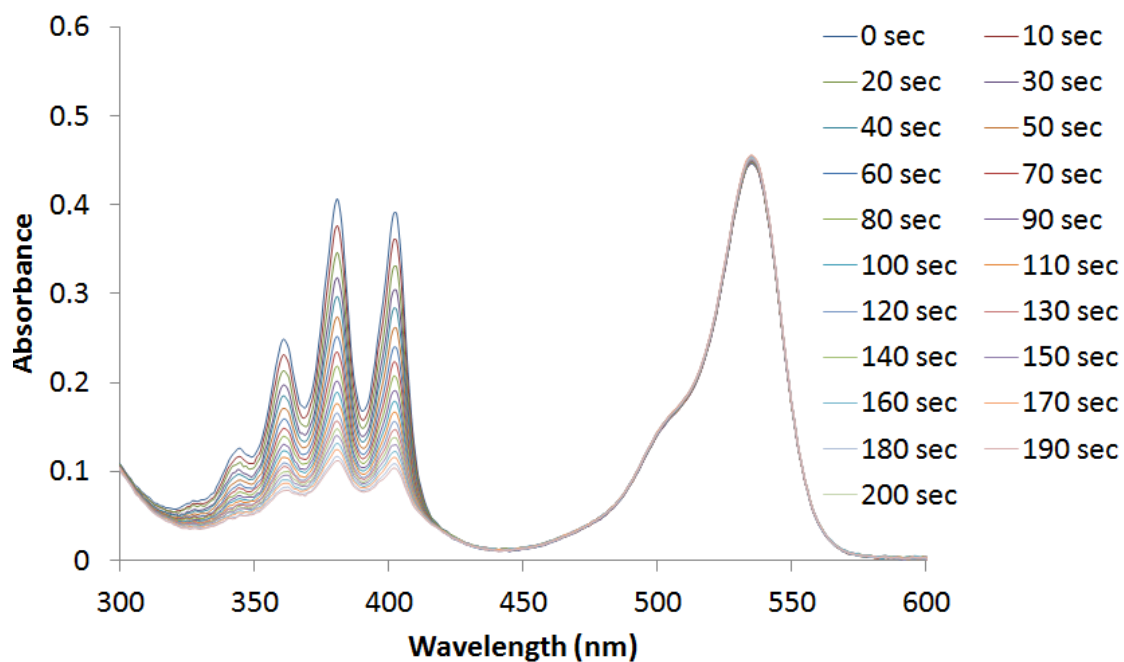
Figure A.58 The change of absorbance of ADPA at 381 nm in the presence of **3I-GB** in H_2O:THF (1:9) under green LED overtime
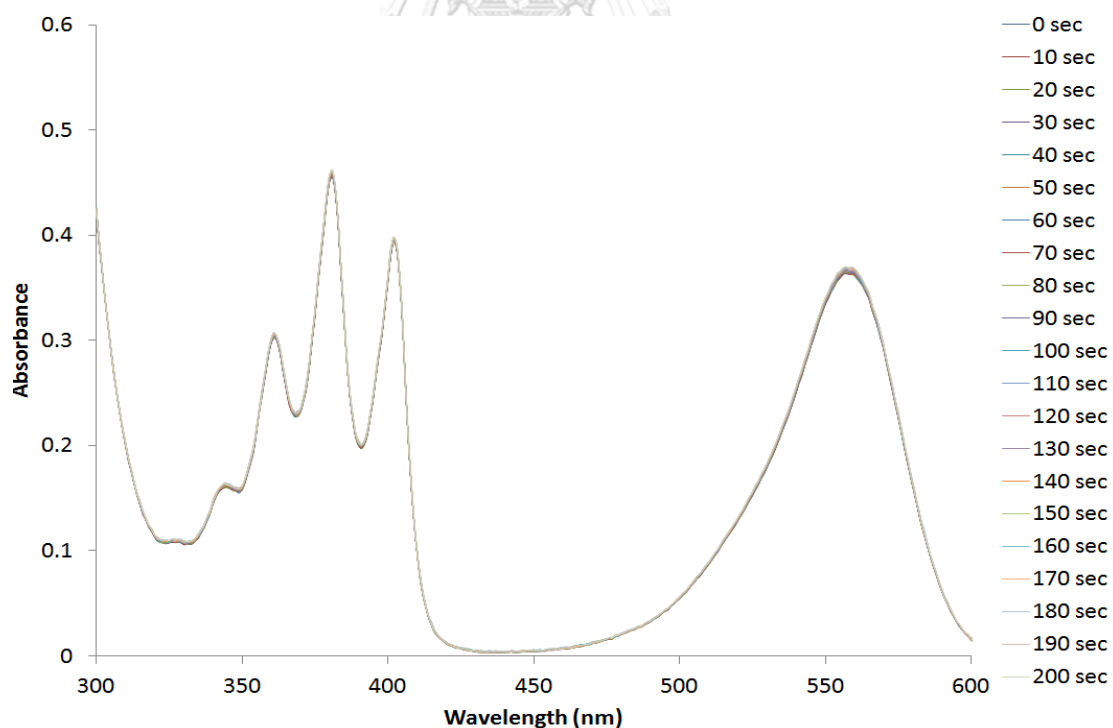

Figure A.59 The change of absorbance of ADPA at 381 nm in the presence of **I-RB** in H_2O:THF (1:9) under green LED overtime
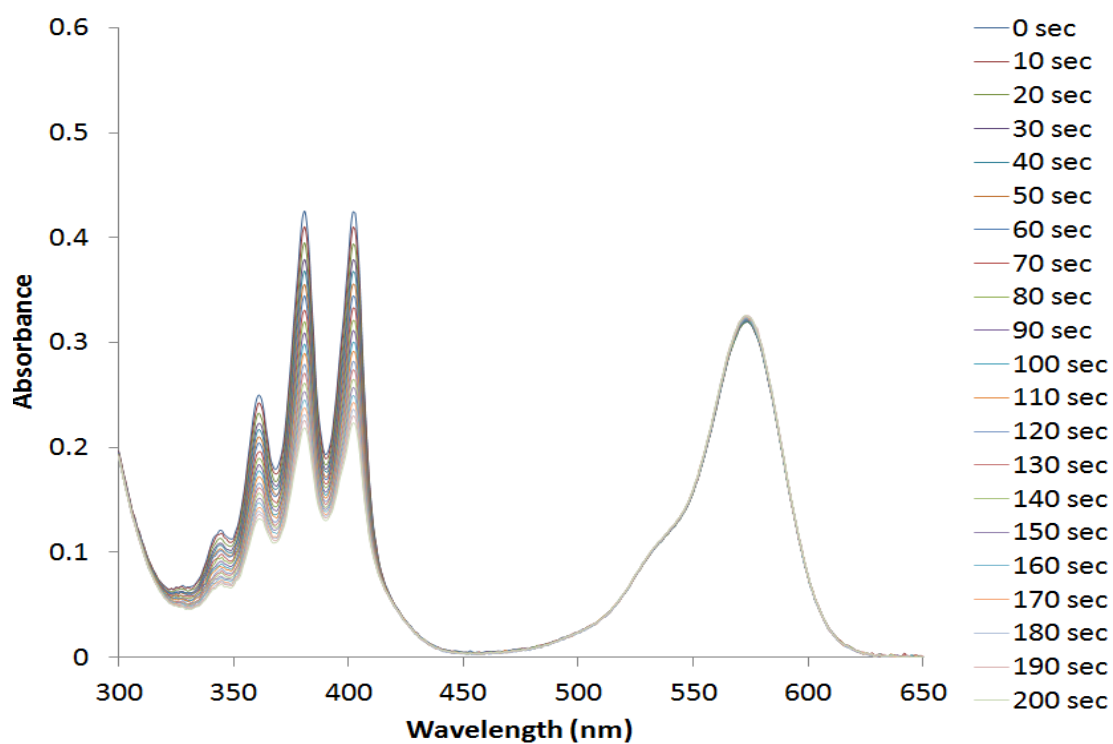
Figure A.60 The change of absorbance of ADPA at 381 nm in the presence of **3I-RB** in H_2O:THF (1:9) under green LED overtime

VITA

Ms. Piyamaporn Tangkasemsamran was born on Thursday 1st October, 1992, in Tak, Thailand. In 2015, she graduated with a Bachelor's degree of Science in Chemistry, from Chulalongkorn University. Next, she has been studied for a Master's degree of Science in Petrochemistry and polymer science, Faculty of Science, Chulalongkorn University. Her poster presentation and proceeding "Photooxidation of organosulfur compounds catalyzed by iodo-BODIPY derivatives under visible light irradiation" have been submitted at the Pure and Applied Chemistry International Conference 2018 (PACCON 2018) in the 60th Anniversary of His Majesty the King's Accession to the Throne International Convention Center, February 7–9, 2018, Hat Yai, Songkhla, Thailand.